NADPH related studies performed with a SoxR based biosensor in *Escherichia coli*

Alina Spielmann

Schlüsseltechnologien / Key Technologies
Band / Volume 207
ISBN 978-3-95806-438-6

Mitglied der Helmholtz-Gemeinschaft

JÜLICH
Forschungszentrum

Schriften des Forschungszentrums Jülich
Reihe Schlüsseltechnologien / Key Technologies Band / Volume 207

Forschungszentrum Jülich GmbH
Institut für Bio-und Geowissenschaften
Biotechnologie (IBG-1)

NADPH related studies performed with a SoxR based biosensor in *Escherichia coli*

Alina Spielmann

Schriften des Forschungszentrums Jülich
Reihe Schlüsseltechnologien / Key Technologies Band / Volume 207

ISSN 1866-1807 ISBN 978-3-95806-438-6

Bibliografische Information der Deutschen Nationalbibliothek.
Die Deutsche Nationalbibliothek verzeichnet diese Publikation in der
Deutschen Nationalbibliografie; detaillierte Bibliografische Daten
sind im Internet über http://dnb.d-nb.de abrufbar.

Herausgeber und Vertrieb:	Forschungszentrum Jülich GmbH Zentralbibliothek, Verlag 52425 Jülich Tel.: +49 2461 61-5368 Fax: +49 2461 61-6103 zb-publikation@fz-juelich.de www.fz-juelich.de/zb
Umschlaggestaltung:	Grafische Medien, Forschungszentrum Jülich GmbH
Druck:	Grafische Medien, Forschungszentrum Jülich GmbH
Copyright:	Forschungszentrum Jülich 2019

Schriften des Forschungszentrums Jülich
Reihe Schlüsseltechnologien / Key Technologies, Band / Volume 207

D 61 (Diss. Düsseldorf, Univ., 2019)

ISSN 1866-1807
ISBN 978-3-95806-438-6

Vollständig frei verfügbar über das Publikationsportal des Forschungszentrums Jülich (JuSER)
unter www.fz-juelich.de/zb/openaccess.

This thesis in hand has been performed at the Institute of Bio- and Geosciences, IBG-1: Biotechnology, Forschungszentrum Jülich GmbH, from May 2015 until July 2018 under the supervision of Prof. Dr. Michael Bott and Dr. Meike Baumgart.

Printed with the permission of
the Faculty of Mathematics and Natural Sciences
of the Heinrich Heine University Düsseldorf

Examiner: **Prof. Dr. Michael Bott**
Institute of Bio- and Geosciences, IBG-1: Biotechnology
Forschungszentrum Jülich GmbH

Co-examiner: **Prof. Dr. Martina Pohl**
Institute of Bio- and Geosciences, IBG-1: Biotechnology
Forschungszentrum Jülich GmbH

The first part of the results described in this thesis have been published in the following original publication:

Spielmann, A., Baumgart, M., Bott, M. (2018). NADPH-related processes studied with a SoxR-based biosensor in *Escherichia coli*. *MicrobiologyOpen*. *0*, e785.
doi: 10.1002/mbo3.785

The second part of the results described in this thesis has been submitted for publication:

Spielmann, A., Brack, Y., van Beek, H., Flachbart, L., Baumgart, M. and Bott, M. (2019). NADPH biosensor-based identification of an alcohol dehydrogenase variant with improved catalytic properties caused by a single charge reversal at the protein surface.
Submitted for publication to Microbial Biotechnology.

Table of contents

Abstract

The SoxRS regulatory system of *Escherichia coli* responds to NADPH, presumably due to the NADPH-dependent reduction of the transcriptional regulator SoxR, switching it to the inactive state. In a previous study, this NADPH-responsiveness was used to construct the genetically encoded NADPH biosensor pSenSox, in which the SoxR-activated *soxS* promoter controls expression of the reporter gene *eyfp*, allowing detection of SoxR activation at the single cell level *via* eYFP fluorescence. The biosensor was reported to sense intracellular NADPH availability, because increased cellular NADPH demands during the biotransformation of methyl acetoacetate (MAA) to *R*-methyl 3-hydroxybutyrate (MHB) by the strictly NADPH-dependent alcohol dehydrogenase of *Lactobacillus brevis* (*Lb*ADH) led to increased *eyfp* expression. Most importantly, the specific eYFP fluorescence of *E. coli* cells catalyzing MAA reduction to MHB correlated not only with the amount of MAA reduced by the cells, and consequently with the NADPH demand, but also with the specific *Lb*ADH activity when a fixed MAA concentration was provided. The latter property enables high-throughput screening of large NADPH-dependent enzyme libraries for variants with improved activity using fluorescence-activated cell sorting (FACS). Based on the correlation of the specific fluorescence of the biosensor with the cellular NADPH demand and the activity of NADPH-dependent enzymes, the pSenSox biosensor was used in this thesis to (1) study NADPH-related processes in *E. coli* and to (2) identify variants of the NADPH-dependent *Lb*ADH with improved catalytic properties.

(1) NADPH plays a crucial role in cellular metabolism for biosynthesis and oxidative stress responses. Here, pSenSox was used to study the influence of various NADPH-related parameters on the *soxRS* response in *E. coli.* Specifically, the influence of different growth media, of the redox-cycling drugs paraquat and menadione, of the SoxR-reducing system RsxABCDGE and RseC, and of transhydrogenases SthA and PntAB on the pSenSox signal was examined. Redox-cycling drugs activated the NADPH biosensor. The absence of RsxABCDGE and/or RseC caused an enhanced biosensor response, in agreement with their function as a SoxR-reducing system. The absence of the membrane-bound transhydrogenase PntAB caused an increased biosensor response, whereas the lack of the soluble transhydrogenase SthA or of SthA and PntAB was associated with a strongly decreased response. These data support the opposing functions of PntAB in $NADP^+$ reduction and of SthA in NADPH oxidation. In conclusion, the biosensor pSenSox was shown to be a useful tool for analyzing environmental conditions and genes with respect to their influence on the NADPH availability in the cell.

(2) The NADPH-dependent *Lb*ADH is widely used in industrial biotechnology for the biocatalytic production of chiral alcohols. To find an optimized *Lb*ADH variant for the substrate 2,5-hexanedione, the biosensor pSenSox was used for FACS-based high-throughput screening of an *Lb*ADH library to isolate clones showing increased fluorescence during the biotransformation of 2,5-hexanedione. Using this approach, the improved variant *Lb*ADH^{K71E} was identified in which lysine-71 was replaced by glutamate, causing a charge reversal at the surface of the protein. Kinetic measurements with purified enzymes revealed that *Lb*ADH^{K71E} has a 16% higher affinity (K_M= 4.3 ± 0.5 mM) and a 17% higher activity (V_{max}= 173.3 ± 11.1 µmol $min^{-1}mg^{-1}$) compared to the wild-type enzyme (K_M= 5.1 ± 0.6 mM; V_{max}= 148.5 ± 12.3 µmol $min^{-1}mg^{-1}$) with 2,5-hexanedione as substrate. Moreover, the *Lb*ADH^{K71E} enzyme also showed higher activity for the alternative substrates acetophenone, acetylpyridine, 2-hexanone, 4-hydroxy-2-butanone, and MAA. The isolation of the optimized variant *Lb*ADH^{K71E} demonstrates that the application of the biosensor combined with high-throughput screening is a powerful workflow for the identification of unexpected beneficial mutations of NADPH-dependent ADHs.

Zusammenfassung

Das SoxRS-Regulationssystem aus *Escherichia coli* reagiert auf NADPH, vermutlich aufgrund der NADPH-abhängigen Reduktion des Transkriptionsregulators SoxR, wodurch dieser in den inaktiven Zustand versetzt wird. In einer früheren Studie wurde diese Eigenschaft genutzt, um den genetisch kodierten NADPH-Biosensor pSenSox zu konstruieren, bei dem der SoxR-aktivierte *soxS*-Promotor die Expression des Reportergens *eyfp* steuert. Damit kann die SoxR-Aktivierung auf Einzelzellebene über die eYFP-Fluoreszenz detektiert werden. Es wurde nachgewiesen, dass SoxR bei erniedrigtem NADPH-Spiegel aktiviert wird, da der erhöhte NADPH-Verbrauch während der Biotransformation von Methylacetoacetat (MAA) zu (*R*)-Methyl-3-hydroxybutyrat (MHB) mit der NADPH-abhängigen Alkoholdehydrogenase aus *Lactobacillus brevis* (*Lb*ADH) zu einer erhöhten *eyfp*-Expression führte. Außerdem wurde gezeigt, dass die spezifische eYFP-Fluoreszenz von *E. coli*-Zellen bei der Biotransformation von MAA zu MHB nicht nur mit der umgesetzten Menge an MAA sondern auch mit der spezifischen *Lb*ADH-Aktivität korreliert. Letzteres ermöglicht das Hochdurchsatz-Screening nach verbesserten Varianten NADPH-abhängiger Enzyme mittels Fluoreszenz-aktivierter Zellsortierung (FACS). Aufgrund der Korrelation der spezifischen Fluoreszenz mit dem zellulären NADPH-Bedarf einerseits sowie der Aktivität von NADPH-oxidierenden Enzymen andererseits wurde pSenSox in der vorliegenden Arbeit verwendet, um (1) verschiedene NADPH-abhängige Prozesse in *E. coli* zu untersuchen und (2) Varianten der *Lb*ADH mit verbesserten katalytischen Eigenschaften zu identifizieren.

(1) Der Biosensor pSenSox wurde benutzt, um den Einfluss verschiedener NADPH-abhängiger Parameter auf die SoxRS-Antwort in *E. coli* zu untersuchen. Insbesondere wurde der Einfluss verschiedener Wachstumsmedien, der redoxaktiven Verbindungen Paraquat und Menadion, der SoxR-Reduktasen RsxABCDGE und RseC sowie der Transhydrogenasen SthA und PntAB auf das pSenSox-Signal untersucht. Die Zugabe von Paraquat oder Menadion aktivierte den Biosensor. Das Fehlen von RsxABCDGE und/oder RseC verstärkte die Biosensor-Antwort, in Übereinstimmung mit der Funktion dieser Proteine als SoxR-Reduktionssystem. Das Fehlen der membrangebundenen Transhydrogenase PntAB führte zu einer erhöhten Biosensor-Antwort, während die Deletion der löslichen Transhydrogenase SthA sowie das gemeinsame Fehlen von SthA und PntAB zu einer stark verminderten Biosensor-Antwort führte. Diese Daten unterstützen die entgegengesetzten Funktionen von PntAB und SthA in NADPH-Bildung bzw. Oxidation. Zusammenfassend wurde gezeigt, dass der pSenSox-Biosensor geeignet ist, um den Einfluss von Umweltbedingungen und Genen auf die NADPH-Verfügbarkeit in der Zelle zu analysieren.

(2) Die NADPH-abhängige *Lb*ADH wird in der industriellen Biotechnologie zur Herstellung von chiralen Alkoholen eingesetzt und ist daher ein interessantes Enzym für eine Biosensor-basierte Optimierung. Zur Verbesserung der *Lb*ADH bezüglich der Umsetzung des Substrates 2,5-Hexandion wurde pSenSox zum Hochdurchsatz-Screening einer *Lb*ADH-Bibliothek mittels FACS verwendet, um Klone zu isolieren, die während der Biotransformation von 2,5-Hexandion eine erhöhte Fluoreszenz zeigten. Dadurch wurde die verbesserte Variante *Lb*ADH^{K71E} identifiziert, bei der Lysin-71 durch Glutaminsäure ersetzt wurde. Dies führte zu einem Ladungswechsel an der Proteinoberfläche, an der Lys-71 lokalisiert ist. Kinetische Messungen ergaben, dass *Lb*ADH^{K71E} eine um 16% erhöhte Substrataffinität (K_M = 4,3 ± 0,5 mM) und eine um 17% erhöhte Aktivität (V_{max}= 173,3 ± 11,1 µmol min^{-1} mg^{-1}) zu 2,5-Hexandion aufweist im Vergleich zum Wildtyp (K_M= 5,1 ± 0,6 mM; V_{max}= 148,5 ± 12,3 µmol min^{-1} mg^{-1}). Zusätzlich setzte *Lb*ADH^{K71E} auch die Substrate Acetophenon, 2-Acetylpyridin, 2-Hexanon, 4-Hydroxy-2-butanon und MAA effizienter um. Die Isolierung von *Lb*ADH^{K71E} zeigt, dass pSenSox in Kombination mit Hochdurchsatz-Screening, die Möglichkeit bietet, unerwartete Mutationen zu identifizieren, die zu einer Verbesserung von NADPH-abhängigen ADHs führen.

Abbreviations

E. coli	*Escherichia coli*
ep-PCR	error-prone polymerase chain reaction
FACS	fluorescence activated cell sorting
*Lb*ADH	alcohol dehydrogenase of *Lactobacillus brevis*
et al.	(lat.) *et alii*
LB	lysogeny broth
K_M	Michaelis constant
v_{max}	maximal turnover rate
MAA	methyl acetoacetate
MHB	(*R*)-methyl 3-hydroxybutyrate
$NADP^+$	nicotinamide adenine dinucleotide phosphate
NADPH	reduced form of $NADP^+$
bp	base pair
OD_{600}	optical density at 600 nm
R. capsulatus	*Rhodobacter capsulatus*
SDS-PAGE	sodium dodecyl sulfate – polyacrylamide electrophoresis
TB	terrific broth
TF	transcription factor
TSS	transcription start site
wt	wild-type

1. Scientific context and key results of this thesis

1.1. Transcription factor-based biosensors

In prokaryotes, transcription factors (TFs) serve as molecular sensors and are needed for the physiological adaptation to environmental and metabolic cues (Ulrich et al., 2005). They control the expression of their target gene(s) as activators or repressors at the level of transcription. TFs respond to a wide variety of signals, including the interaction with small (effector) molecules, ions, physical parameters (e.g. temperature or pH), protein-protein interaction or protein modification (Mahr and Frunzke, 2016).

Genetically encoded, TF-based biosensors usually consist of the TF itself and one of its target promoters fused to a reporter gene. The TF senses the signal, for instance, a high concentration of a certain amino acid, and subsequently activates expression of the reporter gene, typically encoding a fluorescent protein. One major advantage of TF-based biosensors with reporter genes for fluorescent proteins is that these systems enable a correlation of the intracellular concentration of a particular molecule or another signal to a measurable fluorescent signal which can be detected at the single cell level by high-throughput methods such as flow cytometry. Consequently, TF-based biosensors with fluorescent proteins as reporters turned out to be highly useful tools for monitoring physiological responses at the single-cell level and for enabling high-throughput screening in strain and enzyme development (Dietrich et al., 2010; Eggeling et al., 2015; Mahr and Frunzke, 2016; Rogers et al., 2016).

In recent years, TF-based biosensors for amino acids were developed and used to identify novel mutations for overproduction of L-lysine, L-arginine, and L-histidine by fluorescence activated cell sorting (FACS)-based screening of genome-wide, gene-specific, and codon-specific mutant libraries (Binder et al., 2012; Binder et al., 2013; Schendzielorz et al., 2014) or for increasing L-valine production by adaptive laboratory evolution (Mahr et al., 2015). Besides the sensors for amino acids, a TF-based biosensor responding to the intracellular availability of NADPH was developed (Siedler et al., 2014). This NADPH biosensor, which takes advantage of the SoxRS regulatory system of *Escherichia coli*, was the major tool for the realization of the experiments of this thesis (cf. chapter 1.3).

1.2. The SoxRS system of *E. coli*

1.2.1. The oxidative stress regulators SoxR and SoxS

SoxR and SoxS are transcription factors that control the expression of oxidative stress response genes when cells are exposed to superoxide, redox-cycling drugs, or nitric oxide (Hidalgo and Demple, 1994; Kobayashi, 2017). In *E. coli*, the SoxRS system regulates gene expression in a two-step regulatory cascade. First, an oxidation of the iron-sulfur cluster activates the transcriptional regulator SoxR, which then activates *soxS* expression (Greenberg et al., 1990; Tsaneva and Weiss, 1990). SoxR was previously considered to activate expression of *soxS* only, but recent studies uncovered further direct SoxR target genes (Seo et al., 2015). SoxS activates genes, many but not all of which are responsible for coping with damage caused by oxygen radicals, such as *sodA* for superoxide dismutase, *zwf* for the NADPH-generating glucose 6-phosphate dehydrogenase, or *fumC* for fumarase C (Blanchard et al., 2007; Seo et al., 2015).

SoxR is a homodimer with each subunit containing an [2Fe-2S] cluster (Hidalgo and Demple, 1994; Watanabe et al., 2008) (Fig. 1). SoxR activity is controlled by an alteration of the redox state of its [2Fe−2S] clusters, which is associated with conformational changes: SoxR activates *soxS* expression only in the oxidized $[2Fe{-}2S]^{2+}$ state, but not in the reduced $[2Fe{-}2S]^{+}$ state (Ding et al., 1996; Gaudu and Weiss, 1996). Thus, SoxR senses oxidative stress using the redox states of the [2Fe-2S] cluster and regulates the transcription of the *soxS* gene by structural changes between the oxidized and reduced forms.

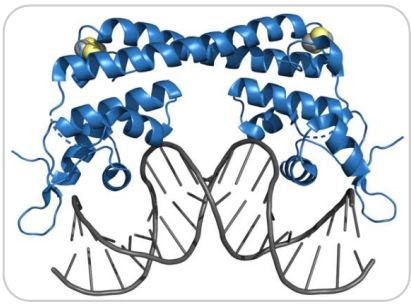

Fig. 1. Structure of the SoxR-*soxS* promoter complex. The SoxR homodimer is shown in blue. The iron and sulfur atoms of the two [2Fe-2S] clusters are represented in light grey and yellow spheres, respectively. The DNA fragment appears in dark grey. The image was generated with the software PyMOL 2.2.0 (PDB code 2ZHG).

SoxR is kept in the reduced state by NADPH-dependent reduction of its oxidized $[2Fe{-}2S]^{2+}$ clusters with the help of NADPH-dependent reductases (Koo et al., 2003). Conversion of

inactive, reduced SoxR into active, oxidized SoxR can be induced by multiple factors. These include direct oxidation of SoxR by superoxide (Liochev and Fridovich, 2011; Fujikawa et al., 2012) and by redox-cycling drugs (Gu and Imlay, 2011), nitrosylation of SoxR (Ding and Demple, 2000), and conditions leading to a diminished $NADPH/NADP^+$ ratio within cells (Liochev and Fridovich, 1992; Krapp et al., 2011).

Upon removal of the oxidative stress inducing signal, SoxR is re-reduced, *soxS* transcription is inactivated and the expression of the genes controlled by the SoxRS system quickly returns to the pre-induced level. It has been shown that the intrinsic instability of SoxS ($t_{1/2}$ ~ 2 min) and the degradation of SoxS, primarily through the Lon protease, are responsible for the rapid return of the SoxRS system to the inactive state when the stimuli activating the system are no longer present (Griffith et al., 2004).

1.2.2. The *soxRS* promoter

In the genome of *E. coli*, the *soxR* gene is located divergently to the *soxS* gene. The *soxS* promoter is located within the 85-nucleotide *soxRS* intergenic region (Wu and Weiss, 1991; Hidalgo et al., 1998) (Fig. 2). The SoxR binding site is located between the -10 and -35 regions of the *soxS* promoter. Interestingly, SoxR binds both in the oxidized and in the reduced state with high affinity (Hidalgo and Demple, 1994; Gaudu and Weiss, 1996).

In literature several transcription start sites (TSSs) are proposed for SoxR. There is a study indicating that the *soxR* promoter is embedded within the *soxS* structural gene (Wu and Weiss, 1991). A subsequent analysis revealed that the promoters of the two genes overlap and that both, the TSS of *soxR* and the TSS of *soxS*, are located in the *soxRS* intergenic region (Hidalgo et al., 1998). According to Hidalgo et al. (1998), the SoxR binding site in the *soxS* promoter covers the TSS of the *soxR* transcript so that binding of SoxR auto-represses its own transcription. In consequence, SoxR does not only activate *soxS* expression but simultaneously acts as a noninducible repressor of its own expression, both in the oxidized and the reduced state (Hidalgo et al., 1998). In a more recent study reporting on a global analysis of TSSs in *E. coli* by RNA sequencing, two TSSs for *soxR* were found (Thomason et al., 2015). One was located only 1 bp upstream of the TSS found by Hidalgo et al. (1998), whereas the second one was located within the *soxS* coding region, but closer to the *soxS* start codon than the TSS found by Wu and Weiss (1991) (Fig. 2).

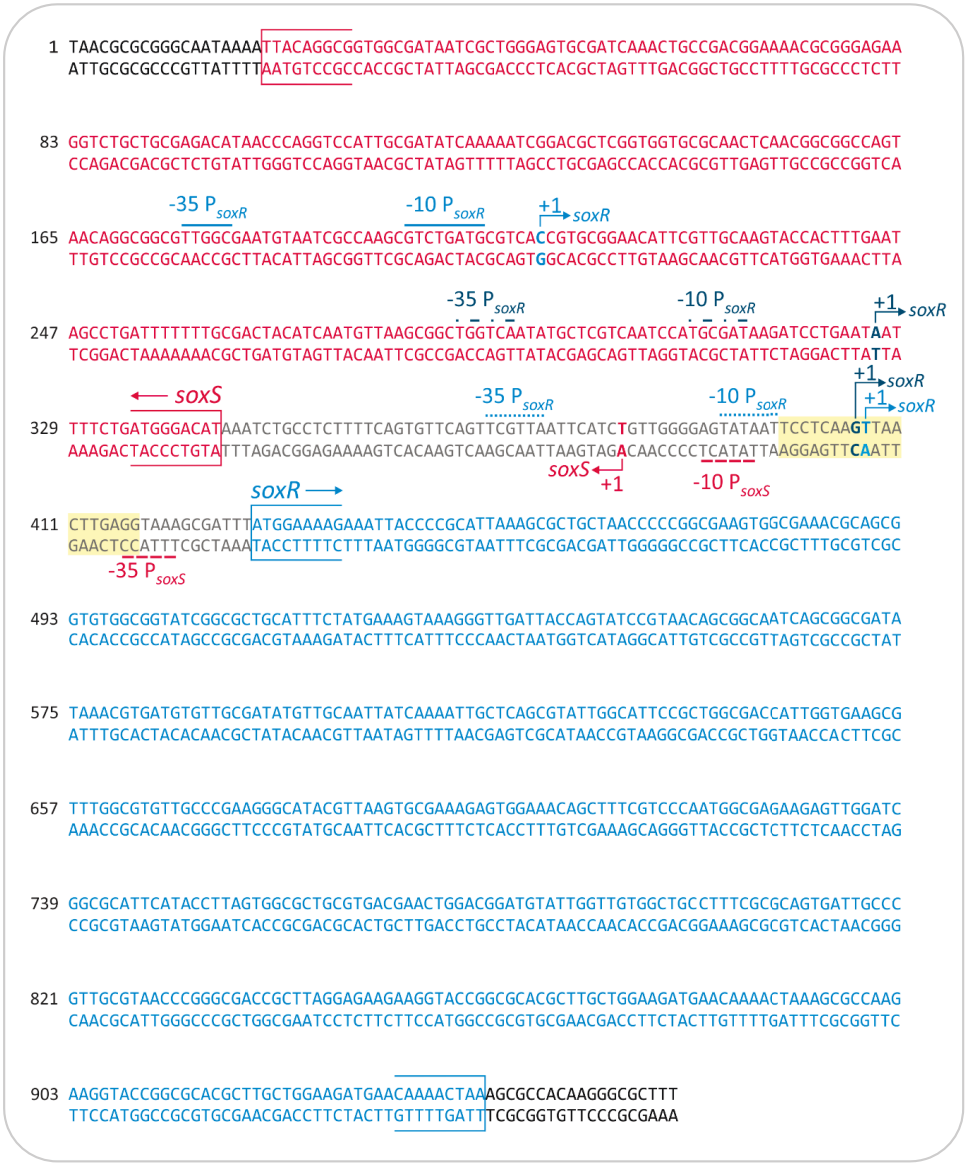

Fig. 2. DNA sequence and features of the *soxRS* region of *E. coli* K-12 MG1655. The *soxS* coding region (nucleotides 19-342), the *soxRS* intergenic region (nucleotides 344-428), and the *soxR* coding region (nucleotides 429-893) are colored in red, grey, and blue, respectively. The beginning and ending of the *soxR* and soxS gene regions are surrounded by open boxes. The positions of the TSS (+1) and the corresponding -10 and -35 regions of the *soxR* promoter according to Wu and Weiss, 1991 are indicated in blue on the upper strand in the nucleotide region 177-212. The -10 and -35 regions are underlined. The positions of the TSS (+1) and the corresponding -10 and -35 regions in the intergenic *soxRS* region (nucleotides 344-428) according to Hidalgo et al., 1998 are indicated in blue on the upper strand for *soxR* and in red on the lower strand for *soxS*. The *soxR* -10 and -35 regions are underlined with dotted lines, whereas the *soxS* -10 and -35 regions are underlined with dashed lines. The two identified *soxR* TSS (+1) according to Thomason et al., 2015 are highlighted in dark blue. For the

identification of the putative -10 and -35 regions corresponding to the *soxR* TSS (+1) at position 326 phiSITE's PromoterHunter Tool (http://www.phisite.org) (Klucar et al., 2009) and its provided search matrix were used. The identified *soxR* -10 and -35 regions are indicated in dark blue on the upper strand in the nucleotide region 285-313 and are underlined with dashdotted lines. The yellow box corresponds to the SoxR-binding site according to Hidalgo & Demple, 1994.

1.2.3. The SoxR-reducing system

By screening an *E. coli* mutant library, mutations in the *rseC* gene and in the *rsxABCDGE* operon were found to cause constitutive expression of a P_{soxS}-*lacZ* reporter gene in a SoxR-dependent manner (Koo et al., 2003). Further studies led to the conclusion that the membrane-integral RsxABCDGE complex and the membrane protein RseC (Daley et al., 2005) constitute a SoxR-reducing system (Koo et al., 2003) (Fig. 3). The statement that purified RsxC exhibits NADPH-dependent cytochrome *c* reduction activity suggests that NADPH serves as electron donor of the Rsx complex (Koo et al., 2003).

The *rsxABCDGE* operon is highly homologous to the *rnfABCDGE* operon of *Rhodobacter capsulatus* (Koo et al., 2003), indicating that the RsxABCDGE complex belongs to the family of Rnf complexes. The presence of *rnf* genes in bacteria suggests the existence of a membrane-bound, redox-driven ion transporter that links translocation of either Na^+ or H^+ across the membrane to redox reactions (Hreha et al., 2015). More specifically, Rnf enzymes drive the endergonic reduction of ferredoxin ($E_0' = -420$ mV) with NAD(P)H ($E_0' = -320$ mV) by the proton- or sodium-motive force *via* import of H^+ or Na^+, or, in the reverse reaction, the exergonic reduction of $NAD(P)^+$ with reduced ferredoxin coupled to the export of H^+ or Na^+ (Biegel et al., 2011). The redox potential of SoxR in its DNA-free and its DNA-bound state was reported to be -293 mV and -320 mV (Kobayashi et al., 2015), respectively, which is in the same range as the one of NAD(P)H. Consumption of proton- or sodium-motive force *via* the Rsx complex to drive reduction of SoxR by NADPH allows the cell to keep most SoxR in the reduced state in the absence of inducing conditions.

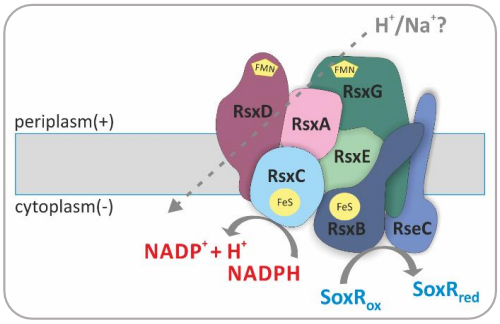

Fig. 3. Model of the SoxR-reducing system based on the topology model of the Rnf complex of *Vibrio cholerae* (Hreha *et al.*, 2015). RsxABCDGE and RseC are predicted to form a membrane-bound complex. This complex reduces active (oxidized) $SoxR_{ox}$ to inactive (reduced) $SoxR_{red}$ with NADPH as reductant at the expense of a transmembrane electrochemical Na^+ or H^+ gradient. Co-factors for electron translocation from NADPH to oxidized SoxR might be present at RsxB and RsxC (iron-sulphur clusters, FeS) as well as RsxD and RsxG (flavin mononucleotides, FMN).

1.2.4. The effect of redox-cycling drugs on the *soxRS* response

Paraquat (1, 1'-dimethyl-4, 4'-bipyridinium dichloride) and menadione (2-methyl-1,4-naphthoquinone) have been reported to induce the *soxRS* response in *E. coli* (Greenberg et al., 1990; Wu and Weiss, 1991; Seo et al., 2015). Paraquat and menadione are redox-cycling drugs, which mediate the transfer of electrons from NADPH to oxygen, leading to the continuous generation of superoxide (Kappus and Sies, 1981) (Fig. 4). Several possibilities exist how redox-cycling drugs might activate the *soxRS* response: (i) the superoxide radical has been shown to directly oxidize the [2Fe-2S] cluster of SoxR (Fujikawa et al., 2012), thus forming active SoxR; (ii) the redox-cycling drug might directly interact with reduced SoxR and oxidize it, leading to active SoxR (Gu and Imlay, 2011); (iii) the reduction of the redox-cycling agent by NADPH might lead to a decreased NADPH/$NADP^+$ ratio, thereby interfering with the NADPH-dependent reduction of SoxR and causing an increased level of oxidized, active SoxR; or (iv) the redox-cycling drug might be directly reduced by the SoxR-reducing system(s) of the cell, thereby inhibiting SoxR reduction and causing increased levels of oxidized, active SoxR. It is also possible that several of these mechanisms contribute to the activation of SoxR by paraquat and menadione.

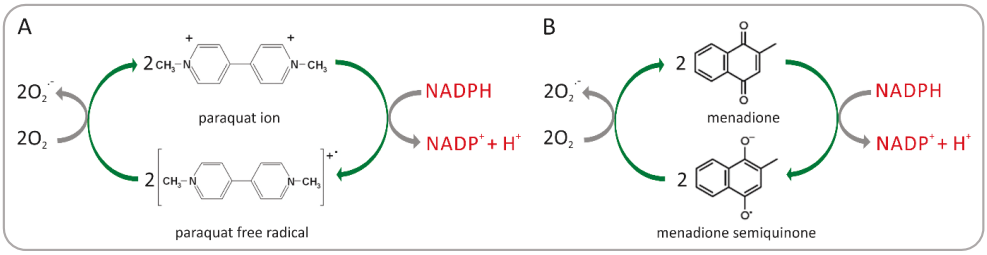

Fig. 4. Redox-cycle of the redox-cycling drugs paraquat (A) and menadione (B). The two redox-cycling drugs mediate the transfer of electrons from NADPH to oxygen, leading to the generation of superoxide.

1.3. The NADPH biosensor pSenSox and its applications

The TF-based NADPH biosensor is encoded by the plasmid pSenSox (Fig. 5A) and takes advantage of the NADPH-responsiveness of the SoxRS system of *E. coli*. The biosensor coding region of pSenSox consists of the *soxR* gene, the SoxR target promoter P_{soxS}, a small part of the *soxS* coding region (63 bp) followed by a stop codon, and the reporter gene *eyfp* (Fig. 5B). Hence, the SoxR-activated *soxS* promoter controls the expression of the *eyfp* gene, allowing detection of SoxR activation at the single cell level by monitoring the intensity of eYFP fluorescence (Siedler et al., 2014). Fluorescence can be measured, for instance, with a FACSAria cell sorter, a BioLector microcultivation system, or a microplate reader. The biosensor responds to NADPH changes, because the enzymatic reduction and inactivation of oxidized SoxR is NADPH-dependent. An increased cellular NADPH demand impairs SoxR reduction and leads to an increased *eyfp* expression (Siedler et al., 2014).

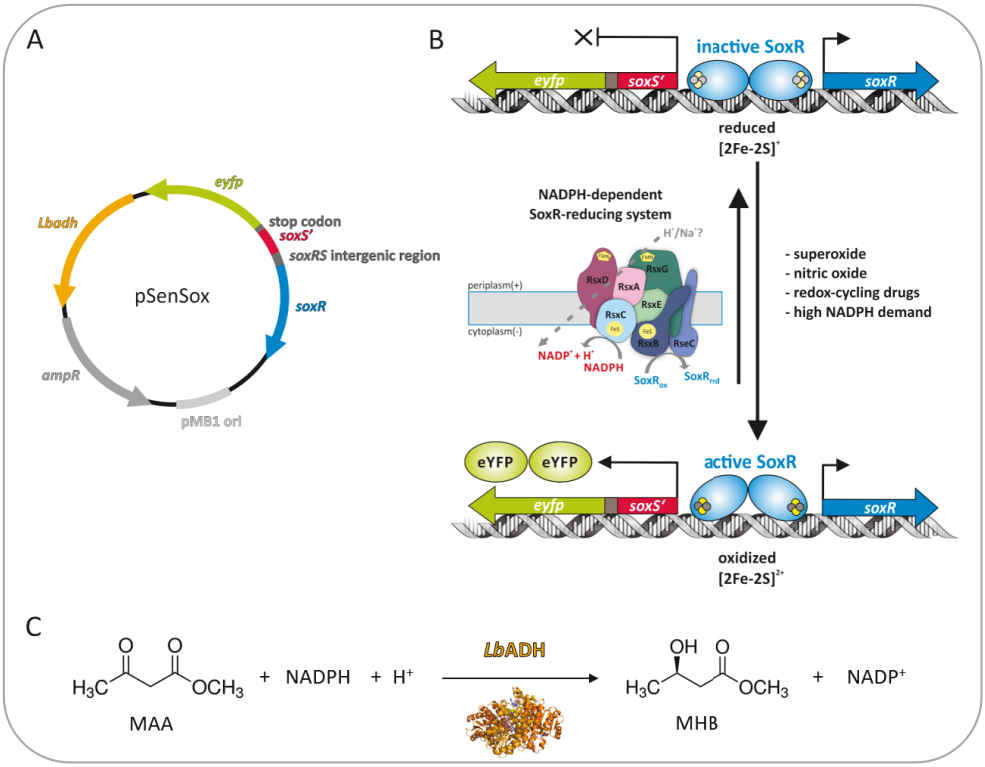

Fig. 5. (A) Scheme of the NADPH biosensor plasmid pSenSox carrying the NADPH biosensor coding region and the *Lbadh* gene. (B) The functional principle of the biosensor: the NADPH biosensor consists of the transcription factor SoxR and its target promoter P_{soxS}, which is fused to the reporter gene *eyfp*. Dimeric SoxR binds to the *soxRS* intergenic region and its activity is controlled by the redox state of its iron-sulfur cluster: in the reduced state it is inactive and there is no *eyfp* expression. In the oxidized state SoxR is active and triggers *eyfp* expression. The sensor responds to changes of the NADPH level because the enzymatic reduction and inactivation of oxidized SoxR is NADPH dependent. An increased cellular NADPH demand impairs SoxR reduction and leads to SoxR activation causing eYFP production. (C) NADPH-dependent reduction of MAA to MHB catalyzed by the *Lb*ADH.

Besides the biosensor, pSenSox carries the gene for the strictly NADPH-dependent alcohol dehydrogenase of *Lactobacillus brevis* (*Lb*ADH) (Fig. 5A). The biosensor response was studied during the reductive whole-cell biotransformation of methyl acetoacetate (MAA) to *R*-methyl 3-hydroxybutyrate (MHB) by the *Lb*ADH (Fig. 5C) using *E. coli* cells carrying pSenSox, and it was found that the cells became fluorescent (Siedler et al., 2014). More specifically, it was shown that the specific eYFP fluorescence of the *E. coli* cells correlated not only with the MAA concentration added to the cells, but also with the specific *Lb*ADH activity when a fixed MAA concentration was provided (Siedler et al., 2014). Due to the latter property, one promising application of the NADPH biosensor is the FACS-based screening of large strain libraries

containing numerous variants of NADPH-dependent enzymes for improved variants. A proof of concept approach led to the identification of one *Lb*ADH variant with a slightly increased activity but reduced affinity for the substrate 4-methyl-2-pentanone (Siedler et al., 2014).

1.4. The (*R*)-specific alcohol dehydrogenase of *Lactobacillus brevis*

The *Lb*ADH is a biotechnologically interesting alcohol dehydrogenase that catalyzes the enantioselective reduction of prochiral ketones into the corresponding, mostly (*R*)-configured secondary alcohols (Rodríguez et al., 2014) (Fig. 6).

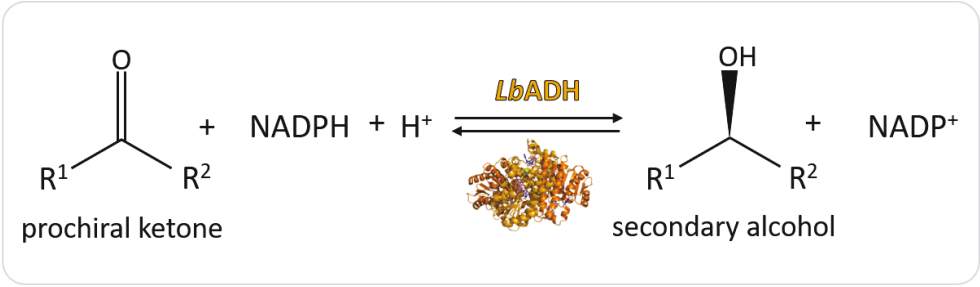

Fig. 6. Reaction scheme for the reduction of prochiral ketones to the corresponding secondary alcohols catalyzed by the (*R*)-specific alcohol dehydrogenase *Lb*ADH using NADPH as cofactor.

The *Lb*ADH is an attractive candidate for biocatalytic transformations, because it is a highly robust and versatile catalyst featuring high regio-and stereoselectivity, a broad substrate range, and the ability to convert sterically demanding substrates (Leuchs and Greiner, 2011). Its preferred *in vitro* substrates are prochiral ketones such as acetophenone with almost invariably a small methyl group as one substituent and a bulky moiety (often aromatic, such as phenyl) as the other (Schlieben et al., 2005). The efficiency of substrate conversion is influenced by, apart from the substrate size, the steric and electronic effects of the used substrate, and the thermodynamic stability of the products (Rodríguez et al., 2014).

The *Lb*ADH is active as a homotetramer with 251 amino acid residues and a molecular mass of 26.6 kDa per subunit (Riebel, 1997; Niefind et al., 2003). It is a short-chain Mg^{2+}-dependent reductase that uses the cofactor NADPH as reducing agent. The crystal structure of the wild-type (wt) *Lb*ADH was solved (Niefind et al., 2003; Schlieben et al., 2005) (Fig. 7). Modelling studies provided the structural basis of its substrate and cosubstrate specificity, as well as an explanation of the enantiospecificity, and the Mg^{2+} dependency of this biocatalyst (Niefind et

al., 2003; Schlieben et al., 2005). It was found that the residues Asn113, Ser142, Tyr155, and Lys159 are involved in the catalytic mechanism. Moreover, the homotetramer contains two Mg^{2+} binding sites and four active centers (one per subunit) (Niefind et al., 2003). Each Mg^{2+} stabilizes the quaternary structure. Their removal, however, does not disrupt the homotetrameric assembly, but fully inactivates the enzyme (Niefind et al., 2003). The non-covalently bound cofactor NADPH is essential for catalysis and has to be recycled efficiently to make the biotransformation economically feasible (Leuchs and Greiner, 2011; Döbber et al., 2018).

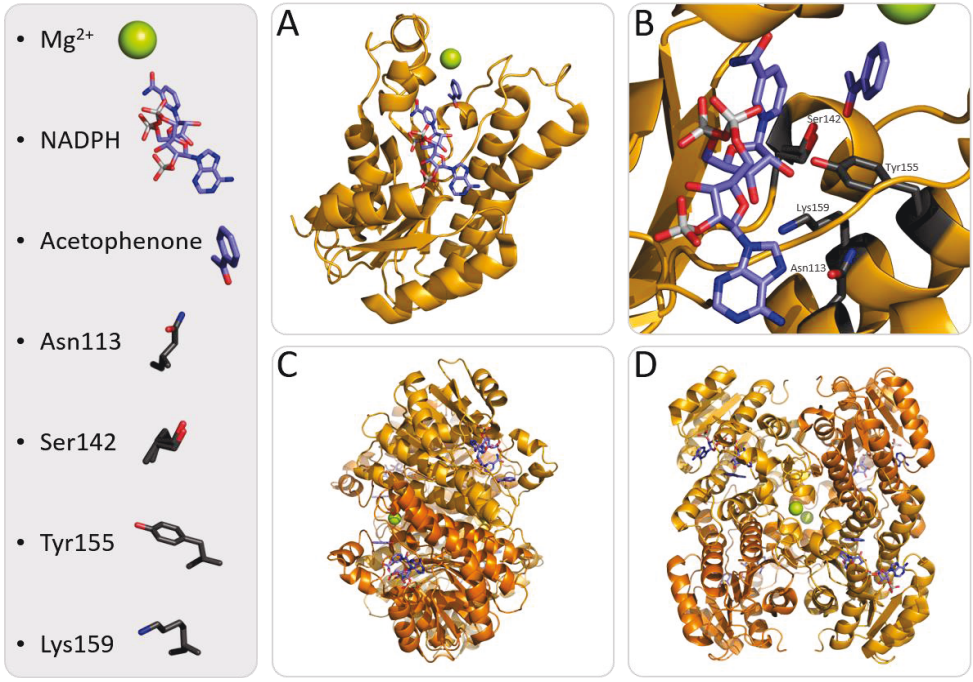

Fig. 7. Crystal structure of the wild-type *Lb*ADH monomer (A), the active center (B) and the homotetramer (C and D) in complex with the substrate acetophenone, the cofactor NADPH and Mg^{2+}. Acetophenone and NADPH are shown as violet sticks. The Mg^{2+} ions are shown as light green spheres. The residues Asn113, Ser142, Tyr155, Lys159 involved in the catalytic mechanism are shown as sticks in grey. The images were generated with the software PyMOL 2.2.0 (PDB code 1ZK4).

1.5. The transhydrogenases of *E. coli*

Transhydrogenases catalyze the reversible interconversion of NADH and NADPH. *E. coli* possesses two transhydrogenases, the membrane-bound, proton-translocating transhydrogenase PntAB and the soluble, energy-independent transhydrogenase SthA (also called UdhA) (Sauer et al., 2004). PntAB is used to produce NADPH from NADH and $NADP^+$

using an electrochemical proton gradient as driving force (Sauer et al., 2004; Kabus et al., 2007), while SthA is mainly involved in NADH production from NADPH (Sauer et al., 2004; Auriol et al., 2011). With these two enzymes, *E. coli* can compensate for imbalances between catabolic NADPH production and anabolic NADPH consumption.

1.6. Economically feasible biotransformations to produce chiral alcohols

Chiral alcohols with high enantiomeric purity are important intermediates for the synthesis of optically active fine chemicals that are, among others, used to produce pharmaceuticals and agrochemicals (Ager et al., 1996; Liese et al., 2001; Breuer et al., 2004). Because of the high chemo-, regio- and enantioselectivities commonly displayed by enzymes, their use as biocatalysts, both in isolated form and in whole-cell systems, for the production of chiral building blocks is of interest. Apart from highly selective reactions, biocatalytic reductions can offer environmentally and economically attractive processes, making the use of biotechnological applications a real alternative to traditional chemical synthesis routes (Munoz Solano et al., 2012; Ni and Xu, 2012). Alcohol dehydrogenases (ADHs) are used for the synthesis of chiral alcohols under very mild reaction conditions due to their high catalytic efficiency and selectivity (Hall and Bommarius, 2011; Zheng et al., 2017). Therefore, the improvement of these enzymes for *in vivo* and *in vitro* applications is of major interest, especially the optimization of specificity, catalytic activity, and the enlargement of the substrate spectrum (Hall and Bommarius, 2011).

1.7. Strategies to find improved enzyme variants

Two classical methods are usually used to isolate improved enzymes: rational protein design and directed evolution through random or semi-rational mutagenesis (Bornscheuer and Pohl, 2001). However, both methods have limits. Purely rational approaches are restricted by the lack of understanding of how protein structure relates to enzyme function. One of the most challenging parts of directed evolution is the identification of improved variants from mutant libraries (Leemhuis et al., 2009). Typically, screenings of mutant libraries involve dedicated assays for a certain substrate or product (Bloch, 2006), as the majority of molecules of interest do not have an easily observable phenotype (Bott, 2015).

In recent years, transcription factor (TF)-based biosensors have been established as a robust method for the identification of productive mutations both within whole genomes or specific enzymes (Bott, 2015; Eggeling et al., 2015; Mahr and Frunzke, 2016). One major advantage of TF-based biosensors with fluorescent reporter genes is that these systems can be used for fluorescence activated cell sorting (FACS) allowing high-throughput screening for promising candidates (Binder et al., 2012; Binder et al., 2013).

1.8. Aims of this thesis

The SoxR-based NADPH biosensor pSenSox was applied in two ways. Firstly, the biosensor was used to study the influence of various conditions on SoxR activity in *E. coli*, including different cultivation media, redox-cycling drugs, mutants lacking known SoxR reductases (RsxABCDGE and RseC), and mutants deficient in the transhydrogenases SthA and PntAB. For these studies the biosensor output was typically recorded during the reductive biotransformation of MAA to MHB by the *Lb*ADH (Fig. 5C).

Secondly, the biosensor pSenSox was used to identify variants of *Lb*ADH with improved activity for the substrate 2,5-hexanedione. This included the construction of a sufficiently large library of *Lb*ADH variants created by random mutagenesis followed by high-throughput FACS screening to isolate clones of the library that showed increased fluorescence during the biotransformation of 2,5-hexanedione. Finally, an *Lb*ADH purification procedure had to be established for *in vitro* enzyme characterization.

1.9. Key results

1.9.1. NADPH-related processes studied with a SoxR-based biosensor in *E. coli*

In the first part of this thesis, the influence of (i) different cultivation media, (ii) redox-cycling drugs, (iii) the lack of known SoxR reductases (RsxABCDGE and RseC), and (iv) the lack of the transhydrogenases SthA and PntAB on SoxR activity were tested using the NADPH biosensor pSenSox. The results have been published in the manuscript entitled “NADPH-related processes studied with a SoxR-based biosensor in *Escherichia coli*” in MicrobiologyOpen (DOI: 10.1002/mbo3.785) (cf. chapter 2.1).

1.9.1.1. The influence of different media on the NADPH biosensor response

To evaluate the influence of different media on the response of the pSenSox-based NADPH biosensor, the biotransformation of MAA to MHB catalyzed by the NADPH-dependent *Lb*ADH (Fig. 5C) was performed with *E. coli*/pSenSox cells in three complex media (TB, 2xTY, or LB) and in a defined minimal medium (M9) with glucose as carbon source. The experiments with the different media included negative controls such as cultures in which MAA was omitted or in which the plasmid pSenNeg, encoding a defective *Lb*ADH, was used. The biotransformation was performed with cells that were cultivated in a BioLector microcultivation system which allows for online recording of eYFP fluorescence (excitation at 485 nm, emission at 520 nm) and biomass gain (change in cell density measured as backscattered light at 620 nm).

Regarding the NADPH biosensor response, it was observed that the specific eYFP fluorescence of the cultures, which corresponds to the ratio of absolute fluorescence over backscatter, increased during reduction of MAA to MHB in all tested media. However, the presence of MAA had a negative influence on growth, even in the absence of *Lb*ADH, and this negative influence was further enhanced in the presence of *Lb*ADH activity, presumably due to NADPH consumption for MAA reduction to MHB. In the absence of either MAA or *Lb*ADH activity, eYFP synthesis was not induced. When comparing the different media with respect to biomass gain after the addition of MAA, the highest cell density was reached in TB medium, followed by 2xTY and LB medium, in which the biomass gain was comparable, and M9-glucose medium, in which almost no further biomass gain occurred. The highest specific fluorescence was obtained in 2xTY medium and LB medium, whereas it was much lower and comparable for TB and M9-glucose medium.

In conclusion, 2xTY and LB media led to a higher biosensor response than media containing an added carbohydrate, such as TB and M9-glucose medium. However, M9-glucose medium can in principle be used to monitor the SoxR-based NADPH biosensor response, which can be necessary or advantageous for experiments in which components of yeast extract or tryptone are disturbing. Overall, the strongest biosensor signal was observed in 2xTY medium, which was therefore chosen for the following experiments with the biosensor.

1.9.1.2. The influence of redox-cycling drugs on the NADPH biosensor response

Redox-cycling drugs such as paraquat and menadione have been reported to induce the *soxRS* response in *E. coli* (cf. chapter 1.2.4). To examine whether the SoxR-based NADPH biosensor responds to the redox-cycling drugs as expected, *E. coli*/pSenSox cells were exposed to different paraquat concentrations (0 µM, 1 µM, 5 µM) and different menadione concentrations (0 µM, 5 µM, 10 µM). The biomass gain and the eYFP fluorescence were monitored in a BioLector after the addition of the redox-cycling drugs to the cultures.

At the concentrations used, both compounds had only minor effects on growth, but clearly triggered a concentration-dependent activation of the SoxR-based biosensor response. These results confirm the strong responsiveness of the SoxR system to paraquat and menadione. Higher concentrations of paraquat (0.01-10 mM) and menadione (15-50 µM) were tested, but did not lead to further increased fluorescence. In conclusion, these experiments are in accordance with the general view that redox-cycling drugs activate the SoxR response (Greenberg et al., 1990; Wu and Weiss, 1991; Seo et al., 2015).

1.9.1.3. The influence of *rseC* and *rsxABCDGE* deletion on the NADPH biosensor response

The RsxABCDGE (Rsx) complex and the protein RseC constitute a membrane-bound SoxR-reducing system, involved in keeping the SoxR iron-sulfur clusters in a reduced state, rendering SoxR transcriptionally inactive (Koo et al., 2003) (cf. chapter 1.2.3). This SoxR-reducing system is supposed to modify the redox state of SoxR in an NADPH-dependent manner (Koo et al., 2003). Due to the suggested NADPH-dependency of the reducing system, the influence of the Rsx and RseC proteins on the SoxR-based NADPH biosensor response was examined using deletion mutants.

Using *E. coli* BL21(DE3) as parent strain, a Δ*rseC* mutant, a Δ*rsx* mutant, and a Δ*rseC*Δ*rsx* double mutant were constructed and analyzed regarding growth and biosensor response. In shake flask experiments with 2xTY medium, all deletion mutants and the parental strain exhibited the same growth behavior, showing that under these conditions RseC and the Rsx complex are dispensable. The changes in fluorescence of the Δ*rseC*, Δ*rsx*, and Δ*rseC*Δ*rsx* mutants carrying pSenSox were studied (i) during the NADPH-dependent biotransformation of MAA to MHB by the *Lb*ADH and (ii) in the presence of the redox-cycling drug paraquat. All deletion mutants showed an increased fluorescence signal compared to the parental strain

both in the presence of MAA and paraquat. The most intense fluorescence signal was recorded in the Δ*rseC* mutant, followed by the Δ*rseC*Δ*rsx* mutant and the Δ*rsx* mutant.

To confirm that the observed effects on the biosensor signal were due to the gene deletions, complementation experiments were performed in the presence of MAA. This required the construction of the plasmids pACYC-*rseC*, pACYC-*rsx*, and pACYC-*rseC*-*rsx*, which were introduced in addition to the plasmid pSenSox into the corresponding deletion mutants. The parental plasmid pACYCDuet-1, which is a T7-based multicopy plasmid carrying an IPTG-inducible promoter, was used as negative control. Already the basal expression of *rseC* and/or *rsx* in the respective deletion mutants without addition of IPTG resulted in decreased biosensor signals compared to the ones obtained in the mutants carrying the control plasmid pACYCDuet-1. However, the complementation was incomplete, because the intensity of the fluorescence signal in the complementation strains was still higher than in the parental strain. Although complementation was only partial, which could be due to an inadequate expression level of the plasmid-encoded genes, it confirmed that the *rseC* and *rsx* deletions were responsible for the increased biosensor response in the mutants.

These results support previously published data stating that RseC and the Rsx complex are involved in SoxR reduction (Koo et al., 2003). An interesting observation made by Koo and coworkers as well as in this study, was that the deletion of both *rseC* and the *rsx* cluster had no additive effect and expression of the reporter gene was even to some extent lower in the Δ*rseC*Δ*rsx* mutant than in the Δ*rseC* single mutant. This leads to the assumption that RseC and the Rsx complex do not function independently but work together to keep SoxR in its reduced state, as proposed previously (Koo et al., 2003). It is also worth mentioning that the Δ*rseC*Δ*rsx* double mutant did not show the highest fluorescence signal among the deletion mutants. The intensity of the biosensor signal in the double mutant suggests that complete deletion of the SoxR-reducing system does not lead to a complete loss of the ability to reduce SoxR. Hence, it could be concluded that apart from the SoxR-reducing system further ways of keeping SoxR in its inactive, reduced state might exist. Moreover, when paraquat was used to induce the NADPH biosensor response, the fluorescence signal was also increased in all mutants compared to the parental strain. The Δ*rseC* mutant showed the highest specific fluorescence followed by the Δ*rseC*Δ*rsx* mutant and the Δ*rsx* mutant. The observation that paraquat and *rsx* and/or *rseC* deletion showed an additive effect on the biosensor response confirms that a fraction of SoxR must still be in the reduced state in the mutants and suggests that paraquat-

based activation of SoxR is not due to interference with SoxR reduction by the Rsx/RseC system.

All in all, this study confirmed that the lack of *rsx* and *rseC* leads to the activation of the pSenSox-based response and therefore supports the previous results obtained by Koo et al., (2003).

1.9.1.4. The influence of the transhydrogenase deletions Δ*pntAB*, Δ*sthA* and Δ*sthA*Δ*pntAB* on the NADPH biosensor response

The transhydrogenases SthA and PntAB of *E. coli* are involved in NADPH metabolism (cf. chapter 1.5). PntAB produces NADPH from NADH and $NADP^+$ using the electrochemical proton gradient as driving force (Sauer et al., 2004), while SthA is mainly involved in NADH production from NADPH (Sauer et al., 2004; Auriol et al., 2011). Due to the relevance of the transhydrogenases in the regulation of cellular NADPH levels, the influence of these enzymes on the NADPH biosensor response was examined using deletion mutants of *E. coli* BL21(DE3) lacking either *sthA*, or *pntAB*, or both.

The growth behavior of the transhydrogenase mutants was tested in shake flask experiments using 2xTY medium. The parental strain *E. coli* BL21(DE3) and the Δ*pntAB* mutant had the same growth behavior, whereas the Δ*sthA* mutant and the Δ*sthA*Δ*pntAB* double mutant showed a growth defect that became apparent during the exponential growth phase. Presumably, an excess of NADPH is formed in this growth phase, which cannot be readily diminished in the absence of SthA. The defect could be largely abolished by plasmid-based expression of *sthA*, confirming that it was caused by the *sthA* deletion.

The influence of SthA and PntAB on the NADPH biosensor signal was analyzed by monitoring the sensor signal in the constructed mutants during the NADPH-dependent biotransformation of MAA by the *Lb*ADH. The Δ*pntAB* mutant showed a slightly increased biosensor signal. The Δ*sthA* mutant and the Δ*sthA*Δ*pntAB* double mutant displayed a decreased biosensor signal by more than 60%. The decreased fluorescence signal in the Δ*sthA*Δ*pntAB* double mutant showed that the effect of *sthA* deletion was dominant over *pntAB* deletion. To confirm that the observed effects were due to the gene deletions, the plasmids pACYC-*pntAB* and pACYC-*sthA* were constructed and introduced into the corresponding deletion mutants in addition to the biosensor plasmid pSenSox. The NADPH biosensor signal in the complementation strains was also measured during the reduction of

MAA by the *Lb*ADH. The parent vector pACYCDuet-1 served as control. Plasmid-based expression of *pntAB* in the Δ*pntAB* mutant completely prevented the increase in the biosensor signal and even reduced it to a small extent. Vice versa, plasmid-based expression of *sthA* in the Δ*sthA* mutant completely prevented the decrease in the sensor response and even increased it.

The increased NADPH biosensor signal in the Δ*pntAB* mutant compared to the parental strain suggests that PntAB catalyzes $NADP^+$ reduction by NADH, resulting in an increased NADPH availability. Hence, the absence of *pntAB* leads to a decrease in NADPH production from NADH and $NADP^+$ and thus an increased biosensor signal. These results support previous studies stating that PntAB is involved in NADPH formation in *E. coli* (Sauer et al., 2004). For instance, overexpression of *pntAB* enhanced conversion of acetophenone to (*R*)-phenylethanol by the NADPH-dependent alcohol dehydrogenase of *Lactobacillus kefir* (Weckbecker and Hummel, 2004) and improved the biosynthesis of 3-hydroxypropionic acid from its precursor malonyl-CoA by an NADPH-dependent malonyl-CoA reductase (Rathnasingh et al., 2012). Moreover, heterologous overexpression of the *E. coli pntAB* genes in *Corynebacterium glutamicum* was shown to enhance production of L-lysine, whose biosynthesis is strongly NADPH-dependent (Kabus et al., 2007). Contrary to PntAB, the results obtained with the Δ*sthA* mutant indicate that SthA catalyzes NADPH oxidation. Thus, the deletion of *sthA* results in an increased NADPH availability, which is reflected by a decreased biosensor signal. These data are in agreement with previous studies showing that SthA is required under conditions leading to excess NADPH formation (Sauer et al., 2004). The decreased fluorescence signal in the Δ*sthA*Δ*pntAB* double mutant suggests that SthA activity is much higher than PntAB activity, which can be expected based on the fact that PntAB catalyzes a reaction coupled to proton transfer across the membrane.

In conclusion, it was shown that PntAB and SthA play an important role in NADPH metabolism and exhibit opposite functions for the NADPH availability in *E. coli*.

1.9.2. Optimization of the NADPH-dependent *Lb*ADH using pSenSox

In the second part of this thesis, the biosensor pSenSox was used for FACS-based screening to find an improved variant of the NADPH-dependent alcohol dehydrogenase *Lb*ADH for the substrate 2,5-hexanedione. FACS is a powerful high-throughput tool for the screening of large libraries containing fluorescent reporter genes to monitor changes in gene expression

(Dietrich et al., 2010). FACS could be applied for the screening of an *Lb*ADH library because of the previous observation that an increased fluorescence of the *E. coli* cells carrying pSenSox variants correlated with higher specific *Lb*ADH activity when a fixed substrate concentration was provided (Siedler et al., 2014).

Prior to FACS screening, a library of *Lb*ADH variants was generated by error-prone PCR (ep-PCR) and cloned into the biosensor plasmid pSenSox replacing the native *Lbadh* gene. The final library was estimated to consist of 1.4×10^6 clones. At first the FACS screening process of the generated *Lb*ADH library comprised three enrichments steps followed by one negative selection step. Subsequently, a final sort on the library was performed with FACS after biotransformation of 2,5-hexanedione. *E. coli* cells carrying the wild-type *Lb*ADH and *E. coli* cells carrying an inactive *Lb*ADH were used as references for electronic gating. After biotransformation, cells carrying more active *Lb*ADH variants should be more fluorescent. Thus, for the last screening step, the sorting gate was set to include variants showing increased fluorescence compared to cells expressing the wild-type *Lb*ADH^{WT}, which enhances the chances for identifying improved variants. In the final sorting step, 2.5×10^5 cells of the library were analyzed and 240 cells falling into the set gate were isolated and spotted on agar plates. Out of the 240 sorted cells, 83 (35%) formed colonies after incubation.

To confirm the increased fluorescence of the isolated clones, single colonies were cultivated in a BioLector microcultivation system, which enables online monitoring of eYFP fluorescence. 65 of the 83 tested clones showed the same fluorescence pattern: all 65 clones displayed a higher fluorescence with similar intensity compared to the fluorescence level of the strain expressing the native *Lbadh* gene in the presence and absence of the substrate 2,5-hexanedione. 12 further clones showed a higher fluorescence than the *E. coli* TOP10/pSenSox strain in the presence and absence of the substrate 2,5-hexanedione, but the fluorescence level was much lower compared to the 65 clones. Six clones showed the same fluorescence level as the *E. coli* TOP10/pSenSox. The plasmids of four of the 65 strains showing higher fluorescence than the *E. coli* TOP10/pSenSox culture were isolated and sequenced to identify mutations. All four clones carried a single G→A transition in the *Lbadh* gene resulting in the amino acid exchange of lysine-71 to glutamic acid, indicating that the used selection approach strongly favored this mutation.

To characterize and compare the *Lb*ADH^{K71E} variant with the wild-type *Lb*ADH^{WT}, both enzymes were successfully produced in *E. coli* C43(DE3), purified with an N-terminal Strep-tag

by affinity chromatography and subsequent gel filtration, and analyzed by SDS-PAGE. The two proteins showed an identical elution profile in the affinity chromatography, but in the size-exclusion chromatography *Lb*ADH^{K71E} eluted slightly before *Lb*ADH^{WT}. Analysis of the purified proteins by SDS-PAGE revealed that *Lb*ADH^{K71E} migrates slower on the gel than *Lb*ADH^{WT}. The slightly different elution profiles of *Lb*ADH^{K71E} and *Lb*ADH^{WT} in the size-exclusion chromatography support a structural change caused by the K71E mutation, whereas SDS-PAGE suggests that the mutation K71E changed the electrostatic properties of the enzyme.

The purified enzymes were used in spectrophotometric enzyme assays to estimate the Michaelis constant (K_M) and the activity (v_{max}) for the substrate 2,5-hexanedione. The kinetic measurements revealed that *Lb*ADH^{K71E} had a 16% higher affinity (K_M= 4.3 ± 0.5 mM) and a 17% higher activity (V_{max}= 173.3 ± 11.1 µmol min^{-1} mg^{-1}) compared to the original enzyme (K_M= 5.1 ± 0.6 mM; V_{max}= 148.5 ± 12.3 µmol min^{-1} mg^{-1}) with 2,5-hexanedione as substrate.

Interestingly, according to the crystal structure of the *Lb*ADH (Niefind et al., 2003; Schlieben et al., 2005), the residue at position 71 is not an active site residue but is located on the surface of the protein and is solvent exposed. Hence, the mutation K71E resulted in a charge reversal on the protein surface. Due to its location, residue K71 seems not to be directly involved in substrate binding. It was assumed that the improved activity of the *Lb*ADH^{K71E} variant might not be limited to the substrate 2,5-hexanedione, which was originally used for FACS screening. Therefore, the kinetic measurements were also performed with other substrates that are known to be reduced by the *Lb*ADH, and it was found that the *Lb*ADH^{K71E} variant had also an increased activity towards the substrates acetophenone, 2-acetylpyridine, 2-hexanone, 4-hydroxy-2-butanone, and methyl acetoacetate. The activity increased 33% for 5 mM acetophenone, 21% for 10 mM 2-acetylpyridine, 22% for 10 mM 2-hexanone, 39% for 10 mM 4-hydroxy-2-butanone, and 46% for 12.5 mM MAA. In addition to that, the K_M and v_{max} values were determined for the substrate MAA. The K_M of the *Lb*ADH^{K71E} decreased by 41% (K_M *Lb*ADH^{WT}: 1.13 ± 0.06 mM, K_M *Lb*ADH^{K71E}: 0.67 ± 0.04 mM) and v_{max} increased by 43% compared to the *Lb*ADH^{WT} (v_{max} *Lb*ADH^{WT}: 154.2 ± 2.2 µmol min^{-1} mg^{-1}, v_{max} *Lb*ADH^{K71E}: 221.2 ± 3.3 µmol min^{-1} mg^{-1}), indicating that the mutant has also a higher affinity and a higher activity for MAA. Obviously, the charge reversal K71E on the surface of *Lb*ADH led to a more active enzyme variant.

In conclusion, the identification of the improved variant *Lb*ADH^{K71E} provides further evidence that random mutagenesis in combination with a high-throughput screening

approach is a powerful tool for the identification of improved enzyme variants not predictable by rational enzyme design.

1.10. Conclusions and outlook

Siedler et al. (2014) constructed the NADPH biosensor pSenSox and introduced it as a useful tool for FACS-based high-throughput screening of libraries of NADPH-dependent enzymes that are of interest in white biotechnology. The results obtained in this thesis broaden the application field of pSenSox by demonstrating that it is a useful tool to study NADPH-related processes in *E. coli*, such as the effect of the transhydrogenases PntAB and SthA. The function of the transhydrogenases has been examined in several studies. However, this is the first study with an NADPH biosensor that confirmed the involvement of PntAB in $NADP^+$ reduction and of SthA in NADPH oxidation. Due to the fact that the biosensor is based on the SoxRS system of *E. coli*, it allows to specifically analyze SoxR activation and enzymes that are involved in SoxR reduction or oxidation. Using the well-studied response of the SoxRS system to redox-cycling drugs, the applicability of the biosensor for analyzing SoxR-related processes could be shown. Moreover, the studies performed in this thesis on the SoxR-reducing system (RsxABCDGE and RseC) represent the first confirmation of the initial results by Koo et al. (2003) and indicate that an alternative system for SoxR reduction should be present in *E. coli*.

For studies that involve monitoring of changes in NADPH more precisely, NADPH sensing proteins can be used as alternative to the TF-based biosensor pSenSox. Recently, another NADPH biosensor was described, which is based on the specific oxygen-independent amplification of the intrinsic fluorescence of NADPH by the mBFP protein (Goldbeck et al., 2018). The mBFP protein was shown to be well suited to study the dynamics of intracellular NADPH availability with a resolution of seconds and to allow the quantitation of NADPH (Goldbeck et al., 2018). The pSenSox biosensor is not suitable to monitor dynamic responses, because it depends on transcription, translation, and oxygen-dependent maturation of eYFP. However, it allows to preserve changed NADPH levels as a stable fluorescence signal, which is a prerequisite, for instance, for FACS-based screening of mutant libraries of NADPH-dependent enzymes. Siedler et al. (2014) demonstrated this potential by the rapid isolation of an *Lb*ADH variant *via* FACS with a slightly increased activity but reduced affinity for the substrate 4-methyl-2-pentanone. In this study the biosensor was successfully used in combination with FACS for the identification of the improved variant *Lb*ADH^{K71E}, showing

increased activity and affinity for several known *Lb*ADH substrates. This provides further proof that using the biosensor combined with a suitable screening approach is useful for the identification of unexpected, promising mutations, which could not have been found with rational protein design.

Taken together, the SoxR-based biosensor proved to be useful for studying NADPH- and SoxR-related processes. It does not allow to quantify NADPH and to study the dynamics of intracellular NADPH availability, but these features can be overcome with the mBFP-based NADPH biosensor. The SoxR-based biosensor reveals its full potential in the FACS-based high-throughput screening of NADPH-dependent enzyme libraries. The FACS-based screening approach depends on the use of viable *E. coli*/pSenSox cells that can express the NADPH-dependent enzyme and perform the NADPH-dependent reaction in the cytoplasm. Thus, important requirements for the substrates and products are that they can enter the biosensor-forming cells and are not toxic to the cells. If this is the case, further high-throughput screenings of randomly mutagenized libraries of NADPH-dependent enzymes might unveil interesting, unforeseen enzyme variants that are attractive for industrial application.

2. Published and submitted publications

2.1. NADPH-related processes studied with a SoxR-based biosensor in *Escherichia coli*

Alina Spielmann, Meike Baumgart, Michael Bott*

IBG-1: Biotechnology, Institute of Bio- and Geosciences, Forschungszentrum Jülich, Jülich, Germany

*Corresponding author

Current state: published in the journal MicrobiologyOpen

Author's contributions:

MBo, MBa, and AS designed the study. AS performed all experiments, wrote the initial version of the manuscript, and prepared the figures. MBa revised the initial version of the manuscript. MBo revised the manuscript and prepared the final published version.

Overall contribution AS: 80%

Received: 4 November 2018 | Revised: 22 November 2018 | Accepted: 23 November 2018
DOI: 10.1002/mbo3.785

ORIGINAL ARTICLE

WILEY MicrobiologyOpen Open Access

NADPH-related processes studied with a SoxR-based biosensor in *Escherichia coli*

Alina Spielmann | Meike Baumgart | Michael Bott

IBG-1: Biotechnology, Institute of Bio- and Geosciences, Forschungszentrum Jülich, Jülich, Germany

Correspondence
Michael Bott, IBG-1: Biotechnology, Institute of Bio- and Geosciences, Forschungszentrum Jülich, Jülich, Germany.
Email: m.bott@fz-juelich.de

Funding information
Bundesministerium für Bildung und Forschung, Grant/Award Number: 031A095B

Abstract

NADPH plays a crucial role in cellular metabolism for biosynthesis and oxidative stress responses. We previously developed the genetically encoded NADPH biosensor pSenSox based on the transcriptional regulator SoxR of *Escherichia coli*, its target promoter P_{soxS} and eYFP as fluorescent reporter. Here, we used pSenSox to study the influence of various parameters on the sensor output in *E. coli* during reductive biotransformation of methyl acetoacetate (MAA) to (*R*)-methyl 3-hydroxybutyrate (MHB) by the strictly NADPH-dependent alcohol dehydrogenase of *Lactobacillus brevis* (*Lb*Adh). Redox-cycling drugs such as paraquat and menadione strongly activated the NADPH biosensor and mechanisms responsible for this effect are discussed. Absence of the RsxABCDGE complex and/or RseC caused an enhanced biosensor response, supporting a function as SoxR-reducing system. Absence of the membrane-bound transhydrogenase PntAB caused an increased biosensor response, whereas the lack of the soluble transhydrogenase SthA or of SthA and PntAB was associated with a strongly decreased response. These data support the opposing functions of PntAB in $NADP^+$ reduction and of SthA in NADPH oxidation. In summary, the NADPH biosensor pSenSox proved to be a useful tool to study NADPH-related processes in *E. coli*.

KEYWORDS
NADPH biosensor, RseC, RsxABCDGE complex, transhydrogenases PntAB and SthA

1 | INTRODUCTION

Genetically encoded biosensors based on transcriptional regulators (TRs) and using fluorescent proteins as reporters are highly useful tools for monitoring physiological responses at the single-cell level and for enabling high-throughput screening in strain and enzyme development (Dietrich, McKee, & Keasling, 2010; Eggeling, Bott, & Marienhagen, 2015; Mahr & Frunzke, 2016; Rogers, Taylor, & Church, 2016). In recent years, we developed TR-based biosensors for amino acids and used them, for example, to identify novel mutations for overproduction of L-lysine, L-arginine, and L-histidine by FACS-based screening of genome-wide, gene-specific, and codon-specific mutant libraries (Binder et al., 2012; Binder, Siedler, Marienhagen, Bott, & Eggeling, 2013; Schendzielorz et al., 2014) or for increasing L-valine production by adaptive laboratory evolution (Mahr et al., 2015).

Besides the sensors for amino acids, we also established a TR-based biosensor responding to the intracellular availability of NADPH (Siedler et al., 2014). It is based on the SoxRS regulatory system of *Escherichia coli*, which governs the expression of oxidative stress response genes by a regulatory cascade, in which synthesis of SoxS depends on transcriptional activation of *soxS* expression by SoxR (Greenberg, Monach, Chou, Josephy, & Demple, 1990; Tsaneva & Weiss, 1990). In the genome, the *soxR* gene is located

divergently to the *soxS* gene. Whereas initial studies indicated that the promoter of *soxR* is located within the *soxS* coding region (Wu & Weiss, 1991), a subsequent analysis revealed that the promoters of the two genes overlap (Hidalgo, Leautaud, & Demple, 1998). The transcription factor SoxR is a homodimer with each subunit containing an [2Fe-2S] cluster (Hidalgo & Demple, 1994; Watanabe, Kita, Kobayashi, & Miki, 2008). SoxR activity is controlled by a change of the redox state of its [2Fe−2S] clusters, which is associated with conformational changes: only in the oxidized $[2Fe{-}2S]^{2+}$ state, but not in the reduced $[2Fe{-}2S]^{+}$ state, SoxR activates *soxS* expression (Ding, Hidalgo, & Demple, 1996; Gaudu & Weiss, 1996). SoxR binds to its target site, which is located between the −10 and −35 regions of the *soxS* promoter and downstream of the −10 region of the *soxR* promoter, both in the oxidized and in the reduced state with high affinity (Gaudu & Weiss, 1996; Hidalgo & Demple, 1994). Besides activating *soxS* expression in the oxidized state, SoxR simultaneously represses expression of its own gene, both in the oxidized and the reduced state (Hidalgo et al., 1998). SoxR was previously considered to activate expression of *soxS* only, but recent studies uncovered further direct SoxR target genes (Seo, Kim, Szubin, & Palsson, 2015).

SoxS functions as a transcriptional activator of genes, many but not all of which are responsible for coping with damage caused by oxygen radicals, such as *sodA* for superoxide dismutase, *zwf* for the NADPH-generating glucose 6-phosphate dehydrogenase, or *fumC* for fumarase C (Blanchard, Wholey, Conlon, & Pomposiello, 2007; Seo et al., 2015). It has been shown that the intrinsic instability of SoxS ($t_{1/2}$ ~ 2 min) and the degradation of SoxS, primarily through the Lon protease, are responsible for the rapid return of the SoxRS system to the inactive state when the stimuli activating the system are no longer present (Griffith, Shah, & Wolf, 2004).

Current evidence indicates that there are multiple ways how the conversion of inactive, reduced SoxR into active, oxidized SoxR can be triggered. These include direct oxidation of SoxR by superoxide (Fujikawa, Kobayashi, & Kozawa, 2012; Liochev & Fridovich, 2011) and by redox-cycling drugs (Gu & Imlay, 2011), nitrosylation of SoxR (Ding & Demple, 2000), and conditions leading to a diminished $NADPH/NADP^{+}$ ratio within cells (Krapp, Humbert, & Carrillo, 2011; Liochev & Fridovich, 1992). The responsiveness to the NADPH availability is presumably due to the fact that SoxR is subject to permanent autoxidation under aerobic conditions, but is kept in the reduced state by NADPH-dependent reductases (Koo et al., 2003).

In a previous study, we made use of the NADPH-responsiveness of the SoxRS system to construct the biosensor pSenSox, in which the SoxR-activated *soxS* promoter controls expression of the *eyfp* gene, allowing detection of SoxR activation at the single-cell level (Siedler et al., 2014). Using the reduction of methyl acetoacetate (MAA) to (*R*)-methyl 3-hydroxybutyrate (MHB) by the strictly NADPH-dependent alcohol dehydrogenase of *Lactobacillus brevis* (*Lb*Adh) as model reaction, we could show that the specific eYFP fluorescence of *E. coli* cells correlated not only with the MAA concentration added to the cells, but also with the specific *Lb*Adh activity when a fixed MAA concentration was provided. The latter property enabled high-throughput screening of an *Lb*Adh mutant library by fluorescence-activated cell sorting (FACS) for variants with improved activity for the alternative substrate 4-methyl-2-pentanone (Siedler et al., 2014).

In this study, we employed pSenSox to test various conditions, including growth media, redox-cycling drugs, mutants lacking SoxR reductases, and mutants lacking transhydrogenases for their influence on SoxR activity.

2 | RESULTS AND DISCUSSION

2.1 | Influence of different media on the NADPH biosensor response

To test the influence of different media on the response of the pSenSox-based NADPH biosensor, the biotransformation of MAA to MHB, catalyzed by the NADPH-dependent *Lb*Adh, was performed in three complex media (TB, 2xTY, or LB) and in a defined minimal medium (M9) with glucose as carbon source using the experimental setup shown in Figure 1 and as described in the methods section. The experiments with the different media, including control cultures in which MAA was omitted or in which pSenNeg, encoding a defective *Lb*Adh, was used, are shown in Figure 2. MAA itself had a negative influence on growth, even in the absence of *Lb*Adh, and this negative influence was further enhanced in the presence of *Lb*Adh activity, when MAA was reduced to MHB with NADPH as reductant. Regarding the response of the SoxRS-based NADPH biosensor, the experiments shown in Figure 2 confirmed that expression of the *eyfp* gene is dependent on the biotransformation of MAA to MHB by the *Lb*Adh. In the absence of either MAA or *Lb*Adh activity, eYFP synthesis was not induced.

When comparing the different media, it became obvious that TB allowed by far the best growth, followed by 2xTY and LB medium, in which the cells grew comparably, and M9 glucose medium, in which almost no growth occurred (Figure A1). When comparing the different media with respect to eYFP synthesis, the highest fluorescence after 24 hr was obtained in 2xTY medium and LB medium, whereas it was much lower and comparable for TB and M9-glucose medium (Figure A1). The almost complete lack of growth in M9-glucose was due to the biotransformation of MAA to MHB, as growth was observed in the absence of MAA or of *Lb*Adh activity (Figure 2). In this medium, cells have to synthesize all cellular components, in particular amino acids, from glucose, whereas in the other media the presence of yeast extract and tryptone provides amino acids and other cellular components that do not need to be synthesized by the cell but can be imported from the medium. Nevertheless, also in these media the NADPH-dependent reduction of MAA to MHB had a strong negative effect on growth, presumably due to a lack of NADPH for biosynthetic purposes. An interesting case is TB medium. Although this medium allowed the best growth, the biosensor response was much lower compared to 2xTY or LB and similar to that in M9-glucose medium. Besides a higher concentration of yeast extract and phosphate buffering, the major difference of TB medium to 2xTY and LB is the presence of glycerol as additional carbon source.

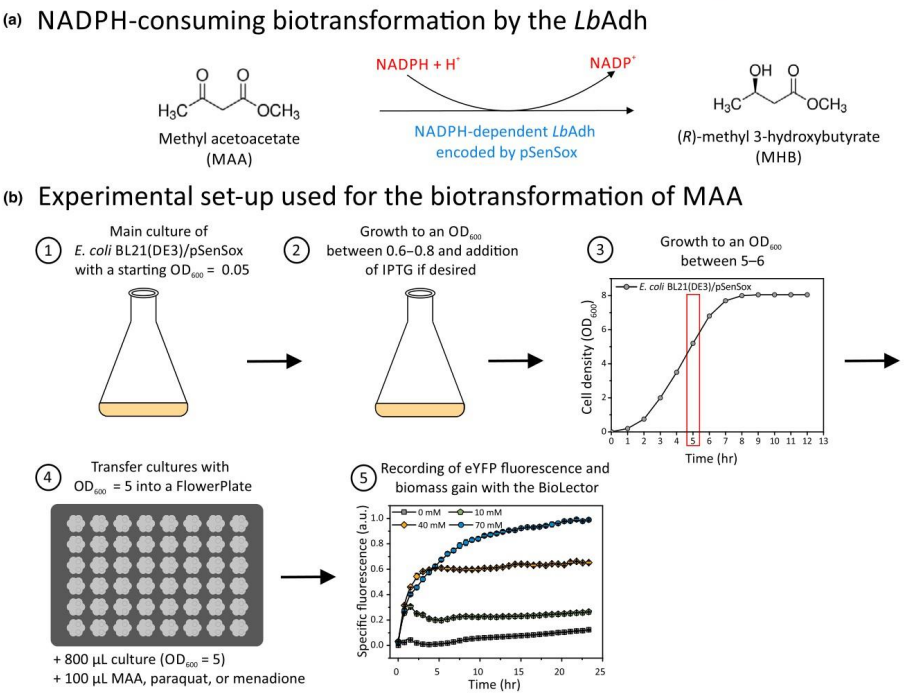

FIGURE 1 (a) NADPH-dependent reduction of MAA to MHB by the *Lb*Adh. (b) Experimental setup used in this work to study the responses of the SoxR-based NADPH biosensor encoded by plasmid pSenSox during whole-cell biotransformation of MAA to MHB. (1) *Escherichia coli* BL21(DE3) carrying pSenSox was cultivated in shake flasks with a starting OD_{600} of 0.05. (2) If desired, IPTG was added to the cultures at an OD_{600} between 0.6 and 0.8. In the absence of IPTG, basal expression of the *Lbadh* gene by the *tac* promoter is sufficient for *Lb*Adh synthesis and biotransformation of MAA to MHB. However, IPTG can be added to maximize *Lbadh* expression. (3) To ensure that enough biomass is formed for the biotransformation, the cultures were grown for at least 5 hr until an OD_{600} of 5 or higher was reached. (4) For the biotransformation, 800 µl of the culture with an OD_{600} adjusted to 5 were transferred into a Flowerplate (m2p-labs, Baesweiler, Germany) and the biotransformation was started by the addition of 100 µl MAA at the desired concentration to these cultures. To study the effect of redox-cycling drugs, either 100 µl paraquat or 100 µl menadione were added to the cultures at the desired concentration. (5) The change in eYFP fluorescence and biomass was monitored for around 24 hr with a BioLector microcultivation system that enables online recording of eYFP fluorescence (excitation at 485 nm, emission at 520 nm) and biomass gain (change in cell density measured as backscattered light at 620 nm (Kensy, Zang, Faulhammer, Tan, & Büchs, 2009). The specific fluorescence over the time course of 24 hr corresponds to the ratio of absolute fluorescence/backscatter

In conclusion, media without a separately added carbohydrate as carbon source, such as 2xTY and LB, led to a higher biosensor response than media containing an added carbohydrate, such as M9-glucose or TB, which contains 4 ml/L glycerol. This is probably due to a higher NADPH availability by carbohydrate catabolism. M9 glucose medium can in principle be used to monitor the SoxR-based NADPH biosensor response, which can be necessary or advantageous for experiments in which components of yeast extract or tryptone are disturbing. Overall, the strongest biosensor signal was observed in 2xTY medium, which was therefore chosen for the following experiments.

2.2 | Influence of redox-cycling drugs on the NADPH biosensor response

Paraquat (1,1′-dimethyl-4,4′-bipyridinium dichloride) and menadione (2-methyl-1,4-naphthoquinone) have been reported to induce the *soxRS* regulon in *E. coli* (Greenberg et al., 1990; Seo et al., 2015; Wu & Weiss, 1991). We therefore monitored the response of *E. coli* BL21(DE3)/pSenSox to different paraquat concentrations (0, 1, 5 µM) and different menadione concentrations (0, 5, 10 µM) using the experimental setup shown in Figure 1, except that paraquat and menadione were added instead of MAA. At the

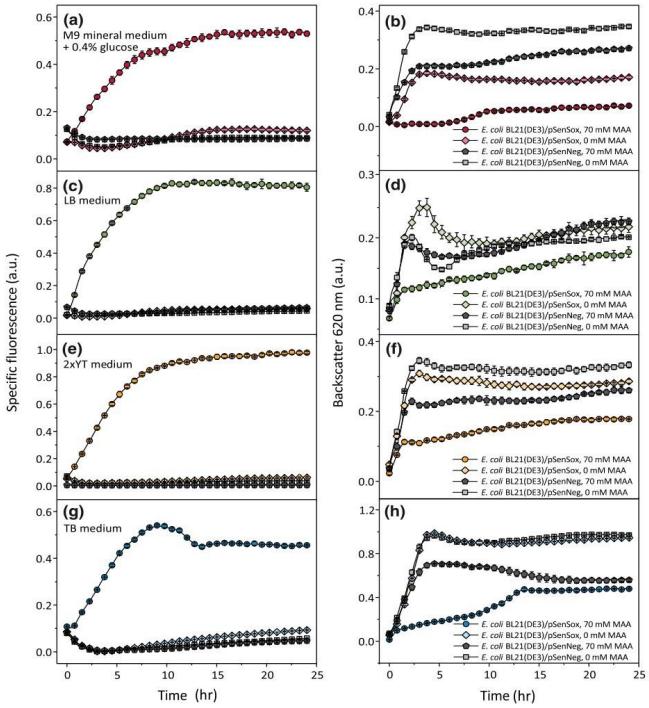

FIGURE 2 Influence of different media on the NADPH biosensor response during biotransformation of MAA to MHB using the experimental setup shown in Figure 1. The changes in fluorescence and biomass were followed during the biotransformation of MAA to MHB by the NADPH-dependent alcohol dehydrogenase of *Lactobacillus brevis* (*Lb*Adh) using *Escherichia coli* BL21(DE3)/pSenSox and *E. coli* BL21(DE3)/pSenNeg cultures cultivated either in M9 mineral medium supplemented with 0.4% (w/v) glucose (a and b), or in LB medium (c and d), or in 2xTY medium (e and f), or in TB medium (g and h). Mean values and standard deviations of three independent biological replicates are shown. The values were normalized to the maximal backscatter value measured in TB medium and to the maximal specific fluorescence measured in 2xYT medium, which were set as 1.0

concentrations used, both compounds had only minor effects on growth (data not shown), but clearly triggered a concentration-dependent activation of the SoxRS-based biosensor response (Figure 3). These results confirm the strong responsiveness of the SoxRS system to paraquat and menadione. Higher concentrations of paraquat (0.01, 0.1, 1, 5, 10 mM) and menadione (15, 20, 25, 50 μM) were tested, but did not lead to further increased fluorescence (data not shown). Addition of up to 5 mM H_2O_2 did not elicit a SoxR response (data not shown).

Paraquat and menadione are redox-cycling drugs, which mediate the transfer of electrons from NADPH to oxygen, leading to the continuous generation of superoxide (Kappus & Sies, 1981). Several possibilities exist how redox-cycling drugs activate the SoxRS response: (a) the superoxide radical has been shown to directly oxidize the [2Fe-2S] cluster of SoxR (Fujikawa et al., 2012), thus forming active SoxR; (b) the redox-cycling drug might directly interact with reduced SoxR and oxidize it, leading to active SoxR (Gu & Imlay, 2011); (c) the reduction of the redox-cycling agent by NADPH might

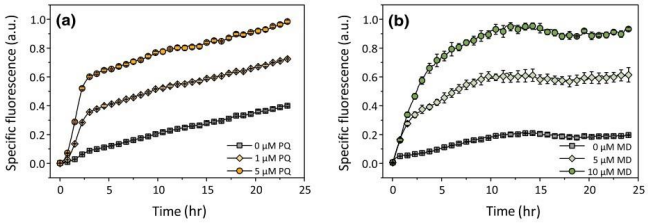

FIGURE 3 Influence of different concentrations of the redox-cycling drugs paraquat (PQ) and menadione (MD) on the NADPH biosensor response using *Escherichia coli*/pSenSox. The changes in fluorescence were followed after the addition of either PQ (a) or MD (b) over a time period of 24 hr. The experimental setup shown in Figure 1 was used for all cultivations in 2xTY medium containing 100 μg/ml carbenicillin. No MAA was added in these experiments. Mean values and standard deviations of three independent biological replicates are shown

lead to a decreased NADPH/NADP$^+$ ratio, thereby interfering with the NADPH-dependent reduction of SoxR and causing an increased level of oxidized, active SoxR; (d) the redox-cycling drugs might be directly reduced by the SoxR-reducing system(s) of the cell, thereby inhibiting SoxR reduction and causing increased levels of oxidized active SoxR. It is possible that several of these mechanisms contribute to the activation of SoxR by paraquat and menadione.

2.3 | Influence of *rseC* and *rsxABCDGE* deletion on the NADPH biosensor response

By screening an *E. coli* mutant library, mutations in the *rseC* gene and in the *rsxABCDGE* operon were found to cause constitutive expression of a P_{soxS}-*lacZ* reporter gene in a SoxR-dependent manner (Koo et al., 2003). Further studies led to the conclusion that the membrane-integral RsxABCDGE complex and the membrane protein RseC constitute a SoxR-reducing system (Koo et al., 2003). The statement that purified RsxC exhibits NADPH-dependent cytochrome *c* reduction activity (Koo et al., 2003) suggests that NADPH serves as electron donor of the Rsx complex. To test the influence of this reducing system on the NADPH biosensor response, we constructed deletion mutants of *E. coli* BL21(DE3) lacking either *rseC* (Δ*rseC*), or *rsxABCDGE* (Δ*rsx*), or all of these genes (Δ*rseC*Δ*rsx*).

When monitoring the growth behavior of the deletion mutants and the parental strain in shake flask experiments with 2xTY medium, all strains exhibited the same growth behavior, showing that under these conditions RseC and the Rsx complex are dispensable (Figure A2). The influence of Δ*rseC*, Δ*rsx*, and Δ*rseC*Δ*rsx* mutations on the NADPH biosensor signal was analyzed according to the standard experimental setup shown in Figure 1 with 30 mM MAA as substrate for the NADPH-dependent *Lb*Adh. As shown in Figure 4, all deletion mutants showed an increased fluorescence signal compared to the parental strain, with the strongest response in the Δ*rseC* mutant, followed by the Δ*rseC*Δ*rsx* mutant and the Δ*rsx* mutant.

To confirm that the observed effects were due to the gene deletions, plasmids pACYC-*rseC*, pACYC-*rsx*, and pACYC-*rseC-rsx* were constructed and transferred into the corresponding deletion mutants. The parent vector pACYCDuet-1 served as control. Basal expression of *rseC* and/or *rsxABCDGE* in the respective deletion mutants without addition of IPTG resulted in decreased biosensor signals compared to the ones obtained in the mutants carrying the control plasmid pACYCDuet-1, but the response was still higher than in the parental strain (Figure A3). Although complementation was only partial, which could be due to an inadequate expression level of the plasmid-encoded genes, it confirmed that the *rseC* and *rsx* deletions were responsible for the increased biosensor response.

The results described above are in agreement with previous data showing a function of RsxABCDGE and RseC in SoxR reduction (Koo et al., 2003). An interesting observation made by Koo and coworkers and by us was that the deletion of both *rseC* and the *rsx* cluster had no additive effect and expression of the reporter gene was even somewhat lower in the Δ*rseC*Δ*rsx* mutant than in the Δ*rseC* single mutant. This indicates that the Rsx complex and RseC do not function independently to reduce SoxR, but work together, as proposed previously (Koo et al., 2003). The RsxABCDGE complex belongs to the family of Rnf complexes, enzymes that drive the endergonic reduction of ferredoxin ($E_0{}' = -420$ mV) with NAD(P)H ($E_0{}' = -320$ mV) by the proton- or sodium-motive force via import of H^+ or Na^+, or, in the reverse reaction, the exergonic reduction of NAD(P)$^+$ with reduced ferredoxin coupled to the export of H^+ or Na^+ (Biegel, Schmidt, Gonzalez, & Müller, 2011). The redox potential of SoxR in its DNA-free and its DNA-bound state was reported to be −293 and −320 mV (Kobayashi, Fujikawa, & Kozawa, 2015), respectively, that is, in the same range as the one of NAD(P)H. Consumption of proton- or sodium-motive force via the Rsx complex to drive reduction of SoxR by NADPH allows the cell to keep most SoxR in the reduced state in the absence of inducing conditions. In fact, it was reported that in wild-type cells overproducing SoxR almost all

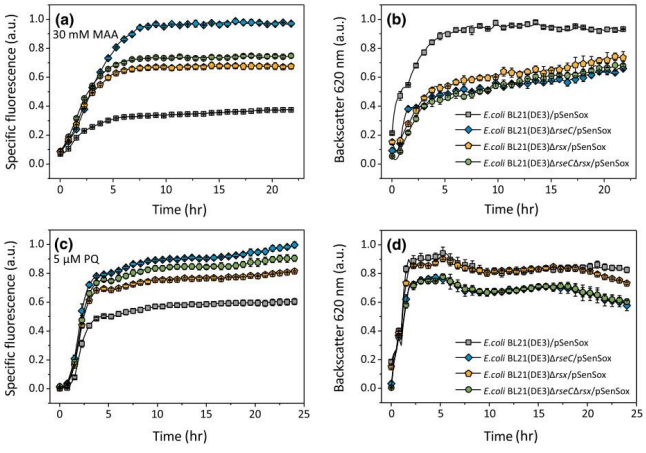

FIGURE 4 Comparison of the NADPH biosensor response (a, c) and cell density (b, d) of *Escherichia coli* BL21(DE3) and its Δ*rseC*, Δ*rsx*, and Δ*rseC*Δ*rsx* mutants during biotransformation of 30 mM MAA to MHB (panels a and b) using the standard experimental setup shown in Figure 1, and in the presence of 5 µM paraquat instead of MAA (panels c and d). Mean values and standard deviations of three independent biological replicates are shown

of the protein was present in the reduced state, but in *rsxC* and *rseC* mutants only about 60% and 56% (Koo et al., 2003). The final steps of electron transfer to SoxR are unknown at present. In the Rnf complexes, RnfB is suggested as electron donor for ferredoxin (Biegel et al., 2011). Therefore, the homologous RsxB protein could serve to reduce SoxR, or alternatively, RseC might transfer electrons from RsxB to SoxR, as a conserved cysteine motif in the N-terminal region of RseC could be part of an iron-sulfur cluster. Further studies are required to solve this issue. The observation that in *rsxC* and *rseC* mutants still about 60% and 56% of SoxR was in the reduced state (Koo et al., 2003) suggests that further enzymes for SoxR reduction exist, which need to be identified.

We also tested the response of the *rsx* and *rseC* mutants in the presence of 5 μM paraquat instead of MAA. Although the parental strain already showed a strong response to paraquat, that of the mutants was still further increased. Again, the *ΔrseC* mutant showed the highest specific fluorescence followed by the *ΔrseCΔrsx* mutant and the *ΔrsxABCDGE* mutant (Figure 4c,d). The observation that paraquat and *rsx* and/or *rseC* deletion showed an additive effect on the biosensor response confirms that a fraction of SoxR must still be in the reduced state in the mutants and suggests that paraquat-based activation of SoxR is not due to interference with SoxR reduction by the Rsx/RseC system.

2.4 | Influence of the transhydrogenase deletions *ΔpntAB*, *ΔsthA*, and *ΔsthAΔpntAB* on the NADPH biosensor response

Transhydrogenases catalyze the reversible interconversion of NADH and NADPH. *E. coli* possesses two transhydrogenases, the membrane-bound, proton-translocating transhydrogenase PntAB and the soluble, energy-independent transhydrogenase SthA (also called UdhA; Sauer, Canonaco, Heri, Perrenoud, & Fischer, 2004). Due to the relevance of transhydrogenases in the regulation of cellular NADPH levels, we studied the influence of these enzymes on the NADPH biosensor response by constructing deletion mutants of *E. coli* BL21(DE3) lacking either *sthA*, or *pntAB*, or both.

The growth behavior of the transhydrogenase mutants was tested in shake flask experiments using 2xTY medium. Whereas the *ΔpntAB* mutant grew like the parental strain, the *ΔsthA* mutant and the *ΔsthAΔpntAB* double mutant showed a growth defect that became apparent during the exponential growth phase (Figure A4). Presumably, an excess of NADPH is formed in this growth phase, which cannot be readily diminished in the absence of SthA. The defect could be largely abolished by plasmid-based expression of *sthA* (Figure A5), confirming that it was caused by the *sthA* deletion.

The influence of SthA and PntAB on the NADPH biosensor signal was analyzed according to the standard experimental setup shown in Figure 1 with 30 mM MAA as substrate for the NADPH-dependent *Lb*Adh. Whereas the *ΔpntAB* mutant displayed a slightly increased biosensor signal, it was decreased by more than 60% in the *ΔsthA* mutant and also in the *ΔsthAΔpntAB* double mutant (Figure 5). The latter result showed that the *sthA* deletion was dominant over the *pntAB* deletion.

To confirm that the observed effects were due to the gene deletions, plasmids pACYC-*pntAB* and pACYC-*sthA* were constructed and transferred into the corresponding deletion mutants. The parent vector pACYCDuet-1 served as control. Plasmid-based expression of *pntAB* in the *ΔpntAB* mutant completely prevented the increase in the biosensor signal and even reduced it to a small extent. Vice versa, plasmid-based expression of *sthA* in the *ΔsthA* mutant completely prevented the decrease in the sensor response and even increased it (Figure A5). The presence of a second plasmid reduced the differences in the biosensor signal between the *ΔsthA* mutant and the parent strain, which might be due to a negative effect on the copy number of pSenSox and thus *Lb*Adh activity.

The results obtained with the *ΔpntAB* mutant indicate that, under the conditions used, PntAB catalyzes $NADP^+$ reduction by NADH, leading to an increased NADPH availability. Absence of *pntAB* therefore results in a lowered NADPH availability and thus an increased biosensor signal. This conclusion is in agreement with previous studies showing that PntAB is involved in NADPH formation in *E. coli* (Sauer et al., 2004) and that overexpression of *pntAB* enhanced conversion of acetophenone to (*R*)-phenylethanol by the NADPH-dependent alcohol dehydrogenase of *Lactobacillus kefir* (Weckbecker & Hummel, 2004) and improved the biosynthesis of 3-hydroxypropionic acid from its precursor malonyl-CoA by an NADPH-dependent malonyl-CoA reductase (Rathnasingh et al., 2012). Moreover, heterologous overexpression of the *E. coli pntAB* genes in *Corynebacterium glutamicum* was shown to enhance production of L-lysine, whose biosynthesis is strongly NADPH-dependent (Kabus, Georgi, Wendisch, & Bott, 2007).

In contrast to PntAB, our results obtained with the *ΔsthA* mutant indicate that under the conditions employed SthA catalyzes NADPH oxidation. Absence of *sthA* thus results in an increased NADPH

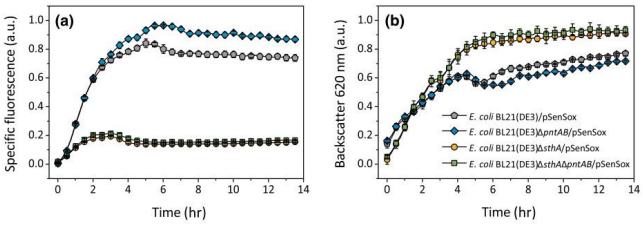

FIGURE 5 Comparison of the NADPH biosensor response (a) and cell density (b) of *Escherichia coli*/pSenSox and its *ΔpntAB*, *ΔsthA*, and *ΔsthAΔpntAB* mutants during biotransformation of MAA (30 mM) to MHB using the standard experimental setup shown in Figure 1. Mean values and standard deviations of three independent biological replicates are shown

availability, which is reflected by a decreased biosensor signal. These data are in agreement with previous studies showing that SthA is required under conditions leading to excess NADPH formation (Sauer et al., 2004). The observation that *pntAB* deletion in the Δ*sthA* mutant did not reverse the decrease in the biosensor signal suggests that SthA activity is much higher than PntAB activity, which can be expected based on the fact that PntAB catalyzes a reaction coupled to proton transfer across the membrane. In conclusion, our data confirm that PntAB and SthA play important and opposite functions for NADPH availability in *E. coli*.

2.5 | Concluding remarks

In this study, we employed the NADPH biosensor pSenSox to study various processes expected to influence the NADPH availability in *E. coli*. We could confirm that the lack of *rsxABCDGE* and *rseC* activated the pSenSox-based response. Paraquat and the Δ*rsx*/Δ*rseC* deletion had an additive effect on the sensor response, indicating that further SoxR-reducing systems exist besides Rsx/RseC and that the paraquat-induced response is presumably not due to interference of paraquat with SoxR reduction by Rsx/RseC. The transhydrogenases

TABLE 1 Bacterial strains and plasmids used in this study

Strain or plasmid	Relevant characteristics	Source or reference
Escherichia coli		
NEB5α	*fhuA2 Δ(argF-lacZ)U169 phoA glnV44 Φ80Δ (lacZ)M15 gyrA96 recA1 relA1 endA1 thi-1 hsdR17*; strain used for general cloning procedures	New England Biolabs
BL21(DE3)	F- *ompT hsdS*$_B$ (r_B^-, m_B^-) *gal dcm* (DE3); parent strain used in this study	Studier and Moffatt (1986)
BL21(DE3)Δ*rseC*	Derivative of BL21(DE3) with an in-frame deletion of *rseC*, locus-tag ECD_02464	This study
BL21(DE3)Δ*rsx*	Derivative of BL21(DE3) with an in-frame deletion of *rsxABCDGE*, locus-tag ECD_01597-ECD_01602	This study
BL21(DE3)Δ*rseC*Δ*rsx*	Derivative of BL21(DE3) with an in-frame deletion of *rseC* and *rsxABCDGE*, locus-tags *ECD_02464*, and *ECD_01597 - ECD_01602*	This study
BL21(DE3)Δ*sthA*	Derivative of BL21(DE3) with an in-frame deletion of Δ*sthA*, locus-tag ECD_03847	This study
BL21(DE3)Δ*pntAB*	Derivative of BL21(DE3) with an in-frame deletion of Δ*pntAB*, locus-tags ECD_01571 and ECD_01572	This study
BL21(DE3)Δ*sthA*Δ*pntAB*	Derivative of BL21(DE3) with an in-frame deletion of Δ*sthA* and Δ*pntAB*), locus-tags ECD_03847, ECD_01571 and ECD_01572	This study
Plasmids		
pSenSox	Amp^R; pBtac-*Lbadh* derivative containing the *soxRS*-based NADPH biosensor and the *Lactobacillus brevis adh* gene under control of the *tac* promoter	Siedler et al. (2014)
pSenNeg	Amp^R; pSenSox derivative with an incomplete Lb*adh* gene preventing synthesis of an active *Lb*Adh	Siedler et al. (2014)
pSIJ8	Amp^R; lambda Red-mediated gene replacement vector expressing lambda Red recombinase and flippase recombinase genes (pKD46, rhaRS-prha-FLP, amp)	Addgene; Jensen et al. (2015)
pKD4	Kan^R; template plasmid for FRT-flanked *kan* cassette needed for lambda Red-mediated gene replacement	Addgene; Datsenko and Wanner (2000)
pACYCDuet-1	Cm^R; vector for the coexpression of two target genes, each under the control of a separate T7 promoter and associated ribosomal binding site (p15A *ori*V_{ec}, 2(P_{T7}), *lacI*	Merck Millipore
pACYC-*rseC*	Cm^R; pACYCDuet-1-derivative for expression of *rseC* under the control of the T7 promoter	This study
pACYC-*rsx*	Cm^R; pACYCDuet-1-derivative for expression of *rsxABCDGE* under the control of the T7 promoter	This study
pACYC-rseC-rsx	Cm^R; pACYCDuet-1-derivative for expression of *rseC* and *rsxABCDGE* under the control of the T7 promoter	This study
pACYC-*sthA*	Cm^R; pACYCDuet-1-derivative for expression of *sthA* under the control of the T7 promoter	This study
pACYC-*pntAB*	Cm^R; pACYCDuet-1-derivative for expression of *pntAB* under the control of the T7 promoter	This study
pACYC-*sthA-pntAB*	Cm^R; pACYCDuet-1-derivative for expression of *sthA* and *pntAB* under the control of the T7 promoter	This study

PntAB and SthA had opposite effects on the biosensor response, in agreement with PntAB being involved in $NADP^+$ reduction and SthA catalyzing NADPH oxidation. In conclusion, the pSenSox-based NADPH biosensor is a useful tool not only for HT-screening of the activity of NADPH-dependent alcohol dehydrogenases (Siedler et al., 2014), but also for analyzing conditions and proteins influencing NADPH availability or SoxR reduction. Recently, another NADPH biosensor was described, which is based on the specific oxygen-independent amplification of the intrinsic fluorescence of NADPH by the mBFP protein (Hwang, Choi, Han, & Kim, 2012). The mBFP protein was shown to be well suited to study the dynamics of intracellular NADPH availability with a resolution of seconds and to allow the quantitation of NADPH (Goldbeck, Eck, & Seibold, 2018). This is not possible with the pSenSox NADPH biosensor, which requires transcription, translation, and oxygen-dependent maturation of eYFP. However, pSenSox allows to preserve changed NADPH levels as a stable fluorescence signal, which is a prerequisite, for example, for FACS-based screening of mutant libraries of NADPH-dependent enzymes, and it allows to specifically analyze the effects of enzymes that are involved in SoxR reduction or oxidation, which is presumably not possible with the mBFP sensor. Thus, mBFP and pSenSox represent two different types of NADPH biosensors, which both have their specific advantages and application fields.

3 | MATERIALS AND METHODS

3.1 | Bacterial strains, plasmids, and growth conditions

All strains and plasmids used in this work are listed in Table 1. *E. coli* BL21(DE3) (Invitrogen, Karlsruhe, Germany) and its derivatives were used for all studies with the NADPH biosensor. *E. coli* NEB5α was employed for cloning purposes. Transformation of *E. coli* cells was performed as described (Hanahan, 1983). Cells were cultivated at 30°C or 37°C in lysogeny broth (LB; Miller, 1972), in 2xTY (16 g/L tryptone, 10 g/L yeast extract, 5 g/L sodium chloride), in M9 mineral medium (33.7 mM $Na_2HPO_4 \times 2H_2O$, 22.0 mM KH_2PO_4, 8.55 mM NaCl, 9.35 mM NH_4Cl, 1 mM $MgSO_4 \times 7H_2O$, 0.3 mM $CaCl_2$, 1 µg/ml biotin, 1 µg/ml thiamin, trace elements) supplemented with 0.4% (w/v) glucose (Sambrook & Russell, 2001), or in terrific broth (TB) medium (12 g/L tryptone, 24 g/L yeast extract, 4 ml glycerol, 12.54 g/L K_2HPO_4, 2.31 g/L KH_2PO_4; pH 7.0). Plasmids were selected by adding antibiotics to the medium to a final concentration of 100 µg/ml carbenicillin, 34 µg/ml chloramphenicol, or 50 µg/ml kanamycin.

3.2 | Recombinant DNA work and construction of deletion mutants

Standard methods such as PCR and DNA restriction enzyme digestion were carried out according to established protocols (Sambrook & Russell, 2001). Oligonucleotides were synthesized by Eurofins Genomics (Ebersberg, Germany) and are listed in Table A1. Construction of pACYC-*rseC*, pACYC-*rsx*, pACYC-*rseC-rsx*, pACYC-*sthA*, and pACYC-*pntAB* was performed by Gibson assembly (Gibson et al., 2009). All plasmids were sequenced by Eurofins Genomics, Ebersberg, Germany. The construction of *E. coli* deletion mutants was performed with the lambda Red recombinase method (Datsenko & Wanner, 2000) using a recent protocol (Jensen, Lennen, Herrgard, & Nielsen, 2015). For the markerless deletion of genes, the arabinose-inducible lambda Red recombineering genes (*exo*, *bet*, and *gam*) and the rhamnose-inducible flippase (FLP) recombinase were introduced into *E. coli* BL21(DE3) using the temperature-sensitive plasmid pSIJ8 (Jensen et al., 2015). The FRT-flanked kanamycin cassette, which was integrated into the *E. coli* genome at the locus of the gene to be deleted, was encoded by plasmid pKD4. For amplification of the FRT-flanked kanamycin cassette of pKD4, oligonucleotides that carried homology regions to the up- and downstream regions of the genes to be deleted were used. All gene deletions were verified by colony PCR using DreamTaq Master Mix 2X (Thermo Scientific, Schwerte, Germany) and the oligonucleotides listed in Table A1.

3.3 | Monitoring the NADPH biosensor response

The NADPH biosensor response during the whole-cell biotransformation of MAA to MHB by the strictly NADPH-dependent *Lb*Adh was measured as described (Siedler et al., 2014). The specific fluorescence is defined as the ratio of fluorescence and backscatter. The biotransformations were performed with *E. coli* BL21(DE3) and its derivatives, such as deletion mutants lacking the genes coding for the SoxR-reducing system or transhydrogenases, and mutant strains carrying expression plasmids for the deleted genes. The *E. coli* BL21(DE3) cells were transformed either with plasmid pSenSox carrying the SoxR-based NADPH biosensor and an intact *Lb*Adh gene or with plasmid pSenNeg, in which a part of the *Lbadh* gene was deleted to prevent synthesis of an active *Lb*Adh (Siedler et al., 2014).

The experimental setup used for the biotransformation experiments is shown in Figure 1. Pre-cultures of three biological replicates of the desired strains were incubated overnight at 37°C and 130 rpm in 5 ml medium containing the appropriate antibiotic(s) as selection marker(s). These pre-cultures were used for the inoculation of the main cultures to an optical density at 600 nm (OD_{600}) of 0.05. The main cultures were grown in 50 ml medium in the presence of the appropriate antibiotics at 37°C and 130 rpm using 500 ml shake flasks. For complementation experiments, the cells were incubated at 30°C. Basal expression of *Lbadh* by the non-induced *tac* promoter allowed for sufficient *Lb*Adh activity in the biotransformation experiments (Siedler et al., 2014). When a higher *Lb*Adh activity was required, IPTG was added to a final concentration of 0.1 mM when the cultures had reached an OD_{600} between 0.6–0.8. To ensure that enough biomass is present for the biotransformation, the cultures were further incubated for at least 5 hr, until an OD_{600} of 5 or higher was reached. Then the cells were harvested by centrifugation (4°C, 4,713 *g* and 15 min) and resuspended in fresh medium supplemented with the corresponding antibiotic to a final OD_{600} of 5. About 800 µl of these

suspensions were transferred into 48-well microtiter Flowerplates (m2p-labs, Baesweiler, Germany). When analyzing the biosensor response under conditions of reductive biotransformation, 100 µl MAA dissolved in ddH_2O at the desired concentration was added to the 800 µl cultures or 100 µl ddH_2O as negative control. To study the effect of redox-cycling drugs and hydrogen peroxide on the biosensor response, the following additions were made to the 800 µl cultures in the Flowerplates: (a) 100 µl paraquat (1,1′-dimethyl-4,4′-bipyridinium dichloride; Sigma-Aldrich) dissolved in ddH_2O to final concentrations of 1 and 5 µM; (b) 100 µl menadione (2-methyl-1,4-naphthoquinone; Sigma-Aldrich) dissolved in DMSO to final concentrations of 5 and 10 µM; (c) 100 µl H_2O_2 to final concentrations of 0.05 or 5 mM. For the negative controls, 100 µl ddH_2O or 100 µl DMSO was added.

After the desired additions, the Flowerplates were incubated in a BioLector microcultivation system (m2p-laps; Baesweiler, Germany) at 30°C and 1,200 rpm (shaking diameter 3 mm), which allows online monitoring of cell density (as backscattered light at 620 nm) and of eYFP fluorescence (excitation wavelength 485 nm, emission wavelength of 520 nm). For the different experiments, the values were normalized to the maximal backscatter and the maximal specific fluorescence observed, which were set as 1.0.

ACKNOWLEDGEMENTS

This work was funded by the German Federal Ministry of Education and Research (BMBF), funding code 031A095B, as part of the project "Molecular Interaction Engineering: From Nature's Toolbox to Hybrid Technical Systems (MIE)".

CONFLICT OF INTEREST

The authors declare no conflict of interest.

AUTHORS CONTRIBUTION

A.S., M.Ba., and M.Bo. designed research; A.S. performed all experiments; A.S., M.Ba., and M.Bo. analyzed the data; A.S. prepared the figures; A.S., M.Ba., and M.Bo. wrote the manuscript.

ETHICS STATEMENT

None required.

DATA ACCESSIBILITY

All data are included in the article.

ORCID

Meike Baumgart https://orcid.org/0000-0002-9874-1151
Michael Bott https://orcid.org/0000-0002-4701-8254

REFERENCES

Biegel, E., Schmidt, S., Gonzalez, J. M., & Müller, V. (2011). Biochemistry, evolution and physiological function of the Rnf complex, a novel ion-motive electron transport complex in prokaryotes. *Cellular and Molecular Life Sciences*, *68*, 613–634. https://doi.org/10.1007/s00018-010-0555-8

Binder, S., Schendzielorz, G., Stäbler, N., Krumbach, K., Hoffmann, K., Bott, M., & Eggeling, L. (2012). A high-throughput approach to identify genomic variants of bacterial metabolite producers at the single-cell level. *Genome Biology*, *13*, R40. https://doi.org/10.1186/gb-2012-13-5-r40

Binder, S., Siedler, S., Marienhagen, J., Bott, M., & Eggeling, L. (2013). Recombineering in *Corynebacterium glutamicum* combined with optical nanosensors: A general strategy for fast producer strain generation. *Nucleic Acids Research*, *41*, 6360–6369. https://doi.org/10.1093/nar/gkt312

Blanchard, J. L., Wholey, W. Y., Conlon, E. M., & Pomposiello, P. J. (2007). Rapid changes in gene expression dynamics in response to superoxide reveal SoxRS-dependent and independent transcriptional networks. *PLoS ONE*, *2*, e1186. https://doi.org/10.1371/journal.pone.0001186

Datsenko, K. A., & Wanner, B. L. (2000). One-step inactivation of chromosomal genes in *Escherichia coli* K-12 using PCR products. *Proceedings of the National Academy of Sciences of the United States of America*, *97*, 6640–6645. https://doi.org/10.1073/pnas.120163297

Dietrich, J. A., McKee, A. E., & Keasling, J. D. (2010). High-throughput metabolic engineering: Advances in small-molecule screening and selection. *Annual Review of Biochemistry*, *79*, 563–590. https://doi.org/10.1146/annurev-biochem-062608-095938

Ding, H., & Demple, B. (2000). Direct nitric oxide signal transduction via nitrosylation of iron-sulfur centers in the SoxR transcription activator. *Proceedings of the National Academy of Sciences of the United States of America*, *97*, 5146–5150. https://doi.org/10.1073/pnas.97.10.5146

Ding, H., Hidalgo, E., & Demple, B. (1996). The redox state of the [2Fe-2S] clusters in SoxR protein regulates its activity as a transcription factor. *Journal of Biological Chemistry*, *271*, 33173–33175. https://doi.org/10.1074/jbc.271.52.33173

Eggeling, L., Bott, M., & Marienhagen, J. (2015). Novel screening methods-biosensors. *Current Opinion in Biotechnology*, *35*, 30–36. https://doi.org/10.1016/j.copbio.2014.12.021

Fujikawa, M., Kobayashi, K., & Kozawa, T. (2012). Direct oxidation of the [2Fe-2S] cluster in SoxR protein by superoxide: Distinct differential sensitivity to superoxide-mediated signal transduction. *Journal of Biological Chemistry*, *287*, 35702–35708. https://doi.org/10.1074/jbc.M112.395079

Gaudu, P., & Weiss, B. (1996). SoxR, a [2Fe-2S] transcription factor, is active only in its oxidized form. *Proceedings of the National Academy of Sciences of the United States of America*, *93*, 10094–10098. https://doi.org/10.1073/pnas.93.19.10094

Gibson, D. G., Young, L., Chuang, R. Y., Venter, J. C., Hutchison, C. A., & Smith, H. O. (2009). Enzymatic assembly of DNA molecules up to several hundred kilobases. *Nature Methods*, *6*, 343–345. https://doi.org/10.1038/nmeth.1318

Goldbeck, O., Eck, A. W., & Seibold, G. M. (2018). Real time monitoring of NADPH concentrations in *Corynebacterium glutamicum* and *Escherichia coli* via the genetically encoded sensor mBFP. *Frontiers in Microbiology*, *9*, 2564. https://doi.org/10.3389/fmicb.2018.02564

Greenberg, J. T., Monach, P., Chou, J. H., Josephy, P. D., & Demple, B. (1990). Positive control of a global antioxidant defense regulon activated by superoxide-generating agents in *Escherichia coli*. *Proceedings of the National Academy of Sciences of the United States of America*, *87*, 6181–6185. https://doi.org/10.1073/pnas.87.16.6181

Griffith, K. L., Shah, I. M., & Wolf, R. E. Jr (2004). Proteolytic degradation of *Escherichia coli* transcription activators SoxS and

MarA as the mechanism for reversing the induction of the superoxide (SoxRS) and multiple antibiotic resistance (Mar) regulons. *Molecular Microbiology*, *51*, 1801–1816. https://doi.org/10.1046/j.1365-2958.2003.03952.x

Gu, M., & Imlay, J. A. (2011). The SoxRS response of *Escherichia coli* is directly activated by redox-cycling drugs rather than by superoxide. *Molecular Microbiology*, *79*, 1136–1150. https://doi.org/10.1111/j.1365-2958.2010.07520.x

Hanahan, D. (1983). Studies on transformation of *Escherichia coli* with plasmids. *Journal of Molecular Biology*, *166*, 557–580. https://doi.org/10.1016/S0022-2836(83)80284-8

Hidalgo, E., & Demple, B. (1994). An iron-sulfur center essential for transcriptional activation by the redox-sensing SoxR protein. *EMBO Journal*, *13*, 138–146. https://doi.org/10.1002/j.1460-2075.1994.tb06243.x

Hidalgo, E., Leautaud, V., & Demple, B. (1998). The redox-regulated SoxR protein acts from a single DNA site as a repressor and an allosteric activator. *EMBO Journal*, *17*, 2629–2636. https://doi.org/10.1093/emboj/17.9.2629

Hwang, C. S., Choi, E. S., Han, S. S., & Kim, G. J. (2012). Screening of a highly soluble and oxygen-independent blue fluorescent protein from metagenome. *Biochemical and Biophysical Research Communications*, *419*, 676–681. https://doi.org/10.1016/j.bbrc.2012.02.075

Jensen, S. I., Lennen, R. M., Herrgard, M. J., & Nielsen, A. T. (2015). Seven gene deletions in seven days: Fast generation of *Escherichia coli* strains tolerant to acetate and osmotic stress. *Scientific Reports*, *5*, 17874. https://doi.org/10.1038/srep17874

Kabus, A., Georgi, T., Wendisch, V. F., & Bott, M. (2007). Expression of the *Escherichia coli pntAB* genes encoding a membrane-bound transhydrogenase in *Corynebacterium glutamicum* improves L-lysine formation. *Applied Microbiology and Biotechnology*, *75*, 47–53. https://doi.org/10.1007/s00253-006-0804-9

Kappus, H., & Sies, H. (1981). Toxic drug effects associated with oxygen metabolism: Redox cycling and lipid peroxidation. *Experientia*, *37*, 1233–1241. https://doi.org/10.1007/BF01948335

Kensy, F., Zang, E., Faulhammer, C., Tan, R. K., & Büchs, J. (2009). Validation of a high-throughput fermentation system based on online monitoring of biomass and fluorescence in continuously shaken microtiter plates. *Microbial Cell Factories*, *8*, 31. https://doi.org/10.1186/1475-2859-8-31

Kobayashi, K., Fujikawa, M., & Kozawa, T. (2015). Binding of promoter DNA to SoxR protein decreases the reduction potential of the [2Fe-2S] cluster. *Biochemistry*, *54*, 334–339. https://doi.org/10.1021/bi500931w

Koo, M. S., Lee, J. H., Rah, S. Y., Yeo, W. S., Lee, J. W., Lee, K. L., … Roe, J. H. (2003). A reducing system of the superoxide sensor SoxR in *Escherichia coli*. *EMBO Journal*, *22*, 2614–2622. https://doi.org/10.1093/emboj/cdg252

Krapp, A. R., Humbert, M. V., & Carrillo, N. (2011). The *soxRS* response of *Escherichia coli* can be induced in the absence of oxidative stress and oxygen by modulation of NADPH content. *Microbiology*, *157*, 957–965. https://doi.org/10.1099/mic.0.039461-0

Liochev, S. I., & Fridovich, I. (1992). Fumarase C, the stable fumarase of *Escherichia coli*, is controlled by the *soxRS* regulon. *Proceedings of the National Academy of Sciences of the United States of America*, *89*, 5892–5896. https://doi.org/10.1073/pnas.89.13.5892

Liochev, S. I., & Fridovich, I. (2011). Is superoxide able to induce SoxRS? *Free Radical Biology and Medicine*, *50*, 1813. https://doi.org/10.1016/j.freeradbiomed.2011.03.029

Mahr, R., & Frunzke, J. (2016). Transcription factor-based biosensors in biotechnology: Current state and future prospects. *Applied Microbiology and Biotechnology*, *100*, 79–90. https://doi.org/10.1007/s00253-015-7090-3

Mahr, R., Gätgens, C., Gätgens, J., Polen, T., Kalinowski, J., & Frunzke, J. (2015). Biosensor-driven adaptive laboratory evolution of L-valine production in *Corynebacterium glutamicum*. *Metabolic Engineering*, *32*, 184–194. https://doi.org/10.1016/j.ymben.2015.09.017

Miller, J. H. (1972). *Experiments in molecular genetics*. Cold Spring Harbor, NY: Cold Spring Harbor Laboratory Press.

Rathnasingh, C., Raj, S. M., Lee, Y., Catherine, C., Ashok, S., & Park, S. (2012). Production of 3-hydroxypropionic acid via malonyl-CoA pathway using recombinant *Escherichia coli* strains. *Journal of Biotechnology*, *157*, 633–640. https://doi.org/10.1016/j.jbiotec.2011.06.008

Rogers, J. K., Taylor, N. D., & Church, G. M. (2016). Biosensor-based engineering of biosynthetic pathways. *Current Opinion in Biotechnology*, *42*, 84–91. https://doi.org/10.1016/j.copbio.2016.03.005

Sambrook, J., & Russell, D. (2001). *Molecular cloning. A laboratory manual*. Cold Spring Harbor, NY: Cold Spring Harbor Laboratory Press.

Sauer, U., Canonaco, F., Heri, S., Perrenoud, A., & Fischer, E. (2004). The soluble and membrane-bound transhydrogenases UdhA and PntAB have divergent functions in NADPH metabolism of *Escherichia coli*. *Journal of Biological Chemistry*, *279*, 6613–6639.

Schendzielorz, G., Dippong, M., Grünberger, A., Kohlheyer, D., Yoshida, A., Binder, S., … Eggeling, L. (2014). Taking control over control: Use of product sensing in single cells to remove flux control at key enzymes in biosynthesis pathways. *ACS Synthetic Biology*, *3*, 21–29. https://doi.org/10.1021/sb400059y

Seo, S. W., Kim, D., Szubin, R., & Palsson, B. O. (2015). Genome-wide reconstruction of OxyR and SoxRS transcriptional regulatory networks under oxidative Stress in *Escherichia coli* K-12 MG1655. *Cell Reports*, *12*, 1289–1299. https://doi.org/10.1016/j.celrep.2015.07.043

Siedler, S., Schendzielorz, G., Binder, S., Eggeling, L., Bringer, S., & Bott, M. (2014). SoxR as a single-cell biosensor for NADPH-consuming enzymes in *Escherichia coli*. *ACS Synthetic Biology*, *3*, 41–47.

Studier, F. W., & Moffatt, B. A. (1986). Use of bacteriophage T7 RNA polymerase to direct selective high-level expression of cloned genes. *Journal of Molecular Biology*, *189*, 113–130. https://doi.org/10.1016/0022-2836(86)90385-2

Tsaneva, I. R., & Weiss, B. (1990). *soxR*, a locus governing a superoxide response regulon in *Escherichia coli* K-12. *Journal of Bacteriology*, *172*, 4197–41205. https://doi.org/10.1128/jb.172.8.4197-4205.1990

Watanabe, S., Kita, A., Kobayashi, K., & Miki, K. (2008). Crystal structure of the [2Fe-2S] oxidative-stress sensor SoxR bound to DNA. *Proceedings of the National Academy of Sciences of the United States of America*, *105*, 4121–4126. https://doi.org/10.1073/pnas.0709188105

Weckbecker, A., & Hummel, W. (2004). Improved synthesis of chiral alcohols with *Escherichia coli* cells co-expressing pyridine nucleotide transhydrogenase, $NADP^+$-dependent alcohol dehydrogenase and NAD^+-dependent formate dehydrogenase. *Biotechnology Letters*, *26*, 1739–1744. https://doi.org/10.1007/s10529-004-3746-2

Wu, J., & Weiss, B. (1991). Two divergently transcribed genes, *soxR* and *soxS*, control a superoxide response regulon of *Escherichia coli*. *Journal of Bacteriology*, *173*, 2864–2871. https://doi.org/10.1128/jb.173.9.2864-2871.1991

How to cite this article: Spielmann A, Baumgart M, Bott M. NADPH-related processes studied with a SoxR-based biosensor in *Escherichia coli*. *MicrobiologyOpen*. 2018;e785. https://doi.org/10.1002/mbo3.785

APPENDIX A

TABLE A1 Oligonucleotides used in this study

Oligonucleotide	Sequence (5′→3′) and properties
Oligonucleotides used for the construction of deletion mutants with the lambda recombination system with 5′-parts corresponding to the upstream or downstream region of the gene(s) to be deleted (shown in bold) and 3′-parts corresponding to the FRT-flanked kanamycin cassette of plasmid pKD4.	
rseC fw	**GAAATGTTCATACCGTATGGATTGTGGTATCTGGAAACGTCCTCGCATTTG TTATGCAAAATGCAACAAAGCCAGTGAAA** GTGTAGGCTGGAGCTGCTTC
rseC rv	**GCCGAAATCACCATTGTCGGTGAACTGCCGCCGCAAACGGCGAAACGCA TTGCCGAGAATATTAAGTTCGGGGCAGCGCA** ATGGGAATTAGCCATGGTCC
rsxABCDGE fw	**GTAATAACCTTACAGTTAACCTGTTGTCGCCTGCTCTGGATTAACGGATAAT AGGCGGCTTTTTTATTTCAGGCCGAAAA** GTGTAGGCTGGAGCTGCTTC
rsxABCDGE rev	**TCAAAAGGCGAACTGAAATTAAGCTCGGTGGTGGGATGAGGATTGTTCTCA CGCAGGCGAGTGAGGATCTCCAGGCGTTT**ATGGGAATTAGCCATGGTCC
pntAB fw	**ATTTAGCTCGTACATGAGCAGCTTGTGTGGCTCCTGACACAGGCAAACCAT CATCAATAAAACCGATGGAAGGGAATATC**GTGTAGGCTGGAGCTGCTTC
pntAB rv	**AAACAGCGGGAGGTCAAAGCATCGCCGTTCTGTTAAGCGATCTCAATAAA GAGTGACGGCCTCAGCAGAGGCCGTCAGGG**ATGGGAATTAGCCATGGTCC
sthA fw	**TGACGGGGATCAATTGGCTTACCCGCGATAAAATGTTACCATTCTGTTG CTTTTATGTATAAGAACAGGTAAGCCCTACC**GTGTAGGCTGGAGCTGCTTC
sthA rv	**CTGGCTCACCGCTGCGCAGCCGCTATGAGCAGCTGGCAGAGGCCATC CGCGCAAGAATGGATGGCCATTTCGATAAAGTT**ATGGGAATTAGC CATGGTCC
Oligonucleotides used for cloning of genes into pACYCDuet-1 with overlapping regions required for Gibson assembly shown in bold.	
rseC-pACYC fw	CTTTAATAAGGAGATATACATGATCAAAGAGTGGGCTACC
rseC-pACYC rv	CATTATGCGGCCGCATCACTGGCTCGCGTCTTC
rsxABC-pACYC-fw	**GGAGATATACATATGGCA**ATGACTGACTACCTGTTAC
rsxABC-rsxDGE rev	**GAATACCAT**TTAGTCCTCGTTTACAACC
rsxDGE-rsxABC fw	**GAGGACTAA**ATGGTATTCAGAATAGCTAGC
rsxDGE-pACYC rev	**GCGTGGCCGGCCGAT**TCAGACATTCCCTGTTTC
Oligonucleotides used for colony-PCRs and sequencing of plasmids	
Δ*rseC* verification fw	GACGGTCGGCGTTATAGGTC
Δ*rseC* verification rev	GGACGCAGAACCGTCAGTACAAGCG
Δ*rsxABCDGE* verification fw	GTTGGCAACCGCATTGATCG
Δ*rsxABCDGE* verification rv	CCCGGCGCAAATTGAGTACG
Δ*sthA* verification fw	TGCTGCGTGAGGTGAAAGTC
Δ*sthA* verification rv	AGTCCGCAAGTTCCGCAATG
Δ*pntAB* verification fw	GCTCAAATGACCGTCTATGC
Δ*pntAB* verification rv	GATTGCTGGCCTTTGCGCTT
pACYCDuet-1 MCS_1 sequencing fw	CAGCAGCCATCACCATCATC
pACYCDuet-1 MCS_2 sequencing fw	CGAAATTAATACGACTCACTATAGG

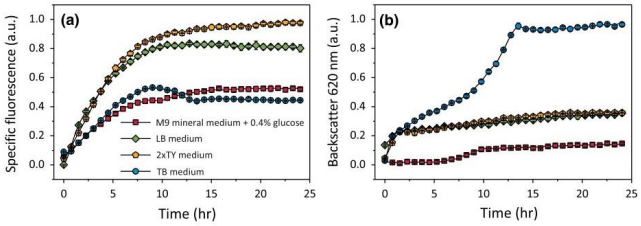

FIGURE A1 Influence of different media on the NADPH biosensor response (A) and cell density (B) of *Escherichia coli*/pSenSox during biotransformation of 70 mM MAA to MHB. The strain was cultivated in either M9 mineral medium with 0.4% (w/v) glucose, or in LB medium, or in 2xTY medium, or in TB medium. The experimental setup shown in Figure 1 was used for all cultivations in one of the media mentioned above containing 100 μg/ml carbenicillin. Mean values and standard deviations of three independent biological replicates are shown

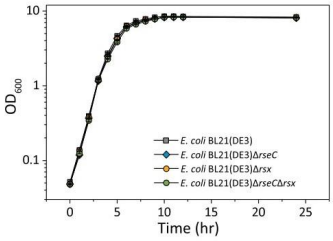

FIGURE A2 Growth behavior of the mutants *Escherichia coli* Δ*rseC*, *E. coli* Δ*rsx*, and *E. coli* Δ*rseC*Δ*rsx* in comparison to the parental strain *E. coli* BL21(DE3). The strains were cultivated in 50 ml 2xTY medium in 500 ml shake flasks at 30°C and 130 rpm and growth was monitored as OD_{600}. Mean values and standard deviations of three independent biological replicates are shown

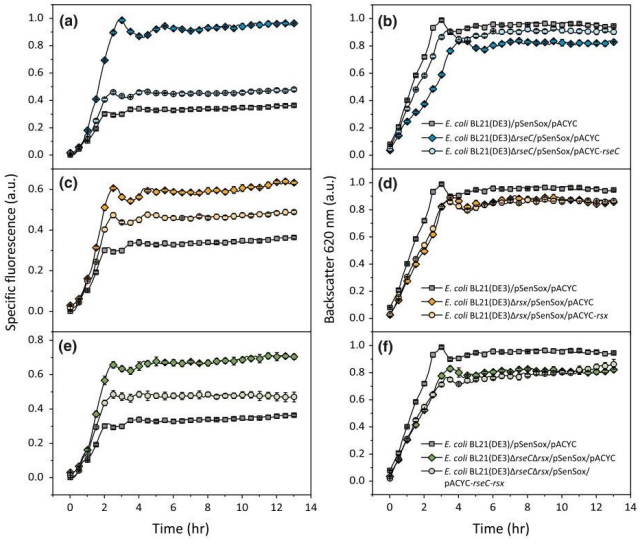

FIGURE A3 Complementation studies of the Δ*rseC*, Δ*rsx*, and Δ*rseC*Δ*rsx* mutants carrying pSenSox using plasmids pACYC-*rseC*, pACYC-*rsx*, and pACYC-*rseC-rsx*. For comparison, the parent strain carrying pSenSox and pACYCDuet-1 was used. The experiment was performed according to the standard setup shown in Figure 1 with 30 mM MAA. IPTG was not added to the cultures as it had a negative effect on growth. Mean values and standard deviations of three independent biological replicates are shown

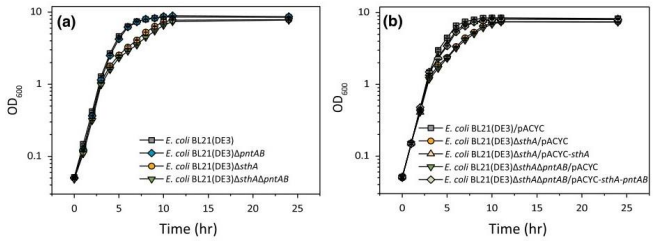

FIGURE A4 Growth (OD_{600}) of the transhydrogenase mutants Δ*pntAB*, Δ*sthA*, and Δ*sthA*Δ*pntAB* compared to the parental strain *Escherichia coli* BL21(DE3) (A) and complementation of the Δ*sthA* and Δ*sthA*Δ*pntAB* strains (B). The strains were cultivated at 30°C and 130 rpm in 500 ml shake flasks with 50 ml of 2xTY medium. Complementation studies were performed in the presence of 0.1 mM IPTG and 34 μg/ml chloramphenicol. Mean values and standard deviations of three independent biological replicates are shown

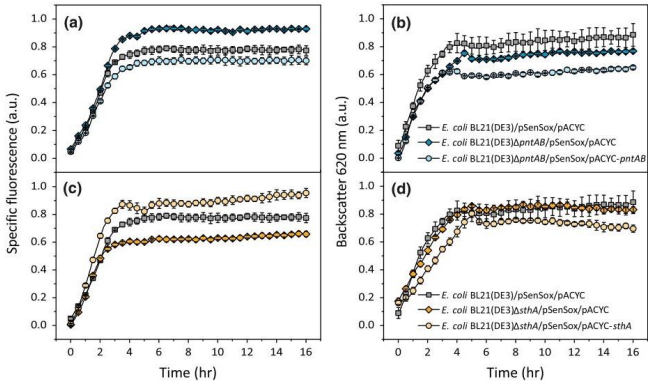

FIGURE A5 Complementation studies of the Δ*pntAB* and Δ*sthA* mutants carrying plasmid pSenSox with plasmids pACYC-*pntAB* or pACYC-*sthA*. For comparison, the parent strain and the mutants carrying pSenSox and pACYCDuet-1 (pACYC) were used. The experiment was performed according to the standard setup shown in Figure 1 with 30 mM MAA. Mean values and standard deviations of three independent biological replicates are shown

2.2. NADPH biosensor-based identification of an alcohol dehydrogenase variant with improved catalytic properties caused by a single charge reversal at the protein surface

Alina Spielmann, Yannik Brack, Hugo van Beek, Lion Flachbart, Meike Baumgart, and Michael Bott*

IBG-1: Biotechnology, Institute of Bio- and Geosciences, Forschungszentrum Jülich, Jülich, Germany

*Corresponding author

Current state: Submitted for publication to the journal Microbial Biotechnology

Author's contributions:

YB constructed the *Lb*ADH library and performed the initial characterization of isolated clones in the BioLector after FACS-screening. YB and AS performed the FACS screening experiments. LF and HB helped to develop the FACS screening approach and with FACS data analysis. AS constructed the plasmid pASK-IBA5plus-*Lbadh*^{K71E}, carried out the purification of *Lb*ADH^{WT} and *Lb*ADH^{K71E}, and performed the biochemical characterization of *Lb*ADH^{WT} and *Lb*ADH^{K71E}. AS wrote major parts of the manuscript and contributed to the finalization of the manuscript. MBa revised the whole manuscript. MBo wrote parts of the manuscript, revised and finalized the whole manuscript.

Overall contribution AS: 50%

Abstract

Alcohol dehydrogenases (ADHs) are used in reductive biotransformations for the production of valuable chiral alcohols. In this study, we used a high-throughput screening approach based on the NADPH biosensor pSenSox and fluorescence-activated cell sorting (FACS) to search for variants of the NADPH-dependent ADH of *Lactobacillus brevis* (*Lb*ADH) with improved activity for the reduction of 2,5-hexanedione to (2*R*,5*R*)-hexanediol. In a library of approx. $1.4x10^6$ clones created by random mutagenesis we identified the variant *Lb*ADH^{K71E}. Kinetic analysis of the purified enzyme revealed that *Lb*ADH^{K71E} had a ~16% higher affinity and a 17% higher activity for 2,5-hexanedione compared to the wild-type *Lb*ADH. Similar improvements were also observed for the alternative substrates acetophenone, acetylpyridine, 2-hexanone, 4-hydroxy-2-butanone, and methyl acetoacetate. K71 is not an active site residue but is located solvent-exposed on the surface of *Lb*ADH and therefore is not an obvious target for rational protein engineering. The study demonstrates that high-throughput screening using the NADPH biosensor pSenSox represents a powerful method to find unexpected beneficial mutations in NADPH-dependent enzymes.

Introduction

Chiral alcohols with high enantiomeric purity are important intermediates for the synthesis of optically active fine chemicals that are used for example to produce pharmaceuticals and agrochemicals (Ager et al., 1996; Liese et al., 2006; Breuer et al., 2004). Alcohol dehydrogenases (ADHs) are used for the synthesis of chiral alcohols under very mild reaction conditions due to their high catalytic efficiency and selectivity (Hall and Bommarius, 2011; Zheng et al., 2017). A prominent example is the NADPH-dependent ADH from *Lactobacillus brevis* (*Lb*ADH), which catalyzes the enantioselective reduction of prochiral ketones to the corresponding, mostly (*R*)-configured secondary alcohols (Hummel, 1999; Rodriguez et al., 2014). *Lb*ADH is an attractive candidate for biotransformations because it is a robust and versatile biocatalyst with high regio- and stereoselectivity, a broad substrate range, and the ability to convert sterically demanding substrates (Leuchs and Greiner, 2011). Its preferred *in vitro* substrates are prochiral ketones such as acetophenone with almost invariably a small methyl group as one substituent and a bulky (often aromatic) moiety (such as phenyl) as the other (Schlieben et al., 2005). The efficiency of substrate conversion by *Lb*ADH is influenced by the substrate size, the steric and electronic effects of the substrate as well as the thermodynamic stability of the products (Rodriguez et al., 2014). *Lb*ADH is active as a homotetramer with 251 amino acid residues and a molecular mass of 26.6 kDa per subunit (Riebel, 1997; Niefind et al., 2003). It is a short-chain Mg^{2+}-dependent reductase that uses the cofactor NADPH as reducing agent. The crystal structure of *Lb*ADH has been solved (Niefind et al., 2003; Schlieben et al., 2005). The non-covalently bound cofactor NADPH is essential for catalysis and must be recycled efficiently to make the biotransformation economically feasible (Leuchs and Greiner, 2011; Döbber et al., 2018).

Because of the industrial relevance of ADHs, their improvement for *in vivo* and *in vitro* applications is of high interest, such as the optimization of specificity or catalytic activity or the broadening of the substrate spectrum (Hall and Bommarius, 2011). The approaches used for obtaining improved ADH variants, such as directed evolution or rational design, have recently been reviewed (Zhang et al., 2015). In directed evolution, a large number of variants of a particular enzyme created by random and/or targeted mutagenesis is screened for the desired property (Farinas et al., 2001). However, the success of this approach is often restricted by the lack of an efficient high-throughput (HT)-screening assay. Typically, screenings of mutant libraries involve dedicated assays for a certain substrate or product, because the majority of molecules of interest do not lead to an easily observable phenotype (Bloch, 2006). In the case of ADHs, the consumption or production of NAD(P)H can be measured or colorimetric assays can be employed (Zhang et al., 2015), but this limits the number of variants that will be tested in practice to several thousands. Therefore, high-throughput (HT) screening and selection methods are highly desirable (van Rossum et al., 2013).

Genetically encoded biosensors based on transcription factors (TFs) controlling the synthesis of a fluorescent reporter protein are highly useful tools for HT-screening in strain and enzyme development (Dietrich et al., 2010; Eggeling et al., 2015; Mahr and Frunzke, 2016; Rogers et al., 2016). We previously reported a TF-based NADPH biosensor allowing HT screening of NADPH-dependent enzymes *via* fluorescence-activated cell sorting (FACS) of an *Escherichia coli*-based mutant library (Siedler et al., 2014). The NADPH biosensor is encoded by the plasmid pSenSox and consists of the TF SoxR, its target promoter P_{soxS}, and the reporter gene *eyfp*. The SoxRS system of *E. coli* triggers the response to oxidative stress (Greenberg et al., 1990; Tsaneva and Weiss, 1990) and SoxR was found to be activated besides other stimuli

by a reduction of the NADPH/$NADP^+$ ratio in the cell (Liochev and Fridovich, 1992; Krapp et al., 2011). We recently confirmed that the pSenSox biosensor responds to various NADPH-related processes in *E. coli*, such as the presence of redox-cycling drugs, the absence of the SoxR-reducing proteins RsxABCDGE and RseC, and the absence of the transhydrogenases PntAB and/or SthA (Spielmann et al., 2018).

E. coli cells carrying pSenSox become fluorescent during NADPH-dependent biotransformation processes due to a high rate of NADPH consumption. Using the reduction of methyl acetoacetate to *R*-methyl 3-hydroxybutyrate by *Lb*ADH as model reaction, it was demonstrated that the specific eYFP fluorescence of cells correlates both with the substrate concentration and, when the substrate concentration is kept constant, with the specific *Lb*ADH activity (Siedler et al., 2014). Due to the latter property, one promising application of the NADPH biosensor is the FACS-based HT screening of libraries with a high number of variants of NADPH-dependent enzymes. A proof of concept approach led to the identification of an *Lb*ADH variant with a slightly increased activity, but reduced affinity for the substrate 4-methyl-2-pentanone (Siedler et al., 2014).

In the present study, we applied the pSenSox biosensor to screen an *Lb*ADH library in *E. coli* by FACS for variants that enable an improved biotransformation of 2,5-hexanedione to (2*R*,5*R*)-hexanediol. This compound serves as a building block for the synthesis of fine chemicals, pharmaceuticals, agrochemicals and chiral phosphine ligands (Haberland et al., 2002; Machielsen et al., 2009). We identified the variant *Lb*ADH^{K71E} and showed that it has an increased activity for the reduction of 2,5-hexanedione, but also various other substrates.

Results

Construction of an LbADH library and FACS screening

We aimed at finding *Lb*ADH variants with improved catalytic properties for the reduction of 2,5-hexanedione to (2*R*,5*R*)-hexanediol by FACS-based HT screening using the NADPH biosensor pSenSox. For this purpose, a library of *Lbadh* variants was generated by error-prone PCR and used to replace the *Lbadh*^{WT} gene of pSenSox. The resulting library pSenSox-*Lbadh*^{Library} present in *E. coli* TOP10 had an estimated size of 1.4×10^6 clones. A culture expressing the *Lbadh*^{Library} was used for the biotransformation of 2,5-hexanedione by incubation for 2.5 h in 2xTY medium supplemented with 70 mM of the diketone. Preliminary studies had revealed that cells expressing *Lbadh*^{WT} showed maximal specific fluorescence during the biotransformation of 2,5-hexanedione after 2 to 3 h.

After biotransformation, the library cells were diluted and subjected to FACS (Fig. 1) as described in detail in the methods section. The entire screening process comprised three positive selection steps for cells showing high fluorescence after biotransformation of 2,5-hexanedione followed by a negative selection step. In the latter, cells showing high fluorescence independent of 2,5-hexanedione were excluded by collecting only those cells in the library that showed the same fluorescence as *E. coli* TOP10/pSenNeg cells lacking an active *Lb*ADH. After propagation, these cells were subjected to a fourth round of positive selection. $2.5x10^5$ cells of the library were analyzed and 240 cells showing a higher fluorescence than the reference strain *E. coli* TOP10/pSenSox containing wild-type *Lb*ADH were spotted on agar plates and incubated overnight at 37°C. 83 cells (35%) formed colonies and were further analyzed.

Initial characterization of isolated clones in the BioLector

To confirm the increased fluorescence of the 83 isolated clones, they were cultivated in a BioLector machine in 2xTY medium with or without 70 mM 2,5-hexanedione. The specific fluorescence of the cultures (the ratio of absolute fluorescence over cell density determined as backscatter at 620 nm) was monitored online for around 24 h. As reference, the strain expressing the wild-type *Lbadh* gene was used. Several of the clones showed an increased specific fluorescence in the presence of 2,5-hexanedione compared to the absence of 2,5-hexanedione and a higher specific fluorescence than the reference strain with wild-type *Lb*ADH. Sequencing of the plasmids isolated from four of these clones revealed that all carried a single G→A transition in the *Lbadh* gene resulting in the amino acid exchange K71E.

To confirm that this mutation, rather than secondary mutations in the pSenSox plasmid or in the genomic DNA, was responsible for the increased fluorescence during the biotransformation of 2,5-hexanedione, the *Lbadh*^{K71E} gene was amplified by PCR and used to replace the wild-type *Lbadh* gene in plasmid pSenSox, and transferred into *E. coli* TOP10. Cultivation of the recombinant strain carrying pSenSox-*Lbadh*^{K71E} in a BioLector machine confirmed that it shows a higher specific fluorescence in the presence of 2,5-hexanedione than in the absence, and higher fluorescence than *E. coli* TOP10/pSenSox with wild-type *Lb*ADH (data not shown). This result supported the assumption that the K71E mutation in *Lb*ADH was responsible for the increased fluorescence and leads to improved properties for 2,5-hexanedione reduction.

Purification and biochemical characterization of LbADH^{WT} and LbADH^{K71E}

To characterize and compare the *Lb*ADH^{K71E} variant with the *Lb*ADH^{WT}, both enzymes containing an N-terminal StrepTag-II were overproduced in *E. coli* C43(DE3) using the

expression plasmids pASK-IBA5plus-*Lbadh*^{WT} and pASK-IBA5plus-*Lbadh*^{K71E} and purified by StrepTactin Sepharose affinity chromatography followed by size-exclusion chromatography (Fig. 2). The two proteins showed an identical elution profile in the affinity chromatography (Fig. 2A), but in the size-exclusion chromatography the *Lb*ADH^{K71E} eluted slightly before *Lb*ADH^{WT} (Fig. 2B). Consequently, the apparent mass calculated from a calibration curve (Fig. 2C) derived from standard proteins of known size was somewhat larger for *Lb*ADH^{K71E} (113 kDa) than for *Lb*ADH^{WT} (95 kDa). The apparent sizes were in agreement with the known tetrameric structure of *Lb*ADH (calculated mass of monomer 26.6 kDa), but also indicated some structural changes associated with the K71E exchange. These structural changes are also apparent after analysis of the purified proteins by SDS-PAGE: *Lb*ADH^{K71E} shows a slightly higher apparent mass than *Lb*ADH^{WT} (Fig. 2D).

The pure enzymes were used for kinetic analysis using a spectrophotometric assay measuring NADPH consumption at 340 nm (see Methods section for details). In initial studies, the affinity and activity for the substrate 2,5-hexanedione were determined using Michaelis-Menten and Lineweaver-Burk plots (Fig. 3, Table 1). The K_M value determined for *Lb*ADH^{K71E} (4.3 ± 0.5 mM) was 16% lower than the one determined for *Lb*ADH^{WT} (5.1 ± 0.6 mM). The maximal activity calculated for *Lb*ADH^{K71E} (173.3 ± 11.1 µmol min^{-1} mg^{-1}) was 17% higher than that of *Lb*ADH^{WT} (148.5 ± 12.3 µmol min^{-1} mg^{-1}). Consequently, *Lb*ADH^{K71E} is more active than *Lb*ADH^{WT} regarding the reduction of 2,5-hexanedione and has a higher substrate affinity. To test whether the improved kinetic properties of *Lb*ADH^{K71E} are specific for 2,5-hexanedione, we determined the K_M and v_{max} values for methyl acetoacetate. Also for this substrate *Lb*ADH^{K71E} showed a better affinity and a higher maximal activity than *Lb*ADH^{WT} (Fig. 3C and 3D, Table 1). In a further set of experiments, the activity of the two enzymes for four other substrates was compared at a single concentration. As summarized in Table 2, *Lb*ADH^{K71E}

showed 21% - 39% higher activity for 2-acetylpyridine, 2-hexanone, acetophenone, and 4-hydroxy-2-butanone, suggesting that the positive effect of the K71E exchange on *Lb*ADH activity was independent of the substrate.

Discussion

A FACS-based HT approach to identify optimized variants of *Lb*ADH for NADPH-dependent reduction of 2,5-hexanedione resulted in the isolation of *Lb*ADH^{K71E}. The exchange of a lysine residue to a glutamic acid residue at position 71 led to an increased activity and a better affinity for 2,5-hexanedione, but also for the substrate methyl acetoacetate. Furthermore, up to 39% increased activities were found for the substrates 2-acetylpyridine, 2-hexanone, acetophenone, and 4-hydroxy-2-butanone. The crystal structure of the *Lb*ADH^{WT} homotetramer in complex with the substrate acetophenone, the cofactor NADPH and Mg^{2+} is available (Schlieben et al., 2005). Interestingly, position 71 is not located close to the active center at the protein core, but solvent-exposed on the protein surface (Fig. 4). According to PyMOL 2.2.0 (Schrödinger, 2015), the distance of position 71 to the substrate acetophenone is around 28.0 Å and to the cofactor NADPH approximately 14.1 Å. The distance to the amino acids involved in catalysis, Asn113, Ser142, Tyr155, and Lys159 (Niefind et al., 2003) of the closest active site, is 19.4 Å, 27.4 Å, 27.1 Å and 25.7 Å, respectively. The distance to the active center suggests that the amino acid at position 71 is not directly involved in substrate binding and reduction.

Apart from the position of the mutation, the nature of the amino acid exchange has to be considered. The mutation led to an exchange of a lysine residue with a positively charged amino group by a glutamate residue with a negatively charged carboxyl group. The enzyme activity assays were performed at pH 7. The K71E exchange on the *Lb*AHD protein surface will

influence its net charge and isoelectric point (pI), as these parameters depend on the content of ionizable groups and their pK_a values (Shaw et al., 2001). According to a protein parameter calculator (https://web.expasy.org/protparam), the K71E exchange resulted in a change of the pI from 5.44 for *Lb*ADH^{WT} to 5.17 for *Lb*ADH^{K71E}. SDS-PAGE also suggested that the mutation K71E changed the electrostatic properties of the enzyme, because *Lb*ADH^{K71E} showed slower migration on the gel than *Lb*ADH^{WT} (Fig. 2D). In SDS-PAGE, proteins with a lower pI might migrate slower due to stronger negative charge repulsion with SDS (Shirai et al., 2008).

The net charge and the ionization state of individual residues affect many aspects of protein behavior including protein structure, stability, solubility, and function (Shaw et al., 2001; Pace et al., 2009). The slightly different elution profiles of *Lb*ADH^{K71E} and *Lb*ADH^{WT} in the size-exclusion chromatography (Fig. 2B) support a structural change caused by the K71E mutation. Moreover, electrostatic effects dominate hydration, denaturation, protein assembly, allostery and salt bridges, thermal stability and enzyme catalysis (Perutz, 1978; Matthew, 1985). Many enzyme reactions proceed *via* charged transition states and therefore stabilization of charges can be a major catalytic factor (Russell and Fersht, 1987). In the case of *Lb*ADH, Tyr155 is assumed to serve as a catalytic acid which is deprotonated in the course of reduction and requires stabilization by the positively charged Lys159 for this purpose (Schlieben et al., 2005; Jörnvall et al., 1995). The K71E exchange might have a positive influence on enzyme catalysis by stabilizing the charged transition state. Charged residues on the surface of proteins can also generate electrical potentials that extend many angstroms out into solution, enhancing substrate association rates and catalytic rates in enzymes (Sharp and Honig, 1990).

It is interesting that a single mutation on the protein surface, as is the case of the *Lb*ADH^{K71E} variant, is sufficient to increase enzyme activity. Several studies have shown that it

is possible to increase protein stability by improving electrostatic interactions among charged groups on the surface of folded proteins through multiple and even single mutations (Akke and Forsen, 1990; Grimsley et al., 1999; Strickler et al., 2006; Gribenko et al., 2009). Therefore, a change in charge-charge interactions on the *Lb*ADH^{K71E} surface might positively influence enzyme stability, leading to increased enzyme activity. More specifically, *Lb*ADH^{K71E} activity might increase because the electrostatic changes on the protein surface have a positive influence on thermodynamic stability. The main factors affecting stability are the relative free energies of the folded (G_f) and the unfolded (G_u) states. Protein stability is defined as the difference in Gibbs free energy, ΔG_u, between the folded and the unfolded state. Specific algorithms have been developed to predict the effects of mutations on protein stability by estimating the changes in the difference in Gibbs free energy ($\Delta\Delta G$) between the wild-type and the mutated enzyme. The mutated enzyme is more stable if $\Delta\Delta G$ is positive. For the proteins *Lb*ADH^{WT} and *Lb*ADH^{K71E} the servers SDM (Pandurangan et al., 2017) and I-Mutant 2.0 (Capriotti et al., 2005) both calculated $\Delta\Delta G$ to be +3.51 kJ/mol. The program iPTREE-STAB (Huang et al., 2007) predicted that the mutation K71E has a stabilizing effect without giving a concrete value for $\Delta\Delta G$. Thus, the charge reversal at position 71 on the protein surface might have decreased the relative free energy of the folded state (G_f) of *Lb*ADH^{K71E} compared to *Lb*ADH^{WT}, resulting in a more stable protein. The increased stability might enable a higher fraction of *Lb*ADH^{K71E} proteins to be in the active, folded state compared to the *Lb*ADH^{WT} proteins, explaining why *Lb*ADH^{K71E} can convert the substrate faster than *Lb*ADH^{WT}.

In conclusion, the charge reversal on the protein surface might be crucial for the higher activity of *Lb*ADH^{K71E} compared to *Lb*ADH^{WT}. Rational protein design has been dominated by algorithms that optimize interactions in the protein core and only few algorithms have been developed that focus on surface interactions (Strickler et al., 2006). This study is another

example for the importance of electrostatic forces on the protein surface regarding enzyme activity. Moreover, this study provides further evidence that random mutagenesis in combination with a HT screening approach is a powerful tool for the identification of promising enzyme variants.

Materials and Methods

Chemicals, bacterial strains, plasmids and growth conditions

Unless specified otherwise the chemicals were purchased from Sigma-Aldrich GmbH (Steinheim, Germany), BD Biosciences (Franklin Lakes, USA), or Carl Roth (Karlsruhe, Deutschland). All bacterial strains and plasmids used in this work are listed in Table 3. One Shot™ TOP10 Electrocomp *E. coli* cells (Invitrogen, Karlsruhe, Germany) were used for cloning and screening purposes. Transformation of *E. coli* cells was performed as described (Hanahan, 1983). Cells were cultivated at 37°C in liquid 2xTY medium consisting of 16 g L^{-1} tryptone (BD Biosciences, Franklin Lakes, USA), 10 g L^{-1} yeast extract, and 5 g L^{-1} sodium chloride, in terrific broth (TB) medium (12 g L^{-1} tryptone, 24 g L^{-1} yeast extract, 4 mL glycerol, 12.54 g L^{-1} K_2HPO_4, 2.31 g L^{-1} KH_2PO_4; pH 7.0), or on LB agar (Carl Roth, Karlsruhe, Deutschland). Plasmids were selected by adding carbenicillin to the medium to a final concentration of 100 µg ml^{-1}. BD™ *FACSFlow* Sheath Fluid for flow cytometry applications was purchased from BD Biosciences (Franklin Lakes, USA).

Recombinant DNA work and library construction

Standard methods such as PCR were carried out according to established protocols (Sambrook and Russell, 2001). Oligonucleotides were synthesized by Eurofins Genomics (Ebersberg, Germany) and are listed in Table 4. All plasmids were sequenced by Eurofins Genomics

(Ebersberg, Germany). For random mutagenesis of the *Lbadh*^{WT} gene, error-prone PCR was performed using the oligonucleotide pair pSenSox-*Lbadh*-fw and pSenSox-*Lbadh*-rv, the plasmid pSenSox as template, and the GeneMorph II Random Mutagenesis Kit (Agilent Technologies, Santa Clara CA, USA). The resulting mutated *Lbadh* fragments were cloned by Gibson assembly (Gibson et al., 2009) into a pSenSox fragment obtained by restriction with EcoRI and HindIII to remove the *Lbadh*^{WT} gene. The Gibson assembly mixture representing the *Lbadh*^{Library} was used to transform electrocompetent cells of *E. coli* TOP10. The resulting library was composed of about 1.4x10^{6} individual clones and was used for preparation of glycerol stocks.

The plasmid pASK-IBA5plus-*Lbadh*^{K71E} was generated by site-directed mutagenesis with pASK-IBA5plus-*Lbadh*^{WT} as template, the oligonucleotide pair *Lbadh*-mutagenesis-A412G-fw and *Lbadh*-mutagenesis-A412G-rv, and the PfuUltra II Hotstart PCR Master Mix (Agilent Technologies, Santa Clara CA, USA). The plasmid pSenSox-*Lbadh*^{K71E} was obtained by amplifying the *Lbadh*^{K71E} gene with the oligonucleotides pSenSox-*Lbadh*-fw and pSenSox-*Lbadh*-rv and pASK-IBA5plus-*Lbadh*^{K71E} as template and cloning the PCR product into plasmid pSenSox cut with HindIII and EcoRI at the former position of the *Lbadh*^{WT} gene.

Fluorescence activated cell sorting (FACS)

Flow cytometric analysis and cell sorting were performed with a FACS ARIA II high-speed cell sorter (BD Biosciences, Franklin Lakes, NJ, USA) and the BD FACSDiva™ software 6.1.3. eYFP fluorescence of single cells was measured by using an excitation wavelength of 488 nm emitted by a blue solid-state laser and an emission wavelength of 533 ± 30 nm at a sample pressure of 70 psi. A threshold was set to exclude non-bacterial particles on the basis of forward scatter (FSC) area versus side scatter (SSC) area. The flow rate was set to analyze

2000–4000 cells per second. For graphical representation of the obtained data as dot plots or histograms the software FlowJo (FlowJo, LLC, Ashland, OR, USA) was used.

The strategy used to isolate cells containing *Lb*ADH variants with improved activity for reduction of 2,5-hexanedione included three enrichments steps with positive selection followed by one negative selection step and another positive selection step. A 1-ml culture of *E. coli* TOP10/pSenSox-*Lbadh*^{Library} in 2xTY medium containing 100 µg ml^{-1} carbenicillin with an initial optical density at 600 nm (OD_{600}) of 0.2 was incubated for 4 h at 37°C and 900 rpm in a 48-well non-transparent Flowerplate (m2p-labs GmbH, Baesweiler, Deutschland). Then the cells were harvested by centrifugation and resuspended in fresh 2xTY medium supplemented with 100 µg ml^{-1} carbenicillin to a final OD_{600} of 3 or higher. 800 µl of these suspensions were transferred into another 48-well Flowerplate and after addition of 100 µL 2,5-hexanedione to a final concentration of 70 mM, the plate was incubated for 2.5 h at 37°C and 900 rpm for NADPH-dependent reduction of 2,5-hexanedione to (2*R*,5*R*)-hexanediol and concomitant NADPH-dependent expression of *eyfp*. Then the cultures were diluted 50-fold in sterile-filtered BD™ FACSFlow Sheath Fluid (BD, Franklin Lakes, USA) and subjected to FACS.

The sorting gate was set to include the 1% most fluorescent cells. $3x10^4$ of these cells were sorted into fresh 2xTY medium containing 100 µg ml^{-1} carbenicillin. After overnight cultivation, a new 1-ml culture was inoculated, incubated for 4 h and then used again for biotransformation of 2,5-hexanedione. Afterwards, the cells were again screened by FACS, $3x10^4$ of the most fluorescent cells were isolated and the positive selection repeated for a third time. After culturing the cells of the third enrichment step, they were subjected to a mock biotransformation in which 2,5-hexanedione was omitted and then analyzed by FACS. In this case, the non-fluorescent cells were sorted in order to remove cells showing high fluorescence independent of *Lb*ADH-catalyzed 2,5-hexanedione reduction. For setting the

sorting gate, cells of *E. coli* TOP10/pSenNeg were used, which lack an active *Lb*ADH. $1x10^5$ library cells within the negative sorting gate were collected in fresh 2xTY medium with 100 µg ml^{-1} carbenicillin. After overnight cultivation, a fourth round of positive selection was performed using cells after 2.5 h biotransformation of 2,5-hexanedione. Cells of *E. coli* TOP10/pSenSox with wild-type *Lb*ADH were used as reference and 240 library cells showing a higher fluorescence than the reference were spotted on LB agar plates with 100 µg ml^{-1} carbenicillin.

83 out of the 240 spotted cells formed colonies after overnight incubation at 37°C and were subsequently analyzed in a BioLector microcultivation system by following eYFP fluorescence and growth as described below. 65 clones showed the same fluorescence pattern with a higher fluorescence compared to the reference strain *E. coli* TOP10/pSenSox expressing the wild-type *Lbadh*^{WT} gene in the presence of the substrate 2,5-hexanedione. The plasmids of four of these strains were isolated and sequenced. All four clones carried a single G→A transition in the *Lbadh* gene resulting in the amino acid exchange K71E.

Biotransformation and monitoring of the NADPH biosensor response

The fluorescence intensity of the NADPH biosensor signal was measured during the whole-cell biotransformation of the substrate 2,5-hexanedione. To test the difference in the fluorescence intensity, pre-cultures of the cultures obtained after FACS screening and the *E. coli* TOP10/pSenSox culture as positive control were incubated overnight at 37°C and 130 rpm in 5 mL 2xTY medium containing 100 µg ml^{-1} carbenicillin. The pre-cultures were used to inoculate main cultures in 2xTY medium with 100 µg ml^{-1} carbenicillin to an OD_{600} of 0.05, which were cultivated at 37°C and 130 rpm. The cells were further cultivated for 5 h, harvested by centrifugation (4°C, 4713 *g*, 15 min) and resuspended in 5 ml fresh 2xTY medium

supplemented with 100 µg ml^{-1} carbenicillin to a final OD_{600} of 5. 800 µl of these suspensions were transferred into a 48-well Flowerplate (m2p-laps, Baesweiler, Germany). To start the biotransformation of the substrates, 100 µL of the substrate 2,5-hexanedione dissolved in ddH_2O was added to the cultures to a final concentration of 70 mM. 100 µL ddH_2O were added to the cultures instead of the substrates as negative controls. After the desired additions, the Flowerplates were incubated in a BioLector microcultivation system (m2p-laps, Baesweiler, Germany) at 30°C and 1200 rpm (shaking diameter 3 mm) and eYFP fluorescence (excitation wavelength 485 nm, emission wavelength of 520 nm) and cell density (as backscattered light at 620 nm) were monitored online (Kensy et al., 2009).

*Lb*ADH *overproduction and purification*

For enzyme production, *E. coli* C43(DE3) carrying pASK-IBA5plus-*Lbadh*^{WT} or pASK-IBA5plus-*Lbadh*^{K71E} was cultivated in TB medium supplemented with 1 mM $MgCl_2$ and 100 µg ml^{-1} carbenicillin. Pre-cultures were used to inoculate 1 l main cultures in a 5 l shaking flask to a starting OD_{600} of 0.1. The main cultures were shaken at 37°C and 130 rpm until an OD_{600} of 0.6 was reached. Then *Lb*ADH overproduction was induced with 0.2 mg l^{-1} anhydrotetracycline and the cultures were then incubated for 20 h at 20°C and 130 rpm. Subsequently, the cells were harvested by centrifugation (4°C, 4713 *g*, 30 min), resuspended in 5 ml lysis buffer (100 mM Tris/HCl buffer at pH 7.2 with 1 mM $MgCl_2$, 1 µg ml^{-1} DNAse and protease inhibitor (cOmplete™ ULTRA Tablets, Mini, EDTA-free, *EASYpack* Protease Inhibitor Cocktail, Roche, Basel, Schweiz), and incubated for 20 min on ice. For cell disruption the cell suspension was passed three times through a French pressure cell at 110 MPa. To sediment intact cells and cell debris the extract was centrifuged for 60 min at 10,000 *g* and 4°C. The resulting supernatant was filtered through a 0.22 µm filter (Millex-GP,

polyethersulfon, Merck Millipore, Tullagreen, Ireland) and used for a two-step purification process with an Äkta™ Pure chromatography system (GE Healthcare Bio-Sciences, Uppsala, Sweden). First, *Lb*ADH was isolated by affinity chromatography using a 1 ml Strep-Trap^{TM} HP column (GE Healthcare Bio-Sciences, Uppsala, Sweden) equilibrated with 100 mM Tris/HCl buffer pH 7.2 containing 1 mM $MgCl_2$ according to the protocol provided by the manufacturer. For elution of specifically bound proteins, equilibration buffer supplemented with 2.5 mM desthiobiotin was used. For the second purification step, size exclusion chromatography was performed using a Superdex^{TM} 200 increase 10/300 GL column (GE Healthcare Bio-Sciences, Uppsala, Sweden) equilibrated with buffer A (50 mM triethanolamine hydrochloride (TEA) containing 1 mM $MgCl_2$ and adjusted to pH 7.0 with 1 M HCl). *Lb*ADH^{WT} and *Lb*ADH^{K71E} were eluted with buffer A at a flow rate of 0.75 mL/min. To determine the molecular mass of the eluted proteins, a calibration curve was established by performing size exclusion chromatography under the same conditions with proteins of known size, namely carbonic anhydrase (29 kDa), bovine serum albumin (66 kDa), alcohol dehydrogenase (150 kDa) and β-amylase (200 kDa). Protein concentrations were determined using a bicinchoninic acid assay (Interchim, Montluçon, France). 1 µg protein of the elution fraction obtained after affinity purification and 1 µg protein of the elution fraction obtained after size exclusion chromatography were analyzed by sodium dodecyl sulfate polyacrylamide gel electrophoresis (SDS-PAGE) using a Mini-PROTEAN® TGX^{TM} Any kD^{TM} gel (Bio-Rad Laboratories, Hercules CA, USA).

Kinetic analysis of LbADH^{WT} and LbADH^{K71E}

The kinetic properties of purified *Lb*ADH^{WT} and *Lb*ADH^{K71E} were analyzed using an assay in which the oxidation of NADPH was followed at 340 nm using a JASCO V560 UV/VIS

spectrophotometer (JASCO, Gross-Umstadt, Germany) equipped with a water bath-heated cell holder set at 30°C. The assay was performed in disposable semi-micro cuvettes made of polystyrene (Sarstedt, Nürnbrecht, Germany) containing 1 ml assay buffer composed of 50 mM TEA pH 7.0, 1 mM $MgCl_2$, 0.3 mM NADPH, 0.7 µg purified *Lb*ADH^{WT} or *Lb*ADH^{K71E}, and different concentrations of the substrate. For 2,5-hexanedione, concentrations from 1 mM to 20 mM were used, for methyl acetoacetate 0.195 mM to 12.5 mM. The activity for acetophenone was determined at 5 mM, the activities for 2-acetylpyridine, 2-hexanone, and 4-hydroxy-2-butanone were determined at 10 mM. The progress of NADPH consumption was measured continuously for 1 min and used to calculate the corresponding enzyme activity using an extinction coefficient for NADPH at 340 nm of 6.22 mM^{-1} cm^{-1}. The data were used to create Michalis-Menten and Lineweaver-Burk plots. K_M and V_{max} values were determined by nonlinear regression of the Michaelis-Menten equation using the software GraphPad Prism 7 (GraphPad Software, La Jolla California USA).

Acknowledgements

We are grateful to Prof. Wolfgang Kroutil (Department of Chemistry, University of Graz, Austria) for providing plasmid pASK-IBA5plus-*Lbadh*^{WT}. This work was funded by the German Federal Ministry of Education and Research (BMBF), funding code 031A095B, as part of the project “Molecular Interaction Engineering: From Nature’s Toolbox to Hybrid Technical Systems (MIE)”.

References

Ager, D.J., Prakash, I., and Schaad, D.R. (1996) 1,2-Amino alcohols and their heterocyclic derivatives as chiral auxiliaries in asymmetric synthesis. *Chem Rev* **96**: 835-876.

Akke, M., and Forsen, S. (1990) Protein stability and electrostatic interactions between solvent exposed charged side chains. *Proteins* **8**: 23-29.

Bloch, W. (2006) J.-L. Reymond (Ed.): Enzyme assays. High-throughput screening, genetic selection and fingerprinting. *Anal. Bioanal. Chem.* **386**: 1583-1584.

Breuer, M., Ditrich, K., Habicher, T., Hauer, B., Kesseler, M., Sturmer, R., and Zelinski, T. (2004) Industrial methods for the production of optically active intermediates. *Angew. Chem. Int. Ed.* **43**: 788-824.

Capriotti, E., Fariselli, P., and Casadio, R. (2005) I-Mutant2.0: predicting stability changes upon mutation from the protein sequence or structure. *Nucleic Acids Res* **33**: W306-310.

Dietrich, J.A., McKee, A.E., and Keasling, J.D. (2010) High-throughput metabolic engineering: advances in small-molecule screening and selection. *Annu Rev Biochem* **79**: 563-590.

Döbber, J., Pohl, M., Ley, S.V., and Musio, B. (2018) Rapid, selective and stable HaloTag-*Lb*ADH immobilization directly from crude cell extract for the continuous biocatalytic production of chiral alcohols and epoxides. *React Chem Eng* **3**: 8-12.

Eggeling, L., Bott, M., and Marienhagen, J. (2015) Novel screening methods - biosensors. *Curr Opin Biotechnol* **35**: 30-36.

Farinas, E.T., Bulter, T., and Arnold, F.H. (2001) Directed enzyme evolution. *Curr Opin Biotechnol* **12**: 545-551.

Gibson, D.G., Young, L., Chuang, R.-Y., Venter, J.C., Hutchison, C.A., and Smith, H.O. (2009) Enzymatic assembly of DNA molecules up to several hundred kilobases. *Nat Meth* **6**: 343-345.

Greenberg, J.T., Monach, P., Chou, J.H., Josephy, P.D., and Demple, B. (1990) Positive control of a global antioxidant defense regulon activated by superoxide-generating agents in *Escherichia coli*. *Proc Natl Acad Sci USA* **87**: 6181-6185.

Gribenko, A.V., Patel, M.M., Liu, J., McCallum, S.A., Wang, C., and Makhatadze, G.I. (2009) Rational stabilization of enzymes by computational redesign of surface charge-charge interactions. *Proc Natl Acad Sci USA* **106**: 2601-2606.

Grimsley, G.R., Shaw, K.L., Fee, L.R., Alston, R.W., Huyghues-Despointes, B.M., Thurlkill, R.L., et al. (1999) Increasing protein stability by altering long-range coulombic interactions. *Protein Sci* **8**: 1843-1849.

Grosch, J.H., Wagner, D., Nistelkas, V., and Spiess, A.C. (2017) Thermodynamic activity-based intrinsic enzyme kinetic sheds light on enzyme-solvent interactions. *Biotechnol Prog* **33**: 96-103.

Haberland, J., Hummel, W., Daussmann, T., and Liese, A. (2002) New continuous production process for enantiopure (2*R*,5*R*)-hexanediol. *Org Proc Res Dev* **6**: 458-462.

Hall, M., and Bommarius, A.S. (2011) Enantioenriched compounds via enzyme-catalyzed redox reactions. *Chem Rev* **111**: 4088-4110.

Hanahan, D. (1983). Studies on transformation of *Escherichia coli* with plasmids. *J Mol Biol* **166**, 557– 580.

Huang, L.T., Gromiha, M.M., and Ho, S.Y. (2007) iPTREE-STAB: interpretable decision tree based method for predicting protein stability changes upon mutations. *Bioinformatics* **23**: 1292-1293.

Hummel, W. (1999) Large-scale applications of NAD(P)-dependent oxidoreductases: recent developments. *Trends Biotechnol* **17**: 487-492.

Jörnvall, H., Persson, B., Krook, M., Atrian, S., Gonzalez-Duarte, R., Jeffery, J., and Ghosh, D. (1995) Short-chain dehydrogenases/reductases (SDR). *Biochemistry* **34**: 6003-6013.

Kensy, F., Zang, E., Faulhammer, C., Tan, R.K., and Büchs, J. (2009) Validation of a high-throughput fermentation system based on online monitoring of biomass and fluorescence in continuously shaken microtiter plates. *Microb Cell Fact* **8**: 31.

Krapp, A.R., Humbert, M.V., and Carrillo, N. (2011) The *soxRS* response of *Escherichia coli* can be induced in the absence of oxidative stress and oxygen by modulation of NADPH content. *Microbiology* **157**: 957-965.

Leuchs, S., and Greiner, L. (2011) Alcohol dehydrogenase from *Lactobacillus brevis*: A versatile robust catalyst for enantioselective transformations. *Chem Biochem Eng* **25**: 267-281.

Liese, A., Seelbach, K., and Wandrey, C. (2006) *Industrial Biotransformation.* Wiley-VCH Verlag GmbH & Co. KGaA, Weinheim, Germany.

Liochev, S.I., and Fridovich, I. (1992) Fumarase C, the stable fumarase of *Escherichia coli*, is controlled by the *soxRS* regulon. *Proc Natl Acad Sci USA* **89**: 5892-5896.

Machielsen, R., Looger, L.L., Raedts, J., Dijkhuizen, S., Hummel, W., Hennemann, H.-G., et al. (2009) Cofactor engineering of *Lactobacillus brevis* alcohol dehydrogenase by computational design. *Eng Life Sci* **9**: 38-44.

Mahr, R., and Frunzke, J. (2016) Transcription factor-based biosensors in biotechnology: current state and future prospects. *Appl Microbiol Biotechnol* **100**: 79-90.

Matthew, J.B. (1985) Electrostatic effects in proteins. *Annu Rev Biophys Biophys Chem* **14**: 387-417.

Miroux, B., and Walker, J.E. (1996) Over-production of proteins in *Escherichia coli*: mutant hosts that allow synthesis of some membrane proteins and globular proteins at high levels. *J Mol Biol* **260**: 289-298.

Niefind, K., Müller, J., Riebel, B., Hummel, W., and Schomburg, D. (2003) The crystal structure of *R*-specific alcohol dehydrogenase from *Lactobacillus brevis* suggests the structural basis of its metal dependency. *J Mol Biol* **327**: 317-328.

Pace, C.N., Grimsley, G.R., and Scholtz, J.M. (2009) Protein ionizable groups: pK values and their contribution to protein stability and solubility. *J Biol Chem* **284**: 13285-13289.

Pandurangan, A.P., Ochoa-Montano, B., Ascher, D.B., and Blundell, T.L. (2017) SDM: a server for predicting effects of mutations on protein stability. *Nucleic Acids Res* **45**: W229-w235.

Perutz, M.F. (1978) Electrostatic effects in proteins. *Science* **201**: 1187.

Riebel, B. (1997) Biochemische und molekularbiologische Charakterisierung neuer mikrobieller NAD(P)-abhängiger Alkoholdehydrogenasen. Dissertation, Heinrich-Heine-Universität Düsseldorf, Germany.

Rodriguez, C., Borzecka, W., Sattler, J.H., Kroutil, W., Lavandera, I., and Gotor, V. (2014) Steric vs. electronic effects in the *Lactobacillus brevis* ADH-catalyzed bioreduction of ketones. *Org Biomol Chem* **12**: 673-681.

Rogers, J.K., Taylor, N.D., and Church, G.M. (2016) Biosensor-based engineering of biosynthetic pathways. *Curr Opin Biotechnol* **42**: 84-91.

Russell, A.J., and Fersht, A.R. (1987) Rational modification of enzyme catalysis by engineering surface charge. *Nature* **328**: 496-500.

Sambrook, J., and Russell, D. (2001) *Molecular Cloning. A Laboratory Manual*. Cold Spring Harbor, New York: Cold Spring Harbor Laboratory Press.

Schlieben, N.H., Niefind, K., Müller, J., Riebel, B., Hummel, W., and Schomburg, D. (2005) Atomic resolution structures of *R*-specific alcohol dehydrogenase from *Lactobacillus brevis* provide the structural bases of its substrate and cosubstrate specificity. *J Mol Biol* **349**: 801-813.

Schrödinger, L.L.C. (2015) The PyMOL molecular graphics system, Version 1.8.

Sharp, K.A., and Honig, B. (1990) Electrostatic interactions in macromolecules: theory and applications. *Annu Rev Biophys Biophys Chem* **19**: 301-332.

Shaw, K.L., Grimsley, G.R., Yakovlev, G.I., Makarov, A.A., and Pace, C.N. (2001) The effect of net charge on the solubility, activity, and stability of ribonuclease Sa. *Protein Sci* **10**: 1206-1215.

Shirai, A., Matsuyama, A., Yashiroda, Y., Hashimoto, A., Kawamura, Y., Arai, R., et al. (2008) Global analysis of gel mobility of proteins and its use in target identification. *J Biol Chem* **283**: 10745-10752.

Siedler, S., Schendzielorz, G., Binder, S., Eggeling, L., Bringer, S., and Bott, M. (2014) SoxR as a single-cell biosensor for NADPH-consuming enzymes in *Escherichia coli*. *ACS Synt Biol* **3**: 41-47.

Spielmann, A., Baumgart, M., and Bott, M. (2018) NADPH-related processes studied with a SoxR-based biosensor in *Escherichia coli. MicrobiologyOpen* **0**: e785.

Strickler, S.S., Gribenko, A.V., Gribenko, A.V., Keiffer, T.R., Tomlinson, J., Reihle, T., et al. (2006) Protein stability and surface electrostatics: a charged relationship. *Biochemistry* **45**: 2761-2766.

Tsaneva, I.R., and Weiss, B. (1990) *soxR*, a locus governing a superoxide response regulon in *Escherichia coli* K-12. *J Bacteriol* **172**: 4197-4205.

van Rossum, T., Kengen, S.W., and van der Oost, J. (2013) Reporter-based screening and selection of enzymes. *FEBS J* **280**: 2979-2996.

Zhang, R., Xu, Y., and Xiao, R. (2015) Redesigning alcohol dehydrogenases/reductases for more efficient biosynthesis of enantiopure isomers. *Biotechnol Adv* **33**: 1671-1684.

Zheng, Y.G., Yin, H.H., Yu, D.F., Chen, X., Tang, X.L., Zhang, X.J., et al. (2017) Recent advances in biotechnological applications of alcohol dehydrogenases. *Appl Microbiol Biotechnol* **101**: 987-1001.

Table 1. Kinetic parameters of purifed *Lb*ADH^{WT} and *Lb*ADH^{K71E} for various substrates.

Substrate	**V_{max} (µmol min^{-1} mg^{-1})**		**K_M (mM)**	
	***Lb*ADH^{WT}**	***Lb*ADH^{K71E}**	***Lb*ADH^{WT}**	***Lb*ADH^{K71E}**
2,5-Hexanedione[1]	148.5 ± 12.3	173.3 ± 11.1	5.1 ± 0.6	4.3 ± 0.5
Methyl acetoacetate[2]	154.2 ± 2.2	221.2 ± 3.3	1.13 ± 0.06	0.67 ± 0.04

[1]Mean values and standard deviation based on three separate protein preparations with three technical replicates per preparation.

[2]Mean values and standard deviation based on a single protein preparation and three technical replicates.

Table 2. Analysis of *Lb*ADH^{WT} and *Lb*ADH^{K71E} activity for the substrates methyl acetoacetate, 2-acetylpyridine, 4-hydroxy-2-butanone, acetophenone, and 2-hexanone. Mean values obtained from a single protein preparation and three technical replicates are shown.

Substrate	**Substrate concentration**	***Lb*ADH^{WT} activity (µmol min^{-1} mg^{-1})**	***Lb*ADH^{K71E} activity (µmol min^{-1} mg^{-1})**	**% increase**
2-acetylpyridine	10 mM	104.1 ± 1.7	125.5 ± 1.1	21%
2-hexanone	10 mM	22.8 ± 0.7	27.9 ± 1.1	22%
acetophenone	5 mM	29.8 ± 0.7	39.5 ± 0.7	33%
4-hydroxy-2-butanone	10 mM	39.5 ± 1.3	54.9 ± 4.6	39%

Table 3. Bacterial strains and plasmids used in this study.

Strain or plasmid	Relevant characteristics	Source or reference
Escherichia coli		
TOP10	*mcrA*, Δ(*mrr-hsd*RMS-*mcrBC*), Phi80*lacZ(del)M15*, Δ*lacX74*, *deoR*, *recA1*, *araD139*, Δ(*ara-leu*)7697, *galU*, *galK*, *rpsL(SmR)*, *endA1*, *nupG,* strain used for general cloning procedures	Invitrogen
C43(DE3)	F– *ompT gal dcm hsdSB(rB- mB-)*(DE3), strain used for protein expression	(Miroux and Walker, 1996)
Plasmids		
pSenSox	Amp^R; pBtac-*Lbadh* derivative containing the *soxRS*-based NADPH biosensor and the $Lbadh^{WT}$ gene under transcriptional control of the *tac* promoter	(Siedler et al., 2014)
pSenNeg	Amp^R; pSenSox derivative with an incomplete $Lbadh^{WT}$ gene preventing synthesis of an active *Lb*ADH^{WT}	(Siedler et al., 2014)
pSenSox-$Lbadh^{K71E}$	Amp^R; pSenSox derivative with the $Lbadh^{K71E}$ gene under control of the *tac*-promoter	This study
pASK-IBA5plus-$Lbadh^{WT}$	Amp^R; pASK-IBA5plus derivative for production of *Lb*ADH^{WT} with N-terminal Strep-tag II under control of the *tet*-promoter/operator	Prof. W. Kroutil, Department of Chemistry, University of Graz, Austria
pASK-IBA5plus-$Lbadh^{K71E}$	Amp^R; pASK-IBA5plus derivative carrying the gene construct for the purification of the mutant *Lb*ADH^{K71E} protein with an N-terminal Strep-Tactin affinity tag (Strep-tag II) under transcriptional control of the *tet*-promoter/operator	This study

Table 4. Oligonucleotides used in this study.[1]

Oligonucleotide	Sequence (5' → 3') and properties
pSenSox-*Lbadh*-fw	**CAATTTCACACAGGAAACAGGCGGCCGC**ATGTCTAACCGTTTGGATG
pSenSox-*Lbadh*-rv	**CTCTCATCCGCCAAAACAGAGAATTC**CTATTGAGCAGTGTAGCC
Oligonucleotides used for colony-PCRs and sequencing of plasmids.	
pSenSox-*Lbadh*^{Library} sequencing fw	TAATCATCGGCTCGTATAATGTGTG
pSenSox-*Lbadh*^{Library} sequencing rv	GCTTCTGCGTTCTGATTTAATCTG
Lbadh-mutagenesis A412G fw	GATGAAGATGGTTGGACCGAACTGTTTGATGCAACC
Lbadh-mutagenesis A412G rv	GGTTGCATCAAACAGTTCGGTCCAACCATCTTCATC
pASK-IBA5plus-*Lbadh*^{K71E} sequencing fw	GAAATAATTTTGTTTAACTTTAAGAAGG
pASK-IBA5plus-*Lbadh*^{K71E} sequencing rv	CCATTTTTCACTTCACAGGTCAAGC

[1] Overlapping regions required for Gibson assembly in oligonucleotides used for cloning of the *Lbadh*^{Library} genes into pSenSox cut with EcoRI and HindIII are shown in bold.

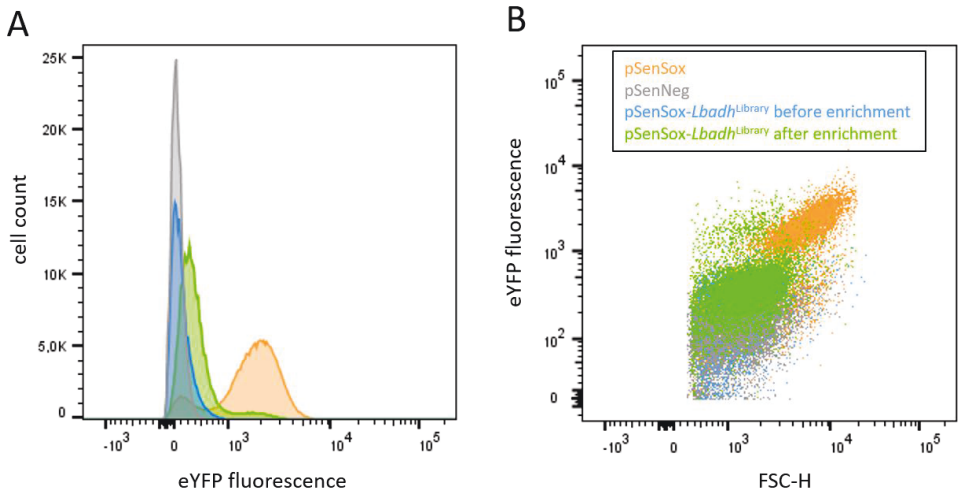

Fig. 1. FACS analysis the *Lb*ADH mutant library. Comparison of the fluorescence distribution of the *E. coli* TOP10/pSenSox-*Lbadh*^{Library} culture before (blue) and after three positive enrichment steps followed by one negative and another positive enrichment step (green). *E. coli* TOP10/pSenSox cells (orange) were used as positive control and *E. coli* TOP10/pSenNeg cells (grey) as negative control. Before FACS analysis, cells of the different cultures were incubated for 2.5 h with the substrate 2,5-hexanedione. Prior to sorting, 2.5×10^5 cells of each culture were analyzed. The plots were generated with the BD DIVA 6.1.3 software. (A) Histogram of the four *E. coli* cultures described above. (B) Dot plots of the four cultures described abvoe displaying the eYFP fluorescence signal against the forward scatter height (FSC-H) reflecting the size of the cells.

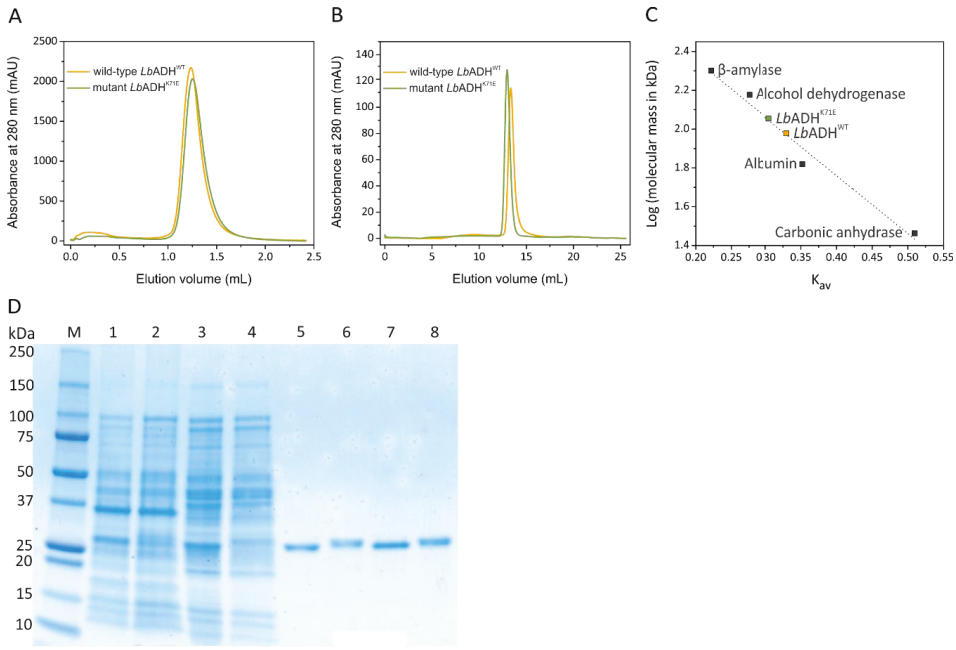

Fig. 2. Purification of *Lb*ADH^{WT} and *Lb*ADH^{K71E}. (A) Chromatogram of the affinity chromatography with the Strep-Trap^{TM} HP column. (B) Chromatogram of the size-exclusion chromatography of the affinity-purified proteins with a Superdex^{TM} 200 increase 10/300 GL column. (C) Calibration curve used for molecular mass determination obtained with proteins of known molecular mass: carbonic anhydrase (29 kDa), bovine serum albumin (66 kDa), alcohol dehydrogenase (150 kDa) and β-amylase (200 kDa). For molecular mass determination the partition coefficient K_{av} was calculated and plotted against the logarithm of the molecular mass. *Lb*ADH^{WT} was shown to be tetrameric with a molecular mass of 107 kDa. *Lb*ADH^{WT} eluted with an apparent molecular mass of 95 kDa and *Lb*ADH^{K71E} with an apparent molecular mass of 113 kDa. (D) SDS-PAGE analysis of crude cell extracts (lanes 1 and 2) and soluble protein fractions (lanes 3 and 4) of *E. coli* C43(DE3)/pASK-IBA5plus-*Lbadh*^{WT} (lanes 1 and 3) and *E. coli* C43(DE3)/pASK-IBA5plus-*Lbadh*^{K71E} (lanes 2 and 4) and of purified *Lb*ADH^{WT} (lanes 5 and 7) and *Lb*ADH^{K71E} (lanes 6 and 8) after StrepTactin affinity chromatography (lanes 5 and 6) and after size-exclusion chromatography (lanes 7 and 8). The Mini-PROTEAN® TGX^{TM} any kD^{TM} gel was stained with GelCode™ Blue Stain Reagent (Thermo Scientific, Rockford, USA). M, protein molecular mass standards.

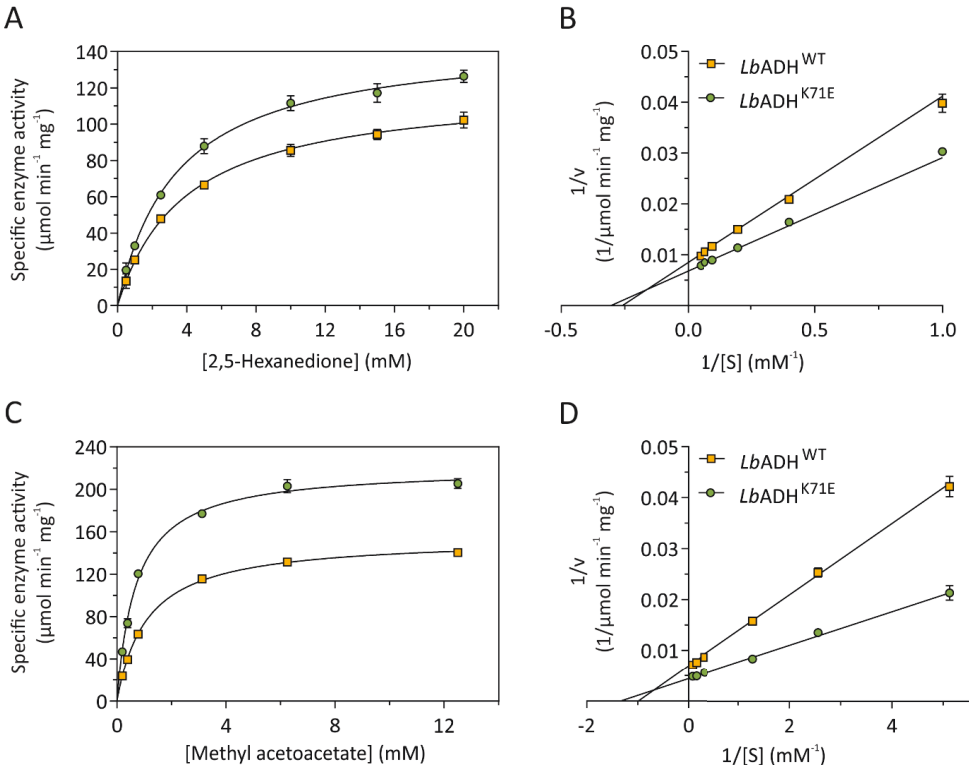

Fig. 3. Representative Michaelis-Menten plots (A, C) and Lineweaver-Burk plots (B, D) for NADPH-dependent reduction of 2,5-hexanedione to (2*R*,5*R*)-hexanediol (A, B) and of methyl acetoacetate to (*R*)-methyl 3-hydroxybutyrate (C, D) by purified *Lb*ADH^{WT} and *Lb*ADH^{K71E}. Data are mean values from three technical replicates of a single protein preparation.

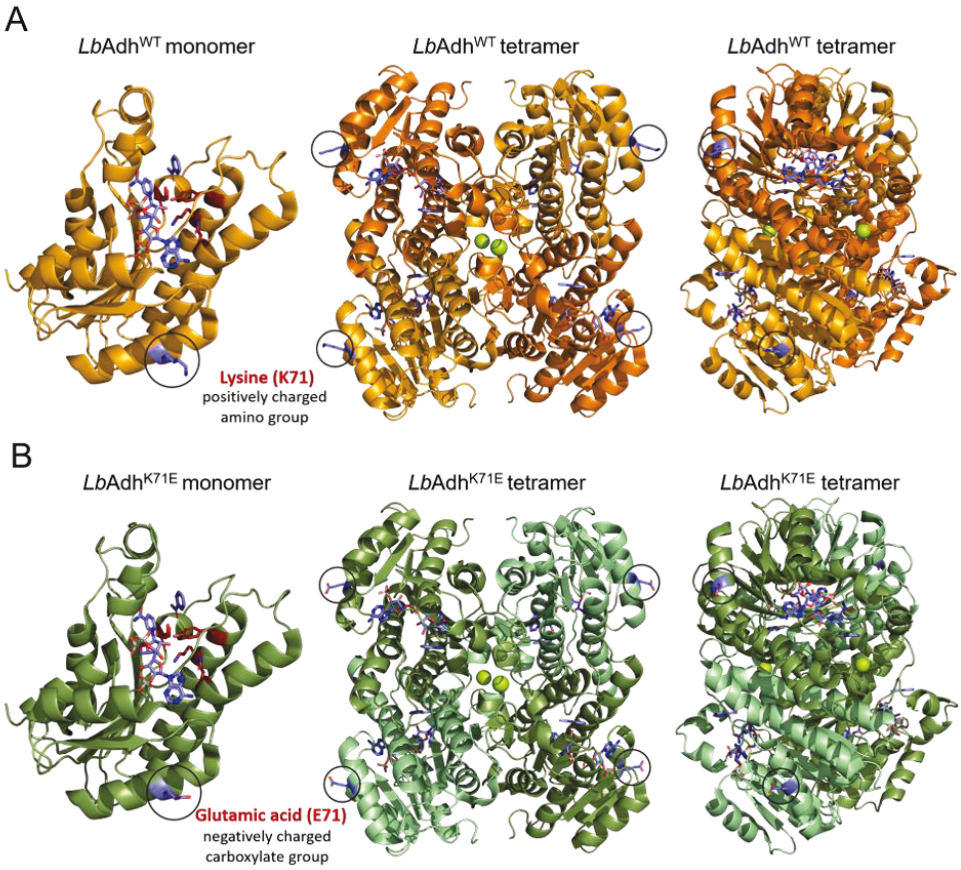

Fig. 4. Crystal structure of the *Lb*ADH^{WT} monomer and the homotetramer in complex with the substrate acetophenone and the cofactor NADPH (Schlieben et al. 2005) (A) and modelled structure of *Lb*ADH^{K71E} (B). In the tetrameric structure, the Mg^{2+} ions needed for structure stabilization are shown as light green spheres. The amino acids at position 71 are shown as sticks and marked with a black circle. The residues Asn113, Ser142, Tyr155, Lys159 involved in the catalytic mechanism are shown in red as sticks in the monomer. The images were generated with the software PyMOL 2.2.0 (PDB code 1ZK4).

3. References

Ager, D.J., Prakash, I., and Schaad, D.R. (1996) 1,2-Amino alcohols and their heterocyclic derivatives as chiral auxiliaries in asymmetric synthesis, *Chemical Reviews* **96**: 835-876.

Auriol, C., Bestel-Corre, G., Claude, J.B., Soucaille, P., and Meynial-Salles, I. (2011) Stress-induced evolution of *Escherichia coli* points to original concepts in respiratory cofactor selectivity, *Proceedings of the National Academy of Sciences of the United States of America* **108**: 1278-1283.

Biegel, E., Schmidt, S., Gonzalez, J.M., and Muller, V. (2011) Biochemistry, evolution and physiological function of the Rnf complex, a novel ion-motive electron transport complex in prokaryotes, *Cellular and molecular life sciences : CMLS* **68**: 613-634.

Binder, S., Schendzielorz, G., Stabler, N., Krumbach, K., Hoffmann, K., Bott, M., and Eggeling, L. (2012) A high-throughput approach to identify genomic variants of bacterial metabolite producers at the single-cell level, *Genome Biol* **13**: R40.

Binder, S., Siedler, S., Marienhagen, J., Bott, M., and Eggeling, L. (2013) Recombineering in *Corynebacterium glutamicum* combined with optical nanosensors: a general strategy for fast producer strain generation, *Nucleic acids research* **41**: 6360-6369.

Blanchard, J.L., Wholey, W.Y., Conlon, E.M., and Pomposiello, P.J. (2007) Rapid changes in gene expression dynamics in response to superoxide reveal SoxRS-dependent and independent transcriptional networks, *PloS one* **2**: e1186.

Bloch, W. (2006) J.-L. Reymond (Ed.): Enzyme assays. High-throughput screening, genetic selection and fingerprinting, *Analytical and Bioanalytical Chemistry* **386**: 1583-1584.

Bornscheuer, U.T., and Pohl, M. (2001) Improved biocatalysts by directed evolution and rational protein design, *Curr Opin Chem Biol* **5**: 137-143.

Bott, M. (2015) Need for speed - finding productive mutations using transcription factor-based biosensors, fluorescence-activated cell sorting and recombineering, *Microb Biotechnol* **8**: 8-10.

Breuer, M., Ditrich, K., Habicher, T., Hauer, B., Kesseler, M., Sturmer, R., and Zelinski, T. (2004) Industrial methods for the production of optically active intermediates, *Angewandte Chemie (International ed. in English)* **43**: 788-824.

Daley, D.O., Rapp, M., Granseth, E., Melen, K., Drew, D., and von Heijne, G. (2005) Global topology analysis of the *Escherichia coli* inner membrane proteome, *Science* **308**: 1321-1323.

Dietrich, J.A., McKee, A.E., and Keasling, J.D. (2010) High-throughput metabolic engineering: advances in small-molecule screening and selection, *Annual review of biochemistry* **79**: 563-590.

Ding, H., and Demple, B. (2000) Direct nitric oxide signal transduction via nitrosylation of iron-sulfur centers in the SoxR transcription activator, *Proceedings of the National Academy of Sciences of the United States of America* **97**: 5146-5150.

Ding, H., Hidalgo, E., and Demple, B. (1996) The redox state of the [2Fe-2S] clusters in SoxR protein regulates its activity as a transcription factor, *The Journal of biological chemistry* **271**: 33173-33175.

Döbber, J., Pohl, M., Ley, S.V., and Musio, B. (2018) Rapid, selective and stable HaloTag-*Lb*ADH immobilization directly from crude cell extract for the continuous biocatalytic production of chiral alcohols and epoxides, *Reaction Chemistry & Engineering* **3**: 8-12.

Eggeling, L., Bott, M., and Marienhagen, J. (2015) Novel screening methods--biosensors, *Current opinion in biotechnology* **35**: 30-36.

Fujikawa, M., Kobayashi, K., and Kozawa, T. (2012) Direct oxidation of the [2Fe-2S] cluster in SoxR protein by superoxide: distinct differential sensitivity to superoxide-mediated signal transduction, *The Journal of biological chemistry* **287**: 35702-35708.

Gaudu, P., and Weiss, B. (1996) SoxR, a [2Fe-2S] transcription factor, is active only in its oxidized form, *Proceedings of the National Academy of Sciences of the United States of America* **93**: 10094-10098.

Goldbeck, O., W Eck, A., and Seibold, G. (2018) *Real time monitoring of NADPH concentrations in Corynebacterium glutamicum and Escherichia coli via the genetically gncoded sensor mBFP*.

Greenberg, J.T., Monach, P., Chou, J.H., Josephy, P.D., and Demple, B. (1990) Positive control of a global antioxidant defense regulon activated by superoxide-generating agents in Escherichia coli, *Proceedings of the National Academy of Sciences of the United States of America* **87**: 6181-6185.

Griffith, K.L., Shah, I.M., and Wolf, R.E., Jr. (2004) Proteolytic degradation of *Escherichia coli* transcription activators SoxS and MarA as the mechanism for reversing the induction of the superoxide (SoxRS) and multiple antibiotic resistance (Mar) regulons, *Mol Microbiol* **51**: 1801-1816.

Gu, M., and Imlay, J.A. (2011) The SoxRS response of *Escherichia coli* is directly activated by redox-cycling drugs rather than by superoxide, *Mol Microbiol* **79**: 1136-1150.

Hall, M., and Bommarius, A.S. (2011) Enantioenriched compounds via enzyme-catalyzed redox reactions, *Chemical reviews* **111**: 4088-4110.

Hess, V., Gallegos, R., Jones, J.A., Barquera, B., Malamy, M.H., and Muller, V. (2016) Occurrence of ferredoxin:NAD(+) oxidoreductase activity and its ion specificity in several Gram-positive and Gram-negative bacteria, *PeerJ* **4**: e1515.

Hidalgo, E., and Demple, B. (1994) An iron-sulfur center essential for transcriptional activation by the redox-sensing SoxR protein, *The EMBO journal* **13**: 138-146.

Hidalgo, E., Leautaud, V., and Demple, B. (1998) The redox-regulated SoxR protein acts from a single DNA site as a repressor and an allosteric activator, *The EMBO journal* **17**: 2629-2636.

Hreha, T.N., Mezic, K.G., Herce, H.D., Duffy, E.B., Bourges, A., Pryshchep, S., et al. (2015) Complete topology of the RNF complex from *Vibrio cholerae*, *Biochemistry* **54**: 2443-2455.

Kabus, A., Georgi, T., Wendisch, V.F., and Bott, M. (2007) Expression of the *Escherichia coli pntAB* genes encoding a membrane-bound transhydrogenase in *Corynebacterium glutamicum* improves *L*-lysine formation, *Applied microbiology and biotechnology* **75**: 47-53.

Kappus, H., and Sies, H. (1981) Toxic drug effects associated with oxygen metabolism: redox cycling and lipid peroxidation, *Experientia* **37**: 1233-1241.

Klucar, L., Stano, M., and Hajduk, M. (2009) phiSITE: database of gene regulation in bacteriophages, *Nucleic acids research* **38**: D366-D370.

Kobayashi, K. (2017) Sensing mechanisms in the redox-regulated, [2Fe–2S] cluster-containing, bacterial transcriptional factor SoxR, *Accounts of Chemical Research* **50**: 1672-1678.

Kobayashi, K., Fujikawa, M., and Kozawa, T. (2015) Binding of promoter DNA to SoxR protein decreases the reduction potential of the [2Fe–2S] cluster, *Biochemistry* **54**: 334-339.

Koo, M.S., Lee, J.H., Rah, S.Y., Yeo, W.S., Lee, J.W., Lee, K.L., et al. (2003) A reducing system of the superoxide sensor SoxR in *Escherichia coli*, *The EMBO journal* **22**: 2614-2622.

Krapp, A.R., Humbert, M.V., and Carrillo, N. (2011) The soxRS response of *Escherichia coli* can be induced in the absence of oxidative stress and oxygen by modulation of NADPH content, *Microbiology* **157**: 957-965.

Leemhuis, H., Kelly, R.M., and Dijkhuizen, L. (2009) Directed evolution of enzymes: Library screening strategies, *IUBMB Life* **61**: 222-228.

Leuchs, S., and Greiner, L. (2011) Alcohol Dehydrogenase from Lactobacillus brevis: A versatile robust catalyst for enantioselective transformations, *Chemical & Biochemical Engineering* **25**: 267-281.

Liese, A., Karsten, S., and Christian, W. (2001) *Industrial Biotransformation*.

Liochev, S.I., and Fridovich, I. (1992) Fumarase C, the stable fumarase of *Escherichia coli*, is controlled by the *soxRS* regulon, *Proceedings of the National Academy of Sciences of the United States of America* **89**: 5892-5896.

Liochev, S.I., and Fridovich, I. (2011) Is superoxide able to induce SoxRS?, *Free Radical Biology and Medicine* **50**: 1813.

Mahr, R., and Frunzke, J. (2016) Transcription factor-based biosensors in biotechnology: current state and future prospects, *Applied microbiology and biotechnology* **100**: 79-90.

Mahr, R., Gätgens, C., Gatgens, J., Polen, T., Kalinowski, J., and Frunzke, J. (2015) Biosensor-driven adaptive laboratory evolution of l-valine production in *Corynebacterium glutamicum*, *Metabolic engineering* **32**: 184-194.

Munoz Solano, D., Hoyos, P., Hernaiz, M.J., Alcantara, A.R., and Sanchez-Montero, J.M. (2012) Industrial biotransformations in the synthesis of building blocks leading to enantiopure drugs, *Bioresource technology* **115**: 196-207.

Ni, Y., and Xu, J.H. (2012) Biocatalytic ketone reduction: a green and efficient access to enantiopure alcohols, *Biotechnology advances* **30**: 1279-1288.

Niefind, K., Müller, J., Riebel, B., Hummel, W., and Schomburg, D. (2003) The crystal structure of *R*-specific alcohol dehydrogenase from *Lactobacillus brevis* suggests the structural basis of its metal dependency, *Journal of molecular biology* **327**: 317-328.

Rathnasingh, C., Raj, S.M., Lee, Y., Catherine, C., Ashok, S., and Park, S. (2012) Production of 3-hydroxypropionic acid via malonyl-CoA pathway using recombinant *Escherichia coli* strains, *Journal of biotechnology* **157**: 633-640.

Riebel, B. (1997) Biochemische und molekularbiologische Charakterisierung neuer mikrobieller NAD(P)-abhängiger Alkoholdehydrogenasen. Heinrich-Heine-Universität Düsseldorf, Germany: Ph.D. thesis.

Rodríguez, C., Borzęcka, W., Sattler, J., Kroutil, W., Lavandera, I., and Gotor, V. (2014) *Steric vs. electronic effects in the Lactobacillus brevis ADH-catalyzed bioreduction of ketones*.

Rogers, J.K., Taylor, N.D., and Church, G.M. (2016) Biosensor-based engineering of biosynthetic pathways, *Current opinion in biotechnology* **42**: 84-91.

Sauer, U., Canonaco, F., Heri, S., Perrenoud, A., and Fischer, E. (2004) The soluble and membrane-bound transhydrogenases UdhA and PntAB have divergent functions in NADPH metabolism of *Escherichia coli*, *The Journal of biological chemistry* **279**: 6613-6619.

Schendzielorz, G., Dippong, M., Grünberger, A., Kohlheyer, D., Yoshida, A., Binder, S., et al. (2014) Taking control over control: use of product sensing in single cells to remove flux control at key enzymes in biosynthesis pathways, *ACS synthetic biology* **3**: 21-29.

Schlieben, N.H., Niefind, K., Muller, J., Riebel, B., Hummel, W., and Schomburg, D. (2005) Atomic resolution structures of R-specific alcohol dehydrogenase from *Lactobacillus brevis* provide the structural bases of its substrate and cosubstrate specificity, *Journal of molecular biology* **349**: 801-813.

Seo, S.W., Kim, D., Szubin, R., and Palsson, B.O. (2015) Genome-wide Reconstruction of OxyR and SoxRS Transcriptional Regulatory Networks under Oxidative Stress in *Escherichia coli* K-12 MG1655, *Cell reports* **12**: 1289-1299.

Siedler, S., Schendzielorz, G., Binder, S., Eggeling, L., Bringer, S., and Bott, M. (2014) SoxR as a single-cell biosensor for NADPH-consuming enzymes in *Escherichia coli*, *ACS synthetic biology* **3**: 41-47.

Spielmann, A., Baumgart, M., and Bott, M. (2018) NADPH-related processes studied with a SoxR-based biosensor in *Escherichia coli* **0**: e785.

Thomason, M.K., Bischler, T., Eisenbart, S.K., Forstner, K.U., Zhang, A., Herbig, A., et al. (2015) Global transcriptional start site mapping using differential RNA sequencing reveals novel antisense RNAs in *Escherichia coli*, *J Bacteriol* **197**: 18-28.

Tsaneva, I.R., and Weiss, B. (1990) *soxR*, a locus governing a superoxide response regulon in *Escherichia coli* K-12, *Journal of Bacteriology* **172**: 4197-4205.

Ulrich, L.E., Koonin, E.V., and Zhulin, I.B. (2005) One-component systems dominate signal transduction in prokaryotes, *Trends in microbiology* **13**: 52-56.

Watanabe, S., Kita, A., Kobayashi, K., and Miki, K. (2008) Crystal structure of the [2Fe-2S] oxidative-stress sensor SoxR bound to DNA, *Proceedings of the National Academy of Sciences of the United States of America* **105**: 4121-4126.

Weckbecker, A., and Hummel, W. (2004) Improved synthesis of chiral alcohols with *Escherichia coli* cells co-expressing pyridine nucleotide transhydrogenase, $NADP^+$-dependent alcohol dehydrogenase and NAD^+-dependent formate dehydrogenase, *Biotechnol Lett* **26**: 1739-1744.

Wu, J., and Weiss, B. (1991) Two divergently transcribed genes, soxR and soxS, control a superoxide response regulon of Escherichia coli, *Journal of bacteriology* **173**: 2864-2871.

Zheng, Y.G., Yin, H.H., Yu, D.F., Chen, X., Tang, X.L., Zhang, X.J., et al. (2017) Recent advances in biotechnological applications of alcohol dehydrogenases, *Applied microbiology and biotechnology* **101**: 987-1001.

Danksagung

Bei **Prof. Dr. Michael Bott** bedanke ich mich für die Überlassung des interessanten Themas, die Übernahme des Erstgutachtens und für die Ratschläge, die den stetigen Fortschritt des Projekts ermöglicht haben.

Prof. Dr. Martina Pohl danke ich für die Übernahme des Zweitgutachtens.

Dr. Meike Baumgart danke ich sehr herzlich für ihre Betreuung und ihr Interesse am Fortgang dieser Arbeit. Insbesondere möchte ich mich bei ihr für die Hilfe bei der Vorbereitung von Vorträgen sowie der Korrektur dieser Arbeit bedanken.

Der Arbeitsgruppe „Metabolic Regulation and Engineering“ danke ich für die gute Arbeitsatmosphäre. Insbesondere danke ich **Maike**, **Kim**, **Julia**, **Cedric**, **Natalie**, **Karen**, **Lingfeng**, **Marcel**, **Hannes**, **Sarah**, **Susanna**, **Kai** und **Brita** für ihre wunderbare Unterstützung im Labor und für spannende wie auch lustige Unterhaltungen, wissenschaftlicher und nicht-wissenschaftlicher Art. Und dafür, dass sie mich in schwierigen Zeiten immer aufgebaut haben und motiviert haben, nicht aufzuhören.

Yannik danke ich für die Mitarbeit am Projekt in Form seiner Masterarbeit. Dank seines engagierten und sorgfältigen Beitrags konnte die verbesserte Variante der Alkohol-Dehydrogenase von *Lactobacillus brevis* identifiziert werden.

Meinen **Eltern** und meinem **Bruder** danke ich besonders für ihre große Unterstützung, ihr Verständnis, und ihre Akzeptanz während der gesamten Studienzeit.

Erklärung

Ich versichere an Eides statt, dass die Dissertation von mir selbständig und ohne unzulässige fremde Hilfe unter Beachtung der „Grundsätze zur Sicherung guter wissenschaftlicher Praxis an der Heinrich-Heine-Universität Düsseldorf“ erstellt worden ist. Die Dissertation wurde in der vorgelegten oder ähnlicher Form noch bei keiner anderen Institution eingereicht. Ich habe bisher keine erfolglosen Promotionsversuche unternommen.

Ingolstadt, den 10.05.2019

Alina Spielmann, M.Sc.

Band / Volume 193
Group IV (Si)GeSn Light Emission and Lasing Studies
D. Stange (2019), vi, 151 pp
ISBN: 978-3-95806-389-1

Band / Volume 194
Construction and analysis of a spatially organized cortical network model
J. Senk (2019), 245 pp
ISBN: 978-3-95806-390-7

Band / Volume 195
Large-scale Investigations of Non-trivial Magnetic Textures in Chiral Magnets with Density Functional Theory
M. Bornemann (2019), 143 pp
ISBN: 978-3-95806-394-5

Band / Volume 196
Neutron scattering
Experimental Manuals of the JCNS Laboratory Course held at Forschungszentrum Jülich and at the Heinz-Maier-Leibnitz Zentrum Garching
edited by T. Brückel, S. Förster, G. Roth, and R. Zorn (2019),
ca 150 pp
ISBN: 978-3-95806-406-5

Band / Volume 197
Topological transport in non-Abelian spin textures from first principles
P. M. Buhl (2019), vii, 158 pp
ISBN: 978-3-95806-408-9

Band / Volume 198
Shortcut to the carbon-efficient microbial production of chemical building blocks from lignocellulose-derived D-xylose
C. Brüsseler (2019), X, 62 pp
ISBN: 978-3-95806-409-6

Band / Volume 199
Regulation and assembly of the cytochrome *bc*$_1$-*aa*$_3$ supercomplex in *Corynebacterium glutamicum*
C.-F. Davoudi (2019), 135 pp
ISBN: 978-3-95806-416-4

Band / Volume 200
Variability and compensation in Alzheimer's disease across different neuronal network scales
C. Bachmann (2019), xvi, 165 pp
ISBN: 978-3-95806-420-1

Schriften des Forschungszentrums Jülich
Reihe Schlüsseltechnologien / Key Technologies

Band / Volume 201
Crystal structures and vibrational properties of chalcogenides: the role of temperature and pressure
M. G. Herrmann (2019), xi, 156 pp
ISBN: 978-3-95806-421-8

Band / Volume 202
Current-induced magnetization switching in a model epitaxial Fe/Au bilayer
P. Gospodarič (2019), vi, 120, XXXVIII pp
ISBN: 978-3-95806-423-2

Band / Volume 203
Network architecture and heme-responsive gene regulation of the two-component systems HrrSA and ChrSA
M. Keppel (2019), IV, 169 pp
ISBN: 978-3-95806-427-0

Band / Volume 204
Spin-orbitronics at the nanoscale: From analytical models to real materials
J. Bouaziz (2019), 228 pp
ISBN: 978-3-95806-429-4

Band / Volume 205
Advanced methods for atomic scale spin simulations and application to localized magnetic states
G. P. Müller (2019), xx, 194 pp
ISBN: 978-3-95806-432-4

Band / Volume 206
Different growth modes of molecular adsorbate systems and 2D materials investigated by low-energy electron microscopy
J. E. Felter (2019), vi, 114, XXXIV pp
ISBN: 978-3-95806-434-8

Band / Volume 207
NADPH-related studies performed with a SoxR-based biosensor in *Escherichia coli*
A. Spielmann (2019), IV, 73 pp
ISBN: 978-3-95806-438-6

Weitere ***Schriften des Verlags im Forschungszentrum Jülich*** unter
http://wwwzb1.fz-juelich.de/verlagextern1/index.asp

Schlüsseltechnologien / Key Technologies
Band / Volume 207
ISBN 978-3-95806-438-6

Mitglied der Helmholtz-Gemeinschaft

JÜLICH
Forschungszentrum